

**MULTIPLY COMPLEX, NON-TOXIC, ANTI-FOULING SURFACES
DESIGNED FOR MARINE AND BIOMEDICAL APPLICATIONS**

A Dissertation

by

KEVIN ANDREW POLLACK

Submitted to the Office of Graduate and Professional Studies of
Texas A&M University
in partial fulfillment of the requirements for the degree of

DOCTOR OF PHILOSOPHY

Chair of Committee,	Karen L. Wooley
Committee Members,	François Gabbai
	Lei Fang
	Melissa A. Grunlan
Head of Department,	François Gabbai

December 2014

Major Subject: Chemistry

Copyright 2014 Kevin Andrew Pollack

ABSTRACT

Biofouling, the undesired accumulation of biological organisms on a surface, is a problem that plagues a wide spectrum of materials. Because of the ban of heavy metal paint formulations, there has been a rapid movement towards the development of novel anti-biofouling coatings based upon various polymeric networks. The main focus of this dissertation is to design and develop unique polymeric networks that display unique heterogeneities in regards to topography, topology and chemical composition on the micro- and nano-scales that can be explored as non-toxic coatings for the deterrence of organisms in the marine environment. These materials also have potential to serve as anti-biofouling coatings for biomedical and other applications.

A two dimensional array of terpolymer networks based on the crosslinking of hyperbranched fluoropolymers (HBFP) with varying concentrations of poly(ethylene glycol) (PEG) and polydimethylsiloxane (PDMS) were generated. Crosslinking coincides with and is followed by degrees of thermodynamically-driven phase separation within the bound network and results in a complex surface that displays dynamically-reorganizing heterogeneity in its topography, topology and chemical composition on both the nano- and the micro-scales. The coatings were characterized using atomic force microscopy (AFM), surface force spectroscopy, and static water contact angle to probe their surface properties.

Because of the performance displayed in anti-biofouling testing for the terpolymer networks, a more industrially-relevant method for applying the networks was sought.

Through the use of a spray coating application method, the terpolymer network could be laid down onto a Naval-approved epoxy barrier coating. The epoxy barrier coating provides functional handles to covalently bond the terpolymer network to the substrate without further modification. The coatings were then tested, through collaborations with the University of Newcastle, Florida Institute of Technology, the University of Hawaii at Manoa and California Polytechnic State University against various marine organisms and in static water immersion testing to test their viability as anti-biofouling coatings.

Additionally, the ability to expand the concept of the terpolymer networks was investigated. These studies included the use of different components for each of the three components of the system. Specifically, the use of silsesquioxanes as a hydrophobic component, zwitterions as a hydrophilic component and a bis-functional fluorinated molecule was explored using AFM, IR, static water contact angle and an anti-biofouling study against *Ulva* zoospores. In summary, both systems studied displayed potential as next-generation anti-biofouling coatings.

DEDICATION

To my mom, Peggy, and my wife, Stephanie

ACKNOWLEDGEMENTS

I would first like to thank my advisor, Prof. Karen L. Wooley, for her guidance, support and help throughout my graduate education at Texas A&M. Without her, none of this work would be possible, and the only reason I was able to achieve so much is because I was influenced so heavily by her. She has instilled confidence in my abilities and has molded me into the researcher that I am today.

I would also like to thank my committee members, Prof. François Gabbai, Prof. Lei Fang, and Prof. Melissa A. Grunlan, for their guidance and support throughout the course of this research. Additionally, I would like to thank all external collaborators who have helped expand this research through their own expertise, including the laboratories of Prof. Jim Callow of the University of Birmingham, Prof. Anthony Clare of Newcastle University, Prof. Michael Hadfield of the University of Hawaii, Prof. Dean Wendt of California Polytechnic State University and Prof. Geoffrey Swain of the Florida Institute of Technology.

For Chapter II, I would like to thank the Office of Naval Research (N00014-10-1-0527 and N00014-14-1-0082). The Welch Foundation is gratefully acknowledged for support through the W. T. Doherty-Welch Chair in Chemistry, Grant No. A-0001. I would also like to thank Dr. Jing Wu of the Materials Characterization Facility at Texas A&M University for her help with the XPS.

For Chapter III, I would like to thank the Office of Naval Research (N00014-14-1-0082, N00014-13-1-0633 and N00014-13-1-0634). The Welch Foundation is gratefully

acknowledged for support through the W. T. Doherty-Welch Chair in Chemistry, Grant No. A-0001. I also gratefully acknowledge Dr. Nick Aldred and Prof. Anthony S. Clare of the University of Newcastle for performing the anti-biofouling assays with *Balanus amphitrite* and *Balanus improvisus*.

For Chapter IV, I would like to thank the Office of Naval Research (N00014-14-1-0082, N00014-14-1-0167, N00014-12-1-0474 and N00014-10-1-0919). The Welch Foundation is gratefully acknowledged for support through the W. T. Doherty-Welch Chair in Chemistry, Grant No. A-0001. I also gratefully acknowledge Ms. Kelli Zargiel and Prof. Geoffrey W. Swain of the Florida Institute of Technology, Ms. Lenora H. Brewer and Prof. Dean E. Wendt of California Polytechnic State University and Ms. Audrey Asahina and Prof. Michael G. Hadfield of University of Hawaii at Manoa for their efforts in performing the static water immersion testing at their respective facilities.

For Chapter V, I would like to thank the Office of Naval Research (N00014-14-1-0082). The Welch Foundation is gratefully acknowledged for support through the W. T. Doherty-Welch Chair in Chemistry, Grant No. A-0001.

I would also like to thank past and present members of the Wooley group, Dr. Jeffery Raymond, Dr. Mahmoud El Sabahy, Dr. Christopher Fidge, Dr. Guorong Sun, Dr. Ritu Shrestha, Dr. Sandani Samarajeewa, Dr. Jiong Zou, Dr. Shiyi Zhang, Mr. Alexander Lonnecker, Mr. Gyu Seong Heo, Ms. Kellie Seetho and Mr. Matthew Svach, who all played a role in my development as a researcher. It has been a privilege to work with such talented individuals on a daily basis that have helped develop my scientific abilities and been there throughout my graduate career.

I would also like to thank some friends I met during my time at Texas A&M, in particular, Dr. Casey Wade, Dr. Thomas Kaiser, Dr. Julian Sculley and Mr. Tyler Hood and Mr. Masato Hirai, for their guidance, support and friendship during the course of my graduate work.

Lastly, I would like to thank my family for their continued support as I pursued my graduate education. Specifically, I would like to thank my mom, Peggy, who always encouraged me to follow my dreams as well as my brother, Adam, and his family for their continuing advice and help. I would also like to thank my beautiful wife, Stephanie, whom I met during my time in the Wooley laboratory at Texas A&M. She has made my life truly special and her presence in my life has pushed me to greater heights than I could imagine alone.

NOMENCLATURE

AF	Anti-fouling
AFM	Atomic force microscopy
ATR-IR	Attenuated total reflectance infrared spectroscopy
ATRP	Atom transfer radical polymerization
ATR-SCVCP	Atom transfer radical-self condensing vinyl copolymerization
BSA	Bovine serum albumin
CA	Contact angle
CDCl ₃	Deuterated chloroform
CuBr	Copper bromide
DCM	Dichloromethane
DIPEA	N,N-diisopropylethylamine
DMA	Dynamic mechanical analysis
DSC	Differential scanning calorimetry
DTMA	Dynamic thermal mechanical analysis
FR	Fouling release
GPC	Gel permeation chromatography
HBFP	Hyperbranched fluoropolymer
HBFP-PEG	Hyperbranched fluoropolymer-poly(ethylene glycol)
HBFP-PEG-PDMS	Hyperbranched fluoropolymer-poly(ethylene glycol)- polydimethylsiloxane

IR	Infrared
MWCO	Molecular weight cutoff
NMR	Nuclear magnetic resonance spectroscopy
PBS	Phosphate buffered saline
PDI	Polydispersity index
PDMS	Polydimethylsiloxane
PEG	Poly(ethylene glycol)
PFS	Pentafluorostyrene
PMDETA	N,N,N',N',N''-pentamethyldiethylenetriamine
POSS	Polyhedral oligomeric silsesquioxane
QNM	Quantitative nanomechanical mapping
RMS	Root mean squared
SFS	Surface force spectroscopy
SIMS	Secondary ion mass spectrometry
TBT	Tributyltin
TEA	Triethylamine
THF	Tetrahydrofuran
TOF	Time of flight
TP	Terpolymer
UV	Ultraviolet
Vis	Visible

TABLE OF CONTENTS

	Page
ABSTRACT	ii
DEDICATION	iv
ACKNOWLEDGEMENTS	v
NOMENCLATURE	viii
TABLE OF CONTENTS	x
LIST OF FIGURES	xii
LIST OF TABLES	xv
CHAPTER	
I INTRODUCTION	1
1.1 Introduction	1
II HYPERBRANCHED FLUOROPOLYMER- POLYDIMETHYLSILOXANE-POLY(ETHYLENE GLYCOL) CROSSLINKED TERPOLYMER NETWORKS DESIGNED FOR MARINE AND BIOMEDICAL APPLICATIONS: HETEROGENEOUS NON-TOXIC ANTI-BIOFOULING SURFACES	10
2.1 Introduction	10
2.2 Experimental Section	13
2.3 Results and Discussions	20
2.4 Conclusions	40
III DEVELOPMENT OF A RAPID METHOD FOR THE APPLICATION OF HYPERBRANCHED FLUOROPOLYMER- POLYDIMETHYLSILOXANE-POLY(ETHYLENE GLYCOL) CROSSLINKED TERPOLYMER NETWORKS FOR USE AS ANTI-BIOFOULING COATINGS	42

3.1	Introduction	42
3.2	Materials and Methods	44
3.3	Results and Discussion.....	51
3.4	Conclusions	64
IV	LONG-TERM STATIC IMMERSION TESTING OF HYPERBRANCHED FLUOROPOLYMER- POLYDIMETHYLSILOXANE-POLY(ETHYLENE GLYCOL) CROSSLINKED TERPOLYMER NETWORKS	66
4.1	Introduction	66
4.2	Materials and Methods	69
4.3	Results	76
4.4	Discussion	87
V	THIOL-ENE CROSSLINKED, MULTIPLY-COMPLEX FLUORINATED-ZWITTERIONIC-SILSESQUIOXANE COATINGS FOR ANTI-BIOFOULING APPLICATIONS	91
5.1	Introduction	91
5.2	Experimental Section	93
5.3	Results and Discussion.....	98
5.4	Conclusions	108
VI	CONCLUSIONS.....	109
	REFERENCES.....	117

LIST OF FIGURES

	Page
Figure 2.1. GPC curves of the three batches of HBFP, 3a-c.	21
Figure 2.2. Synthesis of the crosslinked HBFP-PEG-PDMS terpolymer films.	22
Figure 2.3. Contour graphs of static contact angle measurements of dry (left) and water saturated (right) films.	26
Figure 2.4. Contour graph of the differential static contact angle measurements between dry and water saturated films.	26
Figure 2.5. Topography and SFS Mapping of TP.	28
Figure 2.6. ATR-IR and XPS spectra for TP.	32
Figure 2.7. TGA traces of TP and each of the homopolymer components.	33
Figure 2.8. DSC traces of TP on heating (lower) and cooling (upper).	34
Figure 2.9. DTMA and DMA of TP in air. Top: temperature ramp DTMA. Bottom: frequency ramp DMA at RT.	35
Figure 2.10. Submersion DTMA from 20 to 0 °C in synthetic sea water	38
Figure 2.11. Submersion DMA at 37 °C in PBS.	39
Figure 2.12. Fluorescence signal intensities before and after BSA incubation (left).	40
Figure 3.1. Schematic of the mold used to coat glass microscope slides with Interseal® 670 HS.	45
Figure 3.2. Generation of terpolymer coatings on an epoxy undercoat.	53
Figure 3.3. AFM micrographs of the epoxy barrier coating, 20 micron × 20 micron field of view.	55
Figure 3.4. AFM micrographs of the terpolymer network with 75 wt % PEG and 75 wt % PDMS (left), and an expanded view of the surface topography (right).	55

	Page
Figure 3.5. ATR-IR spectra of the terpolymer network spray coated on the epoxy coating (top three spectra) and an unmodified epoxy coatings (bottom three spectra) after 90 days of immersion in synthetic seawater.	57
Figure 3.6. Cross-section of local maxima (left), minima (center) and intensity profiles for both (left).	59
Figure 3.7. Percent settlement of <i>Balanus amphitrite</i> on the terpolymer coatings after 48 h of exposure.	61
Figure 3.8. Percent settlement of <i>Balanus improvisus</i> on the terpolymer coatings after 48 h of exposure.	62
Figure 3.9. Mean removal strength (in Pa) vs. mean settlement of <i>Balanus improvisus</i> for all samples.	62
Figure 3.10. Percent removal of <i>Balanus improvisus</i> on the terpolymer coatings after 48 h of exposure.	63
Figure 4.1. Percent coverage of hard and soft foulers on experimental coatings after one month of static water immersion testing at Pearl Harbor, Hawaii.	77
Figure 4.2. Mean pressure in kPa required to remove tubeworm, <i>Hydroides elegans</i> , from experimental coatings after one month of static water immersion testing at Pearl Harbor, Hawaii.	78
Figure 4.3. Mean pressure in kPa required to remove the bivalve, <i>Ostrea hanleyana</i> , from experimental coatings after one month of static water immersion testing at Pearl Harbor, Hawaii.	79
Figure 4.4. Percent coverage of hard and soft foulers on experimental coatings after two months of static water immersion testing at Pearl Harbor, Hawaii.	80
Figure 4.5. Mean pressure in kPa required to remove tubeworm, <i>Hydroides elegans</i> , from experimental coatings after two months of static water immersion testing at Pearl Harbor, Hawaii.	80
Figure 4.6. Mean pressure in kPa required to remove the bivalve, <i>Ostrea hanleyanai</i> , from experimental coatings after two months of static water immersion testing at Pearl Harbor, Hawaii.	81

	Page
Figure 4.7. Average percent cover of fouling organisms observed on April 11, 2014.....	82
Figure 4.8. Average relative abundance of fouling organisms observed on April 11, 2014.	83
Figure 4.9. Average water jet pressure required to remove biofilm from panels on April 11, 2014	83
Figure 4.10. Average percent cover of fouling with standard deviation observed on June 18, 2014.....	84
Figure 4.11. Average relative abundance of fouling organisms observed on June 18, 2014.....	84
Figure 4.12. Fouling rating of the terpolymer networks and controls after 1, 2 and 3 months of static water immersion conditions, respectively.....	86
Figure 5.1. Synthesis of the fluorinated small molecule, 1.....	99
Figure 5.2. Synthesis of alkene functionalized sulfobetaine, 2.	99
Figure 5.3. Compounds of the ternary coatings.....	100
Figure 5.4. ATR-IR spectra for coatings A, B, C and D pre- (dry) and post-water (wet) immersion.	102
Figure 5.5. AFM micrographs of coating A (top left), B (top right), C (bottom left) and D (bottom right), 1 mm × 1 mm field of view.....	104
Figure 5.6. Force spectra of the compressive modulus channel transposed on AFM micrographs of coating A (top left), B (top right), C (bottom left) and D (bottom right), 1 mm × 1 mm field of view.....	105
Figure 5.7. Average fluorescence intensity of <i>Ulva</i> zoospores on standard coatings and the different variations of zwitterionic coatings after one week of incubation.	107
Figure 5.8. Confocal micrographs of the surfaces <i>Ulva</i> incubation for one week	107

LIST OF TABLES

	Page
Table 1. Total weight percent of PDMS and PEG in the terpolymer coatings.	23
Table 2. Tapping mode AFM images of the pre-swollen terpolymer networks with RMS roughness and contact angle	24
Table 3. Tapping mode AFM images of the terpolymer networks with RMS roughness and contact angle.....	25
Table 4. Summary of surface force spectroscopy data.....	30
Table 5. Summary of DMA/DTMA with kinetics	37
Table 6. Static water contact angle results of the terpolymer network spray coated on the epoxy coating and an unmodified epoxy coatings after 90 days of immersion in synthetic seawater.....	58
Table 7. Results of water jet testing for all coatings	87
Table 8. Ratios of the compounds in the composition of the ternary coatings.	101
Table 9. Summary of static water contact angle data for all coatings pre- and post-water immersion.....	103
Table 10. Summary of AFM and surface force spectroscopy data for all coatings.....	106

CHAPTER I

INTRODUCTION

1.1 Introduction

Biofouling, or the undesired accumulation of biological material on a surface, is detrimental in various fields.¹⁻² From the medical devices to marine shipping, biofouling can cause many adverse effects on the surfaces where it attaches and proliferates.³⁻⁵ Specifically in the marine shipping industry, biofouling is responsible for numerous increases in the costs of shipping due its effects on the ship hull.⁶⁻⁷ One such way in which it increases the costs for this industry is due to an increase in fuel consumption due to increased drag.⁸ It is estimated that even slight improvements in the performance of coatings on a mid-sized naval surface ship, such as the Arleigh Burke-class destroyer DDG-51, can save an estimated \$300-400k per ship per year, with most savings coming from increase in fuel efficiency.⁷ Fuel consumption is only the first problem caused by marine fouling as well because after an organism attaches to the surface, to prevent further increases in drag, the ship hull needs to be cleaned.⁹ Bringing the vessel into harbor and out of the water for cleaning and further painting applications as the fouling would commonly damage that as well also drives up the associated costs of biofouling in this industry.¹⁰

Traditionally, the shipping and coatings industries have prevented fouling through the use of heavy metal containing paints.¹¹ The most prevalent compound found in these paints were triorganotin compounds, most commonly tributyltin. These coatings were

very effective at minimizing ship hull fouling by preventing the recruitment and growth of organisms on the surface, however, these compounds were toxic and had high instances of bioaccumulation in the organisms and surrounding environments of these areas.¹² The toxicity of the triorganotin compounds eventually led to a ban being placed on them by the International Maritime Organization.¹³

Because many heavy metal containing paints have displayed harmful consequences on the environment, there has been an immense effort towards creating new technologies for anti-biofouling coatings that have little to no negative environmental impact while maintaining the desirable properties of previous coatings.¹⁴⁻¹⁵ Polymers have thus been at the forefront for the development of novel coatings for this industry for the past 15 years.¹⁶⁻¹⁷ Polymeric coatings designed as anti-biofouling coatings focus on various factors to deter or inhibit the fouling of marine organisms on the surface, including topology, surface energy, chemical composition and active deterrents, among others.¹⁸⁻²¹ Siloxanes, PEGylated polymers, fluoropolymers, charged polymers such as zwitterionic polymers and polyurethanes have all been investigated as potential anti-fouling coatings, each because of the unique properties that yield to the surface of the coating, as well as the bulk of the coatings for some of the polymers.²²⁻²⁶ Siloxanes, specifically poly(dimethylsiloxane) (PDMS), is used extensively as an anti-fouling coating because this class of polymers has low surface energy, inertness, stability and pliability.²⁷ The low surface energy is the key component of the anti-fouling properties of siloxanes as it encourages bond fracturing at the surface of the coating.²⁸ PEGylated polymers are effective as anti-fouling coatings because they resist non-specific protein adsorption, and

are also commonly used in combination with hydrophobic components to create amphiphilic network.^{23, 29} Fluoropolymers exhibit low surface energy surfaces and low wettability, and also have a unique chemical stability which leads to an organization of the surface that is able to deter fouling.²⁵ Lastly, zwitterionic polymers function as anti-fouling coatings through a similar mechanism to hydrophilic polymers.²⁴ The zwitterionic polymers have a tightly bound hydration layer on their surface, forming a physical and energetic barrier to prevent fouling of organisms on a surface.³⁰ It has also been observed that the hydrogen bonding of water to zwitterions is much stronger than hydrophilic materials, in general.³¹

While single component systems initially received much interest in the realm of anti-fouling coatings, combinations of the chemical constituents to create more complex systems have been tested as replacement to commercial anti-fouling coatings.³²⁻³⁵ Two constituent systems have a distinct advantage over single constituent systems, in that the multi-constituent system blends two distinctive materials' properties to enhance the overall anti-fouling properties as a whole.³³ Commonly, the materials' properties are blended to create an amphiphilic surface.³⁶⁻³⁷ One example of this research demonstrated that an amphiphilic system was able to deter fouling from both hydrophilic and hydrophobic proteins, while the hydrophilic and hydrophobic surfaces, respectively, could only inhibit settlement of one protein.²⁰ Other examples using other variations of amphiphilic surfaces have displayed similar properties and increased anti-fouling properties against a variety of proteins and marine organisms.³⁸⁻³⁹

Our laboratory has long focused on the development of amphiphilic systems based on two constituent networks.⁴⁰ Our systems differ through the use of a unique fluoropolymer, that of a hyperbranched fluoropolymer (HBFP), which is unique in its macromolecular architecture and multiple functional handles presented in the polymeric structure.^{17, 32, 41-42} While previous generations of HBFP have been hydrophobic, these unique functionalities presented allow it to crosslink with incompatible components, namely hydrophilic polymers such as PEG.⁴⁰ Through the thermodynamically driven phase segregation of the materials followed by kinetic trapping, an amphiphilic surface can be generated which displays unique topography and chemical heterogeneities on both the nanoscopic and microscopic domains.⁴¹ This facet of the coatings is important as many proteins secreted by marine organisms are in the domain of nanometers, and it is hypothesized that the nanoscopic roughness of the surface will deter the preferential settlement of the proteins. HBFP-PEG system have displayed improved anti-fouling properties, including the complete deterrence of select marine organisms.³²

This dissertation focuses on the expansion of the current HBFP-PEG systems through the use of a third component, PDMS. The addition of the PDMS was to incorporate additional heterogeneity into the crosslinked network, while also possibly improving the mechanical properties of the system due to the elastomeric properties of PDMS. With a novel system in place, careful attention was placed on how to develop a more applicable coatings methodology to apply these systems on a larger scale, with emphasis placed on the resultant anti-fouling and fouling release capabilities. The idea of the ternary system was then developed in another direction to determine if the same amount of complexity

can afford coatings which incorporate different functionalities while still maintaining the effective properties of the three individual components.

In Chapter 2, a terpolymer network was generated consisting of three components, the amphiphilic HBFP, the hydrophilic PEG and the hydrophobic PDMS. A series of coatings were made varying in weight percentages of both PEG and PDMS, with respect to HBFP, and displayed unique surface characteristics. AFM and static water contact angle experiments of the films in both a wet and dry state displayed surface reorganization events upon exposure to water. As seen in the static water contact angle measurements, the coatings displayed three responses after water immersion, a normal wetting behavior and films becoming more hydrophilic upon exposure to water, a contraphilic effect with the films becoming more hydrophobic upon water exposure and some films displayed no change after exposure. One film was studied in depth using AFM and surface force spectroscopy (SFS) and was determined to have complex surface topographies which correlated with differences in the chemical composition at the surface which arose due to molecular interactions, phase segregation and compositional gradients between the three components. X-ray photoelectron spectroscopy and ATR-IR spectroscopy were also used to qualitatively probe the surface features and showed good correlation with the SFS data, indicating a surface, which upon wetting, displayed all three chemical components and predominant amounts of PDMS. The thermal and mechanical properties were then measured in relevant environments and exhibited properties that are similar to coatings which are being used commercially. Lastly, anti-biofouling properties of the film were assessed using a non-specific protein adsorption

study with bovine serum albumin, and the terpolymer films were shown to display 60% greater resistance to protein adsorption, indicating a coatings technology which could be explored in more elaborate anti-biofouling assays.

In Chapter 3, a method a rapidly applying the terpolymer coatings to relevant substrates was explored. This methodology would optimally allow for the terpolymer networks and future coatings based off of HBFP to be adhered to a surface without delamination. The first portion of this work was devoted to finding a suitable barrier coating onto which the terpolymer network would be applied. An epoxy barrier coating, Interseal 640®, was chosen because its epoxide functionalities could be exploited using covalent linkages to adhere the terpolymer coating. The networks were then spray coated onto the epoxy barrier coating and tested for loss of surface properties through immersion of the coatings in synthetic seawater for 90 days. Examination of the coatings throughout the study indicated no loss of surface properties as measured through static water contact angle experiments and IR spectroscopy, which was in stark contrast to a bare epoxy coating which displayed increasing hydrophilic properties after 90 days of water immersion. Toxicity studies of the leachates from the terpolymer network were also performed to test if the system was non-toxic. These studies, performed against RAW 264.7 cells, showed 100% cell viability indicating non-toxic properties in a general, non-inclusive model. Confocal microscopy was used to determine the thickness of the terpolymer coating on the epoxy barrier coating and was found to range from $330 \pm 20 \mu\text{m}$ to $380 \pm 20 \mu\text{m}$. Anti-biofouling studies were then performed with three formulation of the terpolymer coatings with 75 wt % PEG and 25,

50 and 75 wt % PDMS with respect to HBFP, respectively, against two species of barnacle cyprids, *Balanus amphitrite* and *Balanus improvisus*. Results from these studies demonstrated that the overall deterrence of fouling increased with increasing amounts of PDMS in the system, and the fouling release properties also increased as a function of the inclusion of PDMS.

In Chapter 4, the terpolymer coatings used in the anti-biofouling assays from Chapter 3 were explored in greater detail in regards to the anti-fouling and fouling release properties they displayed. The coatings were tested using long-term static immersion testing in three sites in the United States, Port Canaveral, Florida, Morro Bay, California and Pearl Harbor, Hawaii. In general, the coatings displayed variable performance dependent on the testing site, however, the coatings with 75 wt % PEG & 50 wt % PDMS and 75 wt % PEG & 75 wt % PDMS were determined to be the best performers of the three in regards to their anti-fouling properties. An increase in the fouling release properties of the terpolymer coatings was also seen with increasing amounts of hydrophobicity in the system. After three months of testing in Port Canaveral, Florida, all coatings were completely fouled, with the only difference being the predominant foulers on each surface. In Morro Bay, California, the coatings fared well initially, with fouling ratings ranging from 74 to 84 after the first month of testing, outperforming the fouling rating of 69 from Intersleek 900, a commercial anti-fouling paint. The coatings after three months in this location displayed variable fouling ratings, but the best performing terpolymer network with 75 wt % PEG and 50 wt % PDMS displayed a fouling rating to Intersleek 900 (62 vs. 67). The results from Pearl Harbor, Hawaii

displayed the most promising results of the study, with less than 20% fouling after two months of submersion in the drydock location. The overall variability in performance depending on location suggests a change in the surface composition and topography after long-term water immersion or post-fouling events in response to different conditions which need to be investigated further in future studies to determine how the surface is changing in regards to its topography and chemical composition in response to these events.

In Chapter 5, the concept of the ternary system was expanded through the creation of a new system comprised of an amphiphilic, fluorinated small molecule, a hydrophobic silsesquioxane and a sulfobetaine zwitterion. The films were prepared using thio-ene click chemistry using the thiol functional handles of the silsesquioxane with the alkene functionalities of the fluorinated small molecule and sulfobetaine zwitterion, respectively. Four coatings were generated from these components varying in the stoichiometric ratios of both the fluorinated and zwitterionic components, with attention being placed on keeping the amount of the bis-functional fluorinated molecule above a certain threshold to generate a robust crosslinked network. The surface features were investigated with static water contact angle and ATR-IR spectroscopy pre- and post-water immersion in synthetic seawater. Through these studies, it was seen that increasing amounts of zwitterions in the system decrease the static water contact angle of the films as there is a greater incorporation of water due to the electrostatic interactions between the sulfobetaine and water. AFM and SFS were then used to determine the surface properties of the systems and films with no sulfobetaine displayed aggregates on

the surface. Films with sulfobetaine showed a consistent topography regardless of the amount of this component in the system. SFS measurements displayed compressive module values ranging from 50 MPa to 90 MPa, with the moduli decreasing with increasing amounts of zwitterionic character in the system. Lastly, an anti-fouling assay was performed with *Ulva* zoospores against a range of standards. This study displayed that all coatings exhibited superior performance to the standards, and that between the four coatings, there was an increase in the deterrence of *Ulva* with an increasing amount of sulfobetaine in the system, indicating a possible greater surface hydration layer present in those films.

CHAPTER II

**HYPERBRANCHED FLUOROPOLYMER-POLYDIMETHYLSILOXANE-
POLY(ETHYLENE GLYCOL) CROSSLINKED TERPOLYMER NETWORKS
DESIGNED FOR MARINE AND BIOMEDICAL APPLICATIONS:
HETEROGENEOUS NON-TOXIC ANTI-BIOFOULING SURFACES***

2.1 Introduction

Biofouling plagues a wide spectrum of applications, from medical devices to maritime vessels.⁴³ For the latter, biofouling increases the fuel consumption of the vessel, in-turn leading to increased operational and maintenance costs.^{7, 43-44} The conventional method of fouling prevention has been achieved through the use of toxic paints and coatings that release biocides, such as cuprous oxide and tributyltin; however, due to the negative effects that these chemicals have on the environment, the use of these systems is in decline.^{12, 45} Various combinations of polymeric materials are currently being investigated for their use as non-toxic anti-biofouling coatings, applying strategies such as hydrophobicity, hydrophilicity, surface complexity and surface energy minimization.^{14, 17, 25, 29, 34, 37-38, 45-51}

Fluoropolymers, siloxanes and poly(ethylene glycol) (PEG) have been researched extensively as anti-biofouling agents, due to their unique chemical and physical

* "Reprinted with permission from "Hyperbranched Fluoropolymer-Polydimethylsiloxane-Poly(ethylene glycol) Crosslinked Terpolymer Networks Designed for Marine and Biomedical Applications: Heterogeneous non-toxic anti-biofouling surfaces" by Kevin A. Pollack, Philip M. Imbesi, Jeffery E. Raymond, Karen L. Wooley. *ACS Advanced Materials & Interfaces*, DOI: 10.1021/am505296n. Copyright 2014 American Chemical Society."

properties.^{34, 37, 40, 45, 49-53} Fluoropolymers typically possess low surface energy, low wettability and chemical stability.⁵⁴ In marine applications, these properties can be exploited to create coatings with increased anti-biofouling performance.^{17, 29, 33, 55-57} Siloxanes, specifically poly(dimethylsiloxane) (PDMS), have shown anti-biofouling characteristics, which are attributed to their low surface energy, in addition to exhibiting inertness, stability, and pliability.^{43, 58} Commercially, PDMS coatings are marketed as non-toxic marine coatings that are capable of rejection and release of biofouling agents under suitable hydrodynamic conditions.^{52, 58} Poly(ethylene glycol) (PEG), or poly(ethylene oxide) (PEO), has been used extensively in the field of marine applications, as well as in the field of biomedical engineering, because of its ability to generate surfaces that resist non-specific protein adsorption.⁵⁹ Previously, combinations of these three chemical constituencies have been utilized in amphiphilic surfaces to generate an enhanced degree of anti-biofouling.³⁷ However, the chemistries involved the incorporation of linear PDMS backbones, with chemical variation achieved *via* side group modification, where significance was placed on gaining amphiphilic character in the resultant coating. While this approach was demonstrated to be effective, we were interested in investigating topological differences of macromolecular components, their ability, in conjunction with chemical heterogeneity, to generate nano- and microscopically-complex surface topographies, and the influences of these parameters in the prevention of biofouling.

The combination of topological, topographical and chemical heterogeneity over a variety of scales drives the development of novel coatings for the prevention of

biofouling in our work. Previously, three generations of hyperbranched fluoropolymers (HBFP) were synthesized to determine the structure-property-function relationships between the fluoropolymer building blocks and ultimate network character.⁴⁰ Each generation of HBFP was developed to afford a polymer that, upon crosslinking with either hydrophilic or hydrophobic components, created an amphiphilic coating possessing chemical and surface heterogeneities on both the nano- and micrometer scales.^{32, 41} Related studies showed that the systems generated *via* crosslinking of HBFP or linear fluoropolymer with PEG moieties could be further modified by the choice of crosslinking reagent and oligomer decoration.³²

This current study involves the development of novel binary and ternary amphiphilic networks through crosslinking of combinations of HBFP, PEG and PDMS. The third generation of HBFP was chosen, due to its amphiphilic character, which enhances anti-biofouling performance while retaining the desired nanoscale surface heterogeneities.³² The advantage of using PDMS as an additional component are because of the anti-biofouling capabilities it displays, specifically, because it rejects fouling *via* a different mechanism when compared to fluoropolymers.²⁷ This complexity from a third component is hypothesized to increase the anti-biofouling performance when compared to the two component system of HBFP-PEG. Additionally, a terpolymer system was chosen over a system of HBFP-PDMS because of the loss of the hydrophilic PEG in that system, detracting from the potential amphiphilic properties of the resultant system. Crosslinking in this system occurred *via* a substitution reaction of the bromoacetyl and bromobenzyl groups of HBFP with the amine termini of both the linear PEG and PDMS

crosslinkers. Deposition of a solution of the three components, followed by a thermal cure, created a thin film that was then characterized using atomic force microscopy (AFM), contact angle experiments, surface force spectroscopy, X-ray photoelectron spectroscopy (XPS) and attenuated total reflectance-infrared spectroscopy (ATR-IR). Non-specific protein binding resistance was investigated and compared against a commercially available anti-biofouling PDMS standard. Thermal and mechanical responses were determined through differential scanning calorimetry (DSC), thermogravimetric analysis (TGA), dynamic mechanical analysis (DMA), and dynamic thermal mechanical analysis (DTMA), as prepared and/or under biologically-relevant conditions.

2.2 Experimental Section

Materials

Reagents and starting materials were purchased from Sigma Aldrich and used as received unless otherwise noted. 2,3,4,5,6-Pentafluorostyrene (PFS) was purchased from Apollo Scientific (UK) and filtered through a plug of neutral alumina prior to use. 2,4,6-tris(bromomethyl)mesitylene was purchased from Combi-Blocks. Bovine serum albumin (BSA) conjugated to Alexa Fluor 680 was purchased from Invitrogen. Sylgard[®] 184 (Dow Corning) was purchased from Ellsworth Adhesives and was prepared as instructed.

Nuclear Magnetic Resonance Spectroscopy and Mass Spectrometry

Briefly, monomers and polymers were characterized by ¹H, ¹³C and ¹⁹F nuclear magnetic resonance (NMR) spectroscopies using a Varian Inova 300 spectrometer.

^1H and ^{13}C NMR spectra were analyzed using the solvent signal as an internal reference and ^{19}F NMR spectra were analyzed with CF_3COOH as an external standard. High-resolution mass spectrometry (HRMS) for the monomers was conducted on an Applied Biosystems PE SCIEX QSTAR. Spectral data for the small molecules are reported elsewhere.³²

Infrared and X-ray Photoelectron Spectroscopy

IR spectra were obtained on a Shimadzu IR Prestige attenuated total reflectance Fourier-transform infrared spectrometer (ATR-IR). Spectra were analyzed using IRsolution software package (Shimadzu). X-ray photoelectron spectroscopy (XPS) measurements were taken with a Kratos Axis Ultra Imaging X-ray photoelectron spectrometer, using Mono Al anode, 12 kV voltage and 10 mA current.

Gel Permeation Chromatography

Gel permeation chromatography was performed on a Waters Chromatography, Inc. (Milford, MA), 1515 isocratic HPLC pump equipped with an inline degasser, a model PD2020 dual-angle (15° and 90°) light scattering detector (Precision Detectors, Inc.), a model 2414 differential refractometer (Waters, Inc.), and four PL_{gel} polystyrene-*co*-divinylbenzene gel columns (Polymer Laboratories, Inc.) connected in series: 5 μm Guard (50×7.5 mm), 5 μm Mixed C (300×7.5 mm), 5 μm 10^4 (300×7.5 mm), and 5 μm 500 Å (300×7.5 mm) using the Breeze (version 3.30, Waters, Inc.) software.

Elemental Analysis

Elemental analysis of the polymers was performed at Midwest Microlab, LLC

(Indianapolis, IN).

Thermal Analysis

Differential scanning calorimetric (DSC) studies were performed on a Mettler-Toledo DSC822^e (Mettler-Toledo, Inc., Columbus, OH), with a heating rate of 10 °C/min. The T_g was taken as the midpoint of the inflection tangent, upon the third heating scan. Thermogravimetric analysis was performed under Ar atmosphere using a Mettler-Toledo model TGA/DSC 1 Star^e system, with a heating rate of 10 °C/min. Measurements were analyzed using Mettler-Toledo Star software version 10.00d.

Atomic Force Microscopy and Surface Force Spectral Mapping

Atomic force microscopy was performed under ambient conditions in air. The AFM instrumentation consisted of a MFP-3D-BIO AFM (Asylum Research; Santa Barbara, CA) and standard silicon tips (type, OTESPA-70; L, 160 μm; normal spring constant, 50 N/m; resonance frequency, 246-282 kHz). Force spectroscopy mapping was performed *via* AFM measurements using a Bruker Multimode 8 system in PeakForceTM tapping mode. This imaging method also provides direct surface maps of modulus, dispersion, deformation and adhesion.⁶⁰ In brief, the PeakForceTM QNMTM imaging mode uses a modified Hertzian model, the DMT model, to directly extract a reduced Young's modulus (E_r).³³ The DMT model takes into account surface-tip interactions neglected in the Hertz model and also allows for mapping of adhesion force, deformation and dissipation energy. This method is described elsewhere in detail.³²

In these measurements, a ScanAsyst-Air (Bruker) with manufacturer specification

for a spring constant of $k = 0.4$ was used. For this study, no formal calibration was performed as the relative values for purposes of chemical identification were sought. Arbitrary values for tip size and the Poisson ratio were used. Thermal tuning of the cantilever gave a resonant frequency of 93 kHz. However, as PeakForce™ imaging uses the cantilever in an off-resonance mode of 2 kHz, this finding is not critical to the qualitative value of the imaging.

Mechanical Analysis

A Mettler Toledo TT-DMA system was used for all dynamic mechanical and dynamic thermal mechanical analysis (DMA/DTMA) studies. Submersion studies were performed in Hyclone (Thermo) calcium/magnesium free phosphate buffered saline solution (1X, PBS) for simulation of an *in-vivo* environment. Submersion studies were performed in synthetic sea water (Ricca Chemicals, cat. no. 8363-5, ASTM D 1141-substitute ocean water) for simulation of a marine environment. All measurements were taken in compression with a dynamic force of 0.1 N.

Static Surface Contact Angle

Contact angles were measured as static contact angles using the sessile drop technique with an Attension Theta optical tensiometer (Biolin Scientific).⁶⁰ Drops were fitted with a Young-Laplace formula to calculate the static contact angle in the Theta software (Biolin Scientific).

Confocal Microscopy and Protein Adhesion Assay

Bovine serum albumin conjugated to AlexaFluor-680 (BSA) was dissolved in phosphate buffered saline (PBS) solution (pH 7.1) to a concentration of 0.1 mg/mL

and stored in the dark. Sylgard[®] 184 was used as a standard to test against the terpolymer film. The surface of the terpolymer network and Sylgard[®] 184 were incubated in fresh PBS buffer for 10 min and dried *via* filtered nitrogen gas. The surfaces were then exposed to Alexa-Fluor-680 conjugate in PBS at 0.1 mg mL⁻¹ for 45 min in a dark chamber. After exposure, the surfaces were washed with 5 mL of PBS buffer and dried *via* filtered nitrogen gas for 1 h. Z-stacked confocal fluorescence images were taken of the BSA exposed surfaces and were discussed in terms of resultant intensity histograms. The imaging platform was a full spectral Olympus FV-1000 laser scanning confocal microscope operating with a 635 nm diode laser and fluorescence collection selected by a wide band monochromator from 650 to 750 nm.

Synthesis of Hyperbranched Fluoropolymers

To a 250 mL Schlenk flask equipped with a stir bar was added **2** (9.00 g, 19.6 mmol), pentafluorostyrene (PFS) (11.4 g, 58.8 mmol), pentamethyldiethylenetriamine (PMDETA) (8.18 mL, 39.2 mmol), CuBr (2.81 g, 10.9 mmol) and anisole (105 mL). The solution was deoxygenated *via* freeze-pump-thaw (×3), the vessel was backfilled with N₂ and then lowered into an oil bath set at 65 °C and the reaction was allowed to proceed for 20 h. The polymerization was quenched by opening the flask to air and submerging the flask in liquid nitrogen. Once thawed, the contents were dissolved in dichloromethane (500 mL), eluted through a plug of alumina to remove the catalyst, concentrated *in vacuo*, and the product was isolated by precipitation into cold hexanes (3 × 1.5 L) to afford a white powder of **3** in 39% yield (7.80 g). IR =

2947, 2878, 2361, 1744, 1651, 1497, 1296, 956 and 864 cm^{-1} . ^1H NMR (CDCl_3 , ppm): δ 0.7-1.5 (br m, C- CH_3), 1.5-3.1 (br m, $\text{CH}_2\text{-CH(R)-}$ backbone), 3.4-4.0 (br m, R-O- $\text{CH}_2\text{-CH}_2\text{-OR}'$), 4.0-4.6 (br m, TFS-O- $\text{CH}_2\text{-CH}_2\text{-OR}$ and R- $\text{CH}_2\text{-CH}_2\text{-O(O)C-R}'$) ppm. ^{13}C -NMR (CDCl_3 , ppm): δ 24.7, 30.7-29.7, 32.1-41.7, 63.6, 68.8, 70.0-70.8, 74.3, 114.7, 122.2, 137.6, 140.7, 144.7, 176.6 ppm. ^{19}F NMR (CDCl_3 , ppm): δ -143 (br m, *o*-F (PFS) and *o*-F (TFS)), -157 (br m, *p*-F (PFS) and *m*-F (TFS)), -162 (br m, *m*-F (PFS)) ppm. The polymerization was repeated to give several batches of HBFP: **3a** $M_w^{\text{GPC}} = 17400$ Da, $M_n^{\text{GPC}} = 8600$ Da, $M_w/M_n = 1.72$. $T_g = 74$ °C. $T_{\text{decomp}}: 385$ °C, 73% mass loss @ 500 °C. **3b** $M_w^{\text{GPC}} = 20100$ Da, $M_n^{\text{GPC}} = 11200$ Da, $M_w/M_n = 1.79$. $T_{g,1} = 48$ °C. $T_{\text{decomp}}: 385$ °C, 67% mass loss @ 500 °C. Anal. calcd. for $\text{C}_{455}\text{H}_{259}\text{Br}_7\text{F}_{238}\text{O}_{35}$: C 48.8%; H, 2.33%; F 40.3%; Br 4.99%; found: C 42.04; H 3.00; F 25.02; Br <0.10%. **3c** $M_w^{\text{GPC}} = 19700$ Da, $M_n^{\text{GPC}} = 13000$ Da, $M_w/M_n = 1.46$. $T_g = 72$ °C. $T_{\text{decomp}}: 385$ °C, 78% mass loss @ 500 °C. Anal. calcd. for $\text{C}_{534}\text{H}_{276}\text{Br}_6\text{F}_{294}\text{O}_{30}$: C 49.3%; H 2.14%; F 42.3%; Br 3.69%; found: C 51.05; H 3.12; F 32.12; Br 0.159%. **3a** was used for the initial AFM imaging and contact angle study, **3b** was used for the AFM data compiled in **Table 1** and **3c** was used for all other studies presented.

Design of the Hyperbranched Fluoropolymer – Poly(ethylene Glycol) – Poly(dimethylsiloxane) Crosslinked Terpolymer Network (HBFP-PEG-PDMS) Two-dimensional Series

A series of HBFP-PEG-PDMS networks was prepared with a constant weight of HBFP (**3b**) and at varying wt % PEG (0-75 wt %, calculated with respect to the

weight of HBFP) and PDMS (25-75 wt %, calculated with respect to the weight of HBFP) to investigate how the relative stoichiometry of the crosslinkers affected surface topography and hydrophilicity.

General Procedure for the Preparation of HBFP-PEG-PDMS Crosslinked Terpolymer Networks

The following general procedure was followed for each sample, as defined here for the terpolymer network having 25 wt% of each PEG and PDMS. To a scintillation vial was added HBFP (100 mg), 1500 Da bis(3-aminopropyl)-terminated PEG (25 mg, 0.017 mmol, 25 wt %), 1500 Da bis(3-aminopropyl)-terminated PDMS (25 mg, 0.010 mmol, 25 wt %), THF (2 mL) and *N,N*-diisopropylethylamine (DIPEA) (0.05 mL, 0.3 mmol) and the mixture was stirred magnetically until homogeneous. The solution was drop cast (0.5 mL per slide) onto pre-cleaned, pre-cut 1 cm² glass microscope slides. A period of *ca.* 30 min allowed for the solvent to evaporate, which afforded a thick pre-gel that was cured at 110 °C for 45 min under N₂ atmosphere to afford the dry coatings. The crosslinked networks were then characterized prior to and after submersion in a nanopure water bath overnight. The thickness of the films were *ca.* 0.3 mm for the ATR-IR, static water contact angle and AFM studies and 1.0 mm for the mechanical analysis studies.

Preparation of PEG Films for ATR-IR and Surface Force Spectral Mapping

To a scintillation vial was added bis(3-aminopropyl)-terminated PEG (100 mg, 0.067 mmol), 2,4,6-tris(bromomethyl)mesitylene (18 mg, 0.045 mmol) and THF (1 mL) and stirred until homogeneous. To the solution was added DIPEA (0.12 mL, 0.69

mmol) and stirred for 30 min. The solution was drop cast onto pre-cleaned, pre-cut 1 cm² glass cover slips. A period of *ca.* 30 min allowed for the solvent to evaporate, which afforded a thick pre-gel that was cured at 110 °C for 45 min under N₂ atmosphere to afford the dry coatings.

Preparation of PDMS Films for ATR-IR and Surface Force Spectral Mapping

To a scintillation vial was added bis(3-aminopropyl) terminated PDMS (130 mg, 0.046 mmol), 2,4,6-tris(bromomethyl)mesitylene (12 mg, 0.030 mmol) and THF (1 mL) and stirred until homogeneous. To the solution was added DIPEA (0.09 mL, 0.52 mmol) and stirred for 30 min. The solution was drop cast onto pre-cleaned, pre-cut 1 cm² glass cover slips. A period of *ca.* 30 min allowed for the solvent to evaporate which afforded a thick pre-gel that was cured at 110 °C for 45 min under N₂ atmosphere to afford the dry coatings.

2.3 Results and Discussions

Synthesis

A series of three HBFP-PDMS binary networks and nine HBFP-PEG-PDMS terpolymer networks was synthesized with varying stoichiometries of the HBFP, PEG (0, 25, 50 and 75 wt%, relative to HBFP) and PDMS (25, 50 and 75 wt%, relative to HBFP) components, to probe the compositional effects on the physical, mechanical and biological properties of the crosslinked materials. This process began with the generation of HBFP. Initially, a precursor molecule, **1**, was prepared through a nucleophilic aromatic substitution of 2,3,4,5,6-pentafluorostyrene (PFS) with an excess of tri(ethylene glycol), followed by esterification of the remaining hydroxyl group by

reaction with 2-bromopropionyl bromide to afford the inimer **2** (Scheme 1). Copolymerization of **2** with PFS using CuBr and PMDETA to facilitate atom transfer radical self-condensing vinyl copolymerization was conducted repeatedly to generate batches of HBFP, **3a-c**.⁴² The three batches of HBFP were synthesized with only subtle differences in molecular weights, molecular weight distributions, and thermal properties (**Figure 2.1**).

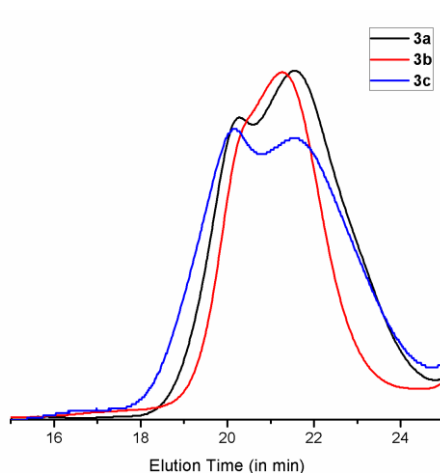


Figure 2.1. GPC curves of the three batches of HBFP, 3a-c.

Because the three samples of HBFP were of similar composition, structure and size, each was able to be taken forward individually to create the series of crosslinked bi/terpolymer networks with bis(3-aminopropyl)-terminated PEG and bis(3-aminopropyl)-terminated PDMS, while allowing for direct comparisons to be made regarding the effects of network composition. Significantly lower % Br contents *vs.* the

theoretical values were measured by elemental analysis, which is expected to be due to biradical coupling and/or elimination reactions during the copolymerization,⁶¹⁻⁶² and is being studied in further detail. Nonetheless, stable networks were established, presumably through a crosslinking between the bromoacetyl and bromobenzyl functional handles of the HBFP with the terminal amines of the PEG and PDMS. The networks were generated through deposition on the surface of a microscope slide through solvent casting followed by a thermal cure at 110 °C (**Figure 2.2**). Post-cure, the films were submerged in distilled water overnight to extract compounds not bound within the network and release the networks as free-standing, water-swollen films from the substrates.

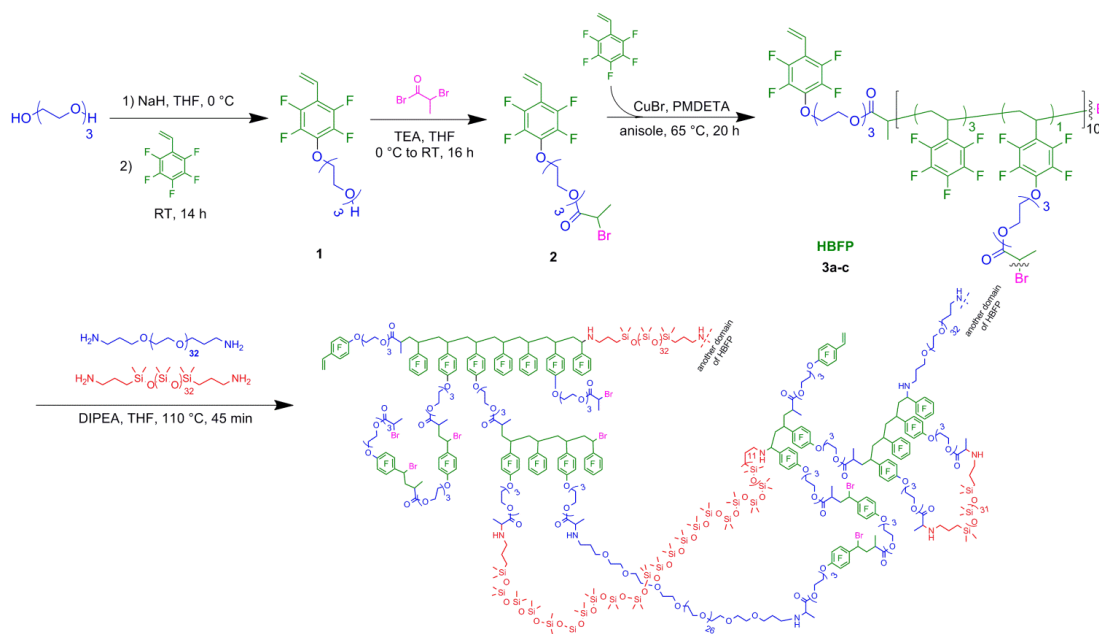


Figure 2.2. Synthesis of the crosslinked HBFP-PEG-PDMS terpolymer films.

Topography and Static Contact Angle

An initial study probed the terpolymer networks with variation of the HBFP-PEG-PDMS weight percent (wt%) ratios to determine the influence of each component on surface character (**Table 1**), as evaluated by AFM and contact angle measurements pre- and post-water immersion (**Table 2** and **Table 3**). In both the dry and wet AFM images, complex topography is seen on the submicrometer scale and surface rearrangement is observed upon water immersion (**Table 2** and **Table 3**). The dynamic reorganization of the surface chemistry during the water immersion was also probed through static water contact angle measurements. The contact angle data of the dry films show an overall decrease in the hydrophobicity of the surface with increasing amounts of PDMS, demonstrating that the HBFP fraction plays an integral role in the surface complexity of the system (**Figure 2.3**).

Table 1. Total weight percent of PDMS and PEG in the terpolymer coatings.

	0 wt % PEG	25 wt % PEG	50 wt % PEG	75 wt % PEG
25 wt % PDMS	20%	33%	43%	50%
50 wt % PDMS	33%	43%	50%	56%
75 wt % PDMS	43%	50%	56%	60%

Table 2. Tapping mode AFM images of the pre-swollen terpolymer networks with RMS roughness and contact angle. Field of view for dry AFM renderings is 50 nm² with a 1.0 nm z-scale.

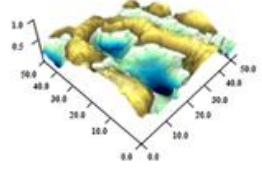
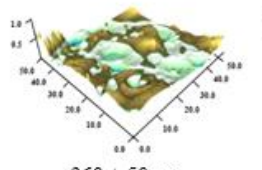
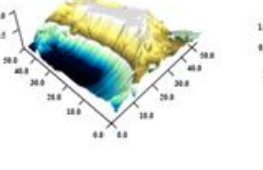
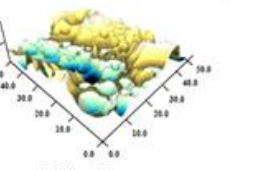
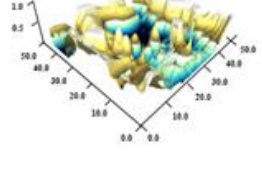
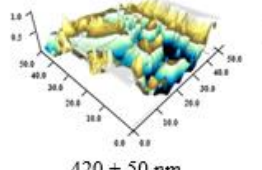
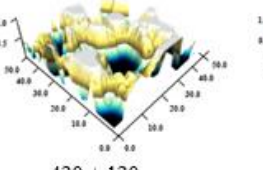
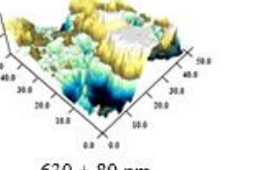
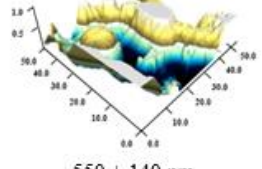
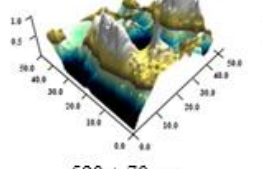
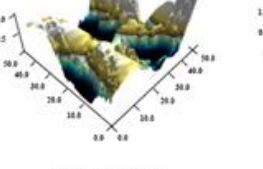
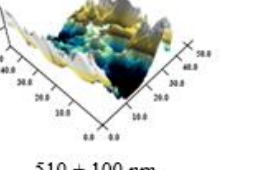
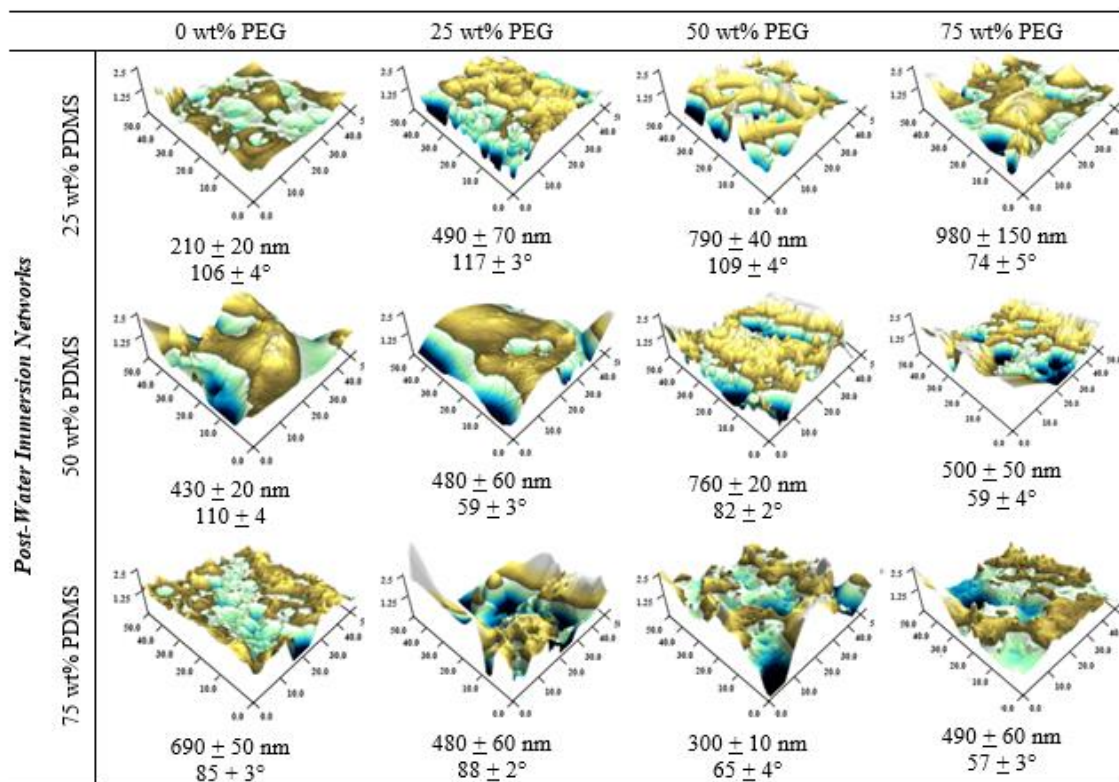
		0 wt% PEG	25 wt% PEG	50 wt% PEG	75 wt% PEG
Pre-Swell Networks	25 wt% PDMS	 210 ± 40 nm 102 ± 3°	 360 ± 50 nm 83 ± 2°	 660 ± 120 nm 106 ± 3°	 410 ± 90 nm 107 ± 3°
	50 wt% PDMS	 250 ± 20 nm 75 ± 3°	 420 ± 50 nm 81 ± 1°	 420 ± 120 nm 83 ± 2°	 630 ± 80 nm 78 ± 3°
	75 wt% PDMS	 550 ± 140 nm 65 ± 4°	 590 ± 70 nm 73 ± 2°	 500 ± 90 nm 76 ± 3°	 510 ± 100 nm 75 ± 2°

Table 3. Tapping mode AFM images of the terpolymer networks with RMS roughness and contact angle. Field of view for wet AFM renderings is 50 nm² with a 2.5 nm z-scale.



Upon water immersion, a general decrease in the contact angle is seen in films with 50 wt% PEG or greater, indicating dynamic surface reorganization occurring in these systems and that the PEG-rich regions are discrete enough for isolated regions of water uptake to occur (**Figure 2.4**).

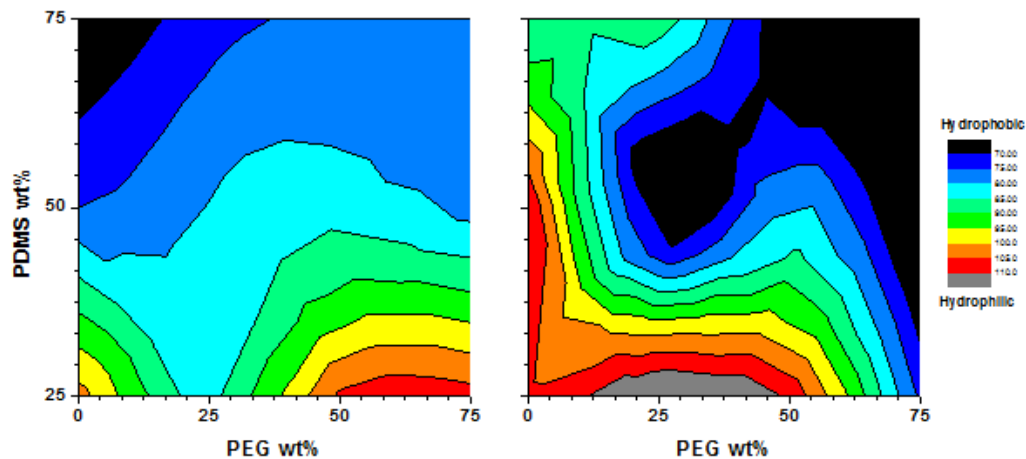


Figure 2.3. Contour graphs of static contact angle measurements of dry (left) and water saturated (right) films.

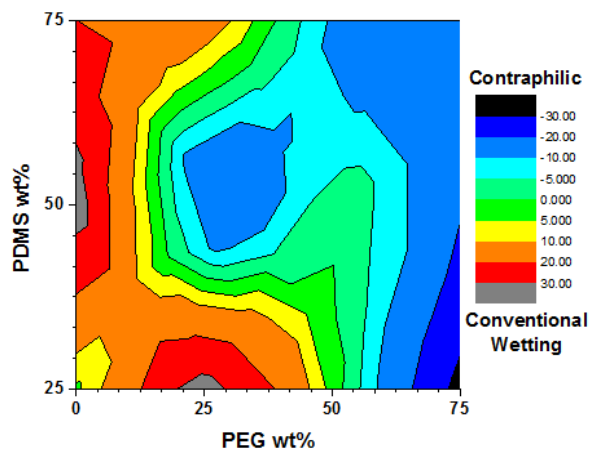


Figure 2.4. Contour graph of the differential static contact angle measurements between dry and water saturated films.

Upon wetting the surfaces having 0 or 25 wt% PEG, an opposite effect was observed, with increases in the static water contact angles. This behavior has been observed for

some amphiphilic materials that are capable of dynamic surface reorganization, where PEG-rich hydrophilic regions swell and promote an increase in the fluorocarbon hydrophobic content at the surface, ultimately, resulting in a contraphilic effect, as supported by previous work using secondary ion mass spectrometry (SIMS) and observed in other systems.^{32, 63}

Surface Compositional Heterogeneity

We next focused attention on the one sample composition that gave the most peculiar behavior. Given the generally high surface topographic roughnesses and trends of either increased or decreased water contact angle, for a minority (0 or 25 wt%) *vs.* majority (50 or 75 wt%) of PEG content relative to HBFP, respectively, the one sample that was unique was that having 50 wt% of each PEG and PDMS, relative to HBFP, which exhibited no change in water contact angle. In order to determine the contribution of the three constituencies to the surface character of the network, surface force spectroscopy (SFS) mapping was performed to differentiate between HBFP-, PDMS- and PEG-rich regions on the surface of the HBFP-PEG-PDMS terpolymer network with 50 wt% PEG and 50 wt% PDMS (**TP**). A particular focus was placed on the qualitative differences in surface response as a function of topography. The results of the SFS study are provided as AFM micrographs, spectral maps and 3D renderings in **Figure 2.5**. Surface topography reveals two sets of features, a raised “lattice” of interconnected regions and a lower region interstitial to the “lattice” with a 6.0 nm height differential between the two. However, topography alone reveals little in regards to the innate composition of the two regions and would, in a less complex system, imply a biphasic material.

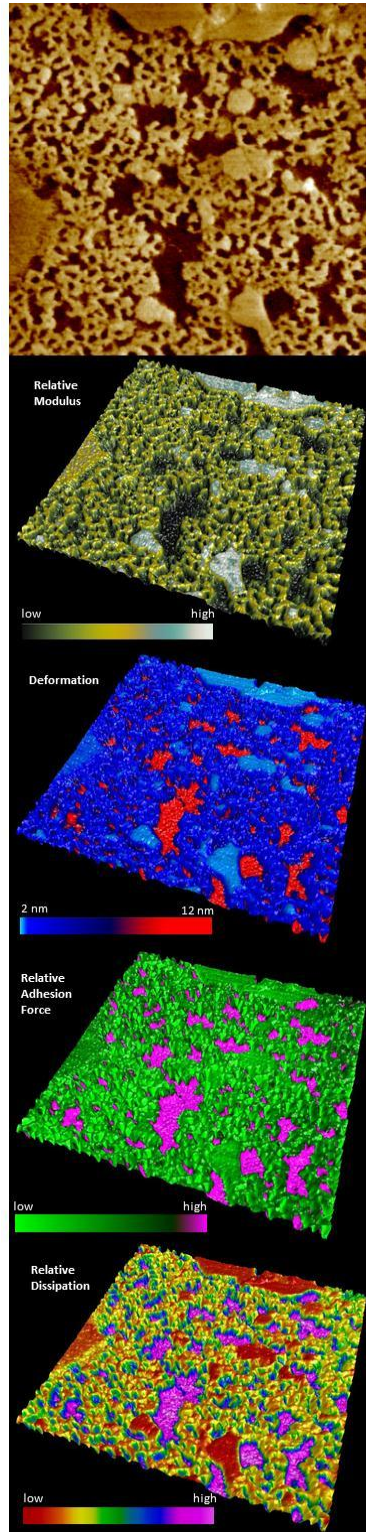


Figure 2.5. Topography and SFS Mapping of TP. Top: AFM micrograph, 4 mm² field of view. Below: Force spectra transposed on 3D renderings of the topography.

To further our understanding of the surface heterogeneity, SFS was used to determine the relative difference in surface character from feature to feature. Modulus mapping shows that the raised “lattice” is composed of two major variations in response, with islands of higher modulus material connected by lower modulus material. The deeper, interstitial material appears the softest. Deformation mapping at constant force provides an inverse relationship to that observed from modulus mapping, with the stiff island regions deforming 2 nm, the raised portions connecting the island regions deforming 4 nm and the soft, lowered interstitial regions deforming 10 nm at a constant tapping force. Adhesion force mapping provides similar phase information as what might be assumed from topography, while also suggesting that the height of the features may be directly related to the surface energy, where the raised regions are lower energy and the lower regions are rich in higher surface energy material. Dissipation mapping provides information about the energy lost to non-restorative forces after deformation, and correlates with deformation. From what is known about fluoropolymer, PDMS and PEG surfaces in general, the following assignments are made:

1. HBFP-rich regions: Raised islands with high modulus, low deformation, low surface energy and low dissipation.
2. PDMS-rich regions: Raised “lattice” regions between islands with moderate modulus, moderate deformation, low surface energy and moderate dissipation.
3. PEG-rich regions: Deeper interstitial regions with low modulus, high deformation, high surface energy and high dissipation.

In addition to the study performed on **TP**, two additional compositions of films were also analyzed using SFS. The three films were tested to determine the difference in their nanomechanical properties at the surface, specifically the Young's moduli of these films. The two additional films chosen were 1) a film that displayed a contraphilic behavior upon wetting, 25 wt% PEG and 25 wt% PDMS, and 2) a film that displayed a normal wetting response, 75 wt% PEG and 75 wt% PDMS. The findings of this study are summarized in **Table 4**. The Young's moduli found at the surfaces were 6.91 MPa, 9.52 MPa and 11.4 MPa for the 25 wt% PEG and 25 wt% PDMS film, 50 wt% PEG and 50 wt% PDMS film and 75 wt% PEG and 75 wt% PDMS film, respectively.

Table 4. Summary of surface force spectroscopy data.

HBFP-PEG-PDMS	Height R_q [nm]	Height R_a [nm]	Modulus Mean [MPa]	Modulus R_q [MPa]	Modulus R_a [MPa]
4:1:1	58.2	42.8	6.91	6.28	3.94
4:2:2	78.5	67.1	9.52	15.2	11.7
4:3:2	27.5	23.4	11.4	48.1	12.5

Surface Spectroscopy

To further support the results of the SFS findings, attenuated total reflectance-infrared spectroscopy (ATR-IR) and X-ray photoelectron spectroscopy (XPS) were used to investigate the surface composition of **TP**. ATR-IR provides IR spectra for the first hundreds of nanometers of the sample network surface, making it a viable method for tracking chemical changes in a polymeric surface.⁶⁴ Assessment of the surface of **TP** pre- and post- water exposure was performed. The assessment was also done for a

PDMS and PEG film and pure HBFP powder. These results are provided in **Figure 2.1**. It can be seen that both the PEG and HBFP samples express water signals almost exclusively after swelling. These results are reasonable, as both the PEG coating and the raw HBFP possess glycol domains, which readily uptake water when other constraints do not exist. The PDMS surface displayed only a small water signature, which is also reasonable. Considering the effects on the surface chemistry of the terpolymer system after wetting, several changes become immediately apparent. From comparison to the PEG surface, it can be seen that the PEG contribution to the 974 cm^{-1} and 1460 cm^{-1} signals are greatly diminished after wetting the terpolymer surface. There is also a possibility of diminished PEG in the final system as a result of not fully crosslinking with HBFP. This possible outcome will be analyzed further in the future by characterizing the media in which the film was submerged. It can also be observed that the HBFP signals at 1497 cm^{-1} and 1734 cm^{-1} are expressly present in the terpolymer surface after wetting. Neither of these findings is unique to this system as other HBFP-PEG networks have shown similar behaviors.³² The uniqueness of this system is in the gross expression of PDMS character after wetting, where the 1010 cm^{-1} , 1080 cm^{-1} and 1258 cm^{-1} PDMS peaks dominate the spectra, thus, making the overall spectra for the terpolymer surface after wetting most closely mimic the PDMS surface spectral signature. The dominance of the PDMS signature is an important result, as it implies that HBFP, in the presence of mobile PDMS after water incubation, does not dominate the surface as in other HBFP-PEG systems.

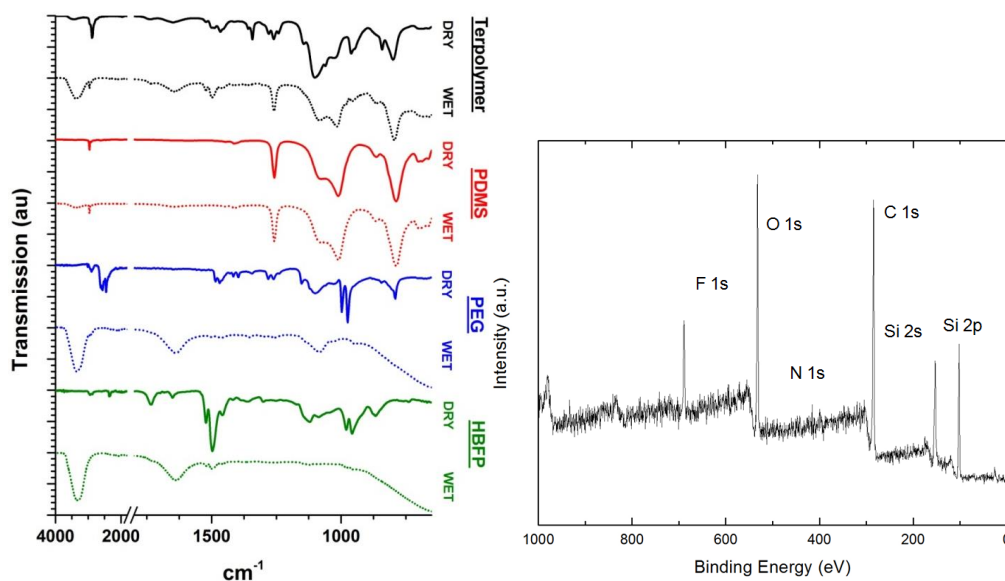


Figure 2.6. ATR-IR and XPS spectra for TP.

While not necessarily applicable to all the terpolymer systems, this result presents an entirely new method for controlling surface reorganization in these amphiphilic heterogeneous systems via variations in the hydrophilic and hydrophobic components of the HBFP-PEG-PDMS system, opening a full range of surface controls previously unrealized. XPS results clarify that the surface initially possessed all three functionalities in sufficient quantities to have comparable spectral signatures (**Figure 2.6**).

Thermal Response

TP was investigated by thermogravimetric analysis to determine how crosslinking influences the thermal stability of the network (**Figure 2.7**). From ambient temperature to 250 °C, 5 percent mass loss is seen in the network, consistent with a partial degradation of PDMS. There are then two degradation events that can be seen in the

network, the first occurring from 250 °C to *ca.* 350 °C corresponding to a continued degradation of PDMS, and then from 350 °C to 500 °C resulting in an 80 percent mass loss of the sample in total, corresponding to the decomposition of HBFP and PEG. It can be seen through this study that the crosslinks in the system do not infer any additional thermal benefit to the network, but overall, this finding should not detract from the intended uses for this material, under temperatures that vary from -2 °C to 33 °C and 36 °C to 38 °C for the marine environment and biomedical uses, respectively.

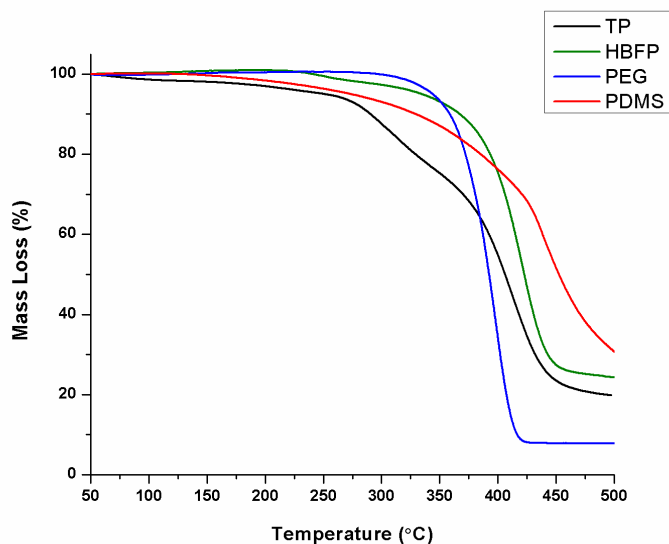


Figure 2.7. TGA traces of TP and each of the homopolymer components.

Differential scanning calorimetry was used to probe the phase transitions present in the terpolymer network (**Figure 2.8**). Upon heating, a melting transition can first be seen at

33 °C, which can be attributed to the PEG in the network, followed by a T_g at 63 °C, attributed to HBFP.

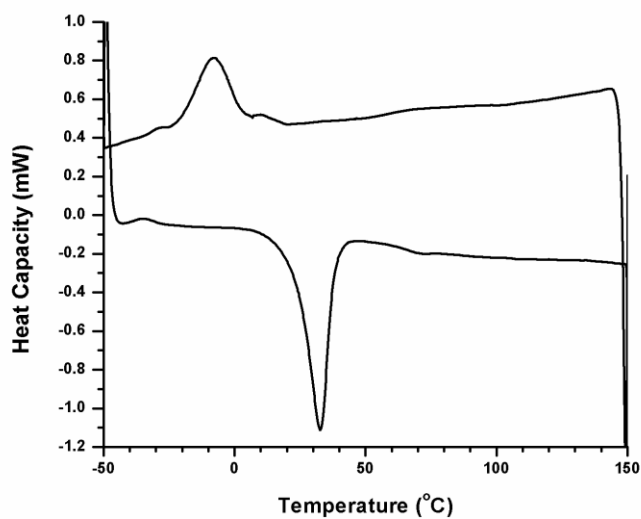


Figure 2.8. DSC traces of TP on heating (lower) and cooling (upper).

Mechanical Response

Response under atmospheric conditions. The mechanical properties of **TP** were investigated with a combination of dynamic mechanical analysis (DMA), dynamic thermal mechanical analysis (DTMA) and static stress-strain analysis. Initial investigation of **TP** by DTMA at 1 Hz (**Figure 2.9**) showed two phase transitions *via* $\tan \delta$ peaks at 89 (A1) and 129 °C (A2).

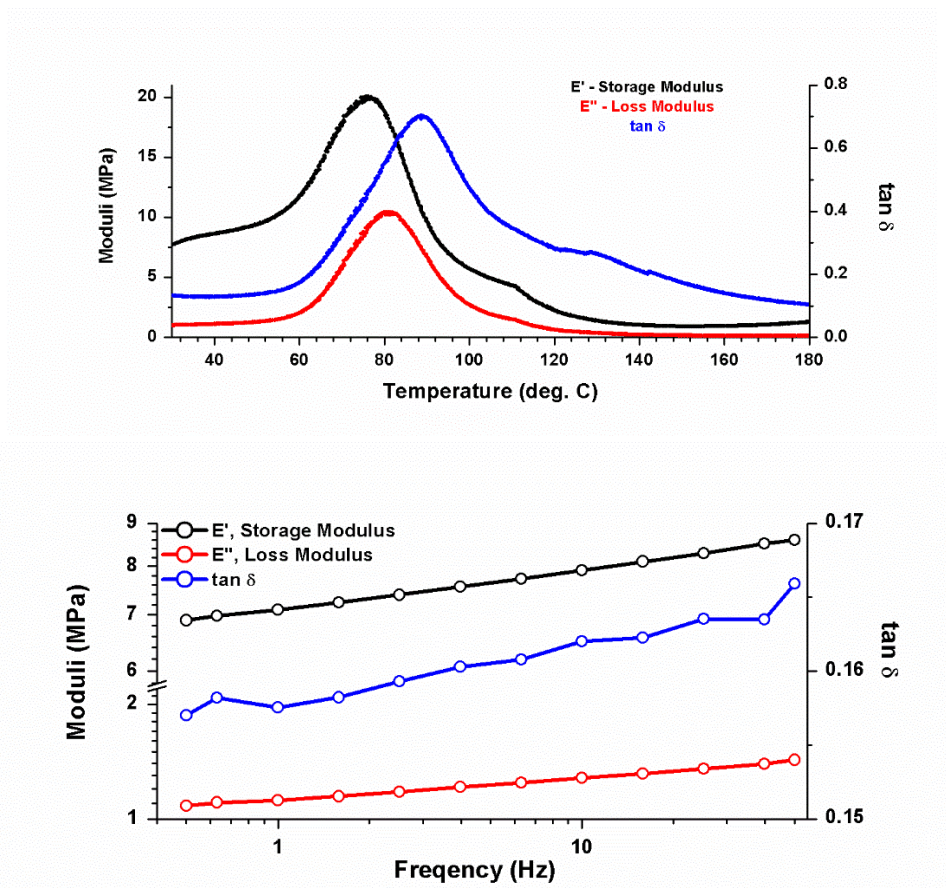


Figure 2.9. DTMA and DMA of TP in air. Top: temperature ramp DTMA. Bottom: frequency ramp DMA at RT.

Room temperature (A0) storage modulus (E') was found to be 7.1 MPa with a loss modulus (E'') of 1.1 MPa. A quasi-steady state character was reached near 150 °C (A3), resulting in post-phase transition values of 0.92 and 0.16 MPa for E' and E'' . A frequency sweep at room temperature displayed frequency dependence typical of an amorphous material without significant phase separations or low temperature phase transitions. A summary of DMA and DTMA data can be found in **Table 5**. Static stress-strain measurements resulted in a characteristic Young's modulus of 37 ± 1 MPa

for deformations of less than 1%.

Response in a marine environment. In order to assess the response in a marine setting, one of the target application environments for these materials, **TP** was assessed by DTMA in synthetic sea water. The temperature was decreased from 20 (M0) to 0 °C over a 2.5 h period and allowed to equilibrate (M2). The mechanical response of the system over this period is summarized in **Table 4**, including the $E'/E''/\tan \delta$ inflection point (M1) observed at 10 °C and the equilibration time constant after reaching 0 °C. Results of this portion of the mechanical assessment are presented in **Figure 2.10** with a plot of the change in E'/E'' per degree change in temperature, as a function of temperature, to display that at temperatures below 15 °C the effect of temperature on stiffness decreases linearly. The ultimate character of **TP** at 0 °C was a 25% increase in stiffness over initial submersion response and was 50% more resistant to deformation when compared to the ambient condition response in air.

Table 5. Summary of DMA/DTMA with kinetics

	Temp. [°C]	solvent	E' [MPa]	E'' [MPa]	tan δ	time [h]	τ [h]	notes
A0	25	atmosphere	7.1	1.1	0.158	0	-	initial
A1	89	atmosphere	10.6	7.5	0.703	1.1	-	tan δ peak
A2	129	atmosphere	1.5	0.39	0.270	1.8	-	tan δ peak
A3	150	atmosphere	0.92	0.16	0.173	2.1	-	high T ss
M0	20	sea water	10.4	1.6	0.159	0	-	initial
M1	10	sea water	12.5	2.2	0.178	0.3	-	-
M2	0	sea water	12.8	2.5	0.193	2	0.07±0.01	ss
B0	37	PBS	28.0	4.6	0.164	0	-	initial
B1	37	PBS	13.1	1.9	0.104	0.1	0.03 ±0.01	solvation 1
B2	37	PBS	9.8	1.5	0.151	0.4	0.12 ±0.01	solvation 2
B3	37	PBS	12.5	2.0	0.161	1.7	0.32 ±0.04	swell
B4	37	PBS	11.7	2.1	0.180	5	0.61 ±0.09	ss

Response at physiological conditions. This system also has potential application as a coating on biomedical devices, where a decreased likelihood of biomacromolecule or whole cell adhesion is sought. Therefore assessment of the mechanical response of the **TP** was performed at conditions that simulate a physiological environment. DMA was performed upon submersion in a pH 7.4 PBS solution at 37 °C (B0), with *in-situ* monitoring to observe solvent uptake (B1 & B2), swelling (B3) and the steady state (B4) response of the film after reaching solvent equilibrium (**Figure 2.11**). Two (relatively) fast phases of initial solvent uptake are observed with transition lifetimes of 0.03 and 0.12 h, and are assigned to rapid association of the buffer solution with the PEG domains and the hydrophilic regions of the amphiphilic HBFP domains, respectively. These

processes resulted in a decrease in E' of 65%. After initial solvent intercalation into the matrix, a swell period of 1.3 h with a transformation lifetime of 0.32 h occurred before beginning an equilibration process resulting in storage and loss moduli of 12.5 MPa and 2.0 MPa, respectively.

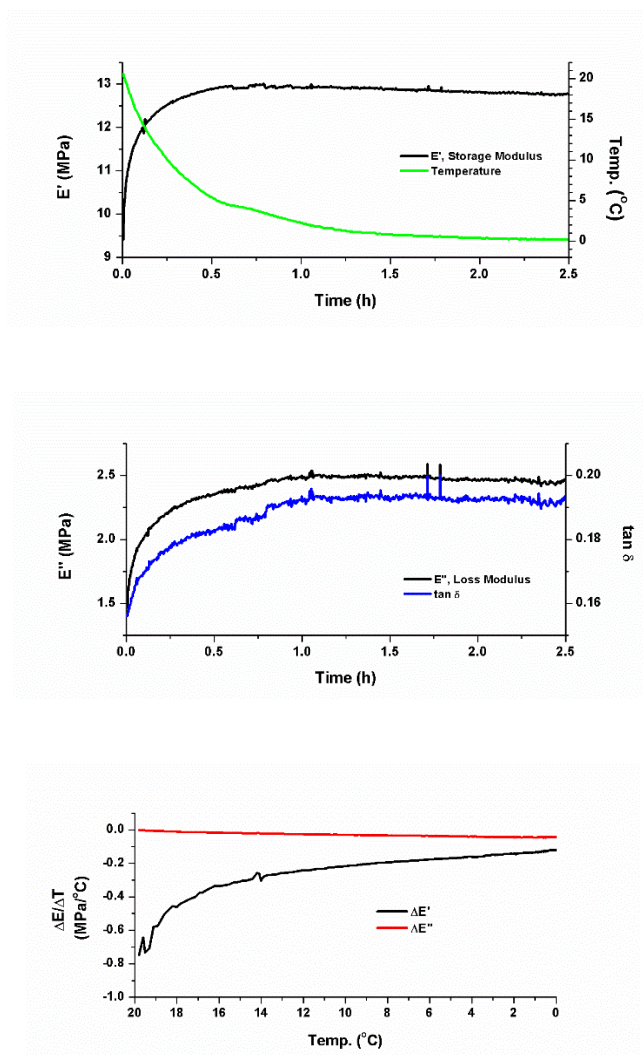


Figure 2.10. Submersion DTMA from 20 to 0 °C in synthetic sea water. Top: storage modulus and temperature v. time. Middle: loss modulus and $\tan \delta$ v. time. Bottom: total change in modulus per unit change in temperature v. temperature.

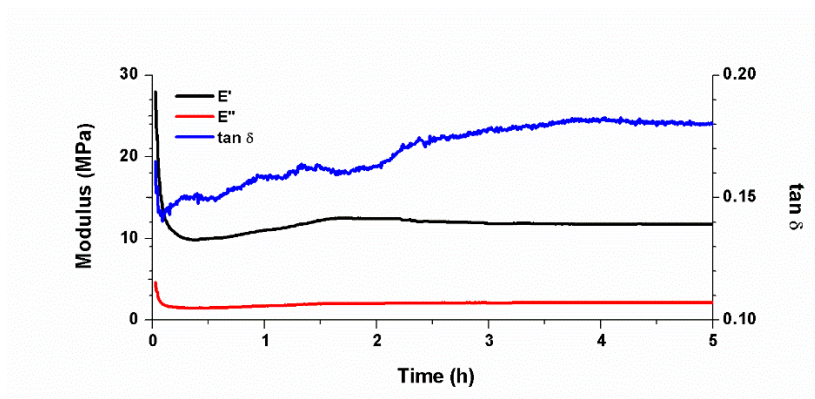


Figure 2.11. Submersion DMA at 37 °C in PBS.

Non-specific Protein Resistance

In an attempt to assess the resistance of the terpolymer network to non-specific protein binding, an assay was performed using bovine serum albumin (BSA) coupled to Alexa Fluor-680. Both **TP** and a PDMS standard (Sylgard[®] 184) were evaluated after 45 min of incubation with a 0.1 mg/mL BSA in PBS buffer *via* confocal fluorescence microscopy. Comparison of the 650 nm to 750 nm emission histograms of the two surfaces after 635 nm excitation can be found in **Figure 2.12**, along with the integrated z-stack images. The change in relative intensities, with identical excitation and collection regimes, shows **TP**'s surface to be *ca.* 60% less susceptible to BSA adsorption than the standard Sylgard[®] 184 PDMS surface.

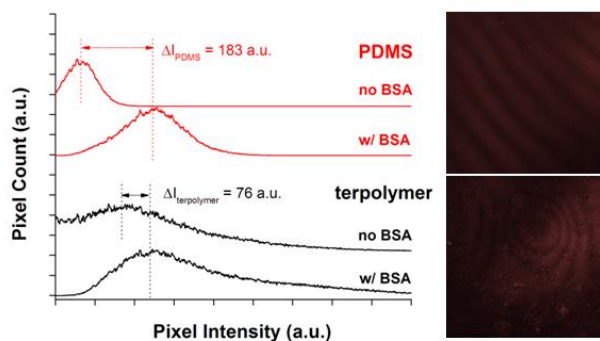


Figure 2.12. Fluorescence signal intensities before and after BSA incubation (left). Confocal micrographs of the PDMS standard (top right) and TP (bottom right) after BSA incubation. Each micrograph is a combined z-stack image of a 10 mm depth field of view taken at 1 μm increments. The x-y field of view is 2 mm. Excitation occurred *via* a 635 nm diode laser, with emission collection selected from 650 nm to 750 nm using a monochromator and a PMT.

2.4 Conclusions

A series of ternary amphiphilic coatings utilizing HBFP, PEG and PDMS with unique surface characteristics were synthesized and characterized. It was shown that heterocomplexity and surface energy are explicitly functions of chemical composition, and that these systems show promise for use as anti-biofouling coatings.

Differing from previous fluoropolymer-PEG systems through incorporation of PDMS, the synthesized terpolymer system expands on the current generation of coatings and displays distinctive topographical, compositional and morphological features, as seen specifically through analysis of the surfaces by surface force and ATR-IR spectroscopies. The materials presented here provide a direct route to enhanced surface complexity with no significant increase in the synthetic or cure conditions. This system also provides an entirely new mode of dynamic surface reorganization, as shown by

preferential emergence of PDMS character on the surface after water immersion, and differing from the predominant fluoropolymer expression observed in previous HBFP-PEG formulations.

By varying the compositional ratios of the three constituents, a wide range of topographical, morphological and compositional variations were displayed. Microscopic characterization revealed a highly disordered heterogeneous surface that varied both topographically and chemically at the micro- and nanometer-scales. Investigation of non-specific protein adsorption of the terpolymer network provided encouraging results; with significantly better resistance to protein adsorption than a commercially-available anti-biofouling PDMS standard. Bulk thermal and mechanical characterization revealed the kinetics and degree of matrix change at both marine and physiological conditions. All of these features provide a new type of amphiphilic surface uniquely qualified for further investigation as a new branch of anti-biofouling material.

In this work, the complications of low bromine content in HBFP is of concern. It is possible that chain-chain bicoupling reactions as well as elimination reactions from the ligand PMDETA may be causing a loss of bromide functionality in the chain ends which can affect future abilities to crosslink with polymer. Further studies will aim to address this issue through the use of different ligands and polymerization conditions to generate polymers with higher chain end functionality.

CHAPTER III

**DEVELOPMENT OF A RAPID METHOD FOR THE APPLICATION OF
HYPERBRANCHED FLUOROPOLYMER-POLYDIMETHYLSILOXANE-
POLY(ETHYLENE GLYCOL) CROSSLINKED TERPOLYMER NETWORKS
FOR USE AS ANTI-BIOFOULING COATINGS**

3.1 Introduction

Biofouling is a persistent problem that plagues numerous fields and can be difficult to fully control.⁶⁵⁻⁶⁶ In particular, marine biofouling poses its own unique set of problems, most notably, the diversity of marine life and the subsequent methods of surface adhesion.⁶⁷⁻⁶⁸ Biofouling can disrupt marine ecosystems through the transport of invasive species on ship hulls travelling into different water systems.⁶⁹ While traditional methods of deterring fouling of marine organisms were effective, the toxicity of these formulations proves detrimental to the environment because of their heavy metal content and subsequent bioaccumulation of these compounds in marine species over time which has led to bans from the international maritime communities.⁷⁰⁻⁷² These factors have led to the development of anti-biofouling and fouling release coatings which take advantage of the properties of the different materials to inhibit the settlement of organisms on the surface or to be used as fouling release coatings as the shear forces at the vessel's cruising speed can detach organisms from the surface.^{32, 73-75}

Of the polymers that have been focused on for the generation of anti-biofouling coatings, fluoropolymers, siloxanes and poly(ethylene glycol) (PEG) and their resultant

systems have been widely investigated due to the unique characteristics present in each class of polymer.^{14, 29, 76} Various formulations combining these polymers have also been explored because of the beneficial properties that can be obtained such as amphiphilicity, chemical heterogeneity, topographical variations and surface energy variations on the surface of the coatings.^{29 50 35} Of note, coatings combining fluoropolymers and PEGylated polymers have led to decreased settlement of both hydrophobic and hydrophilic glycoproteins, and other coatings using this combination have had complete deterrence of specific marine organisms.^{29, 32, 77}

Previously, our laboratory has investigated the use of a terpolymer network composed of hyperbranched fluoropolymer (HBFP), PEG and polydimethylsiloxane (PDMS) to generate surfaces that displayed complex surface topographies and chemical compositions on the nano- and microscales. The network also displayed an improved inhibition of the settlement of a non-specific protein, bovine serum albumin, when compared to a PDMS standard (Sylgard[®] 184). While the initial performance of the network is promising, there are synthetic challenges facing the use of this network in further anti-biofouling assays. Synthetic challenges include the possible delamination of the networks due to water swelling in the PEGylated regions of the film resulting in the difficulty in adhering the terpolymer network to substrates because of the chemical nature of both the siloxane and fluoropolymer components and the ability to create a rapid procedure for applying these networks to relevant substrates. Herein, we report the generation of anti-biofouling coatings comprised of HBFP, PEG and PDMS, which are covalently adhered to substrates through spray coating to a Naval approved epoxy

barrier coating, Interseal[®] 670 HS and the subsequent testing of the anti-biofouling and fouling release performance of the systems again *Balanus amphitrite* and *Balanus improvisus*.

3.2 Materials and Methods

Reagents were purchased from Sigma Aldrich and used as received unless otherwise noted. Interseal[®] 670 HS was purchased from Richmond Supply, Inc. Standard sized microscope slides (25 × 75 × 1 mm) were purchased from VWR. Synthetic seawater was purchased from Ricca Chemical. RAW 264.7 cells and Dulbecco's Modified Eagle's Medium (DMEM) were obtained from the American Type Culture Collection. Media additives (fetal bovine serum, penicillin/streptomycin) were obtained from Sigma Aldrich. Cell culture 96-well flat bottom plates were purchased from Corning Costar Co. HBFP was synthesized according to literature; $M_w = 18.9$ kDa; $M_n = 8.43$; PDI = 2.23. Anal. calcd. for C₇₆₁H₃₉₉Br₉F₄₂₂O₄₅: C 48.4%; H 2.13%; F 42.4%; Br 3.80%; found: C 49.23; H 2.61; F 34.94; Br 4.35%.⁴² It should be noted that previous conditions using PMDETA as a ligand for ATR-SCVP produced polymers with low bromine content and, thus, a decreased ability to be crosslinked. Through changing the ligand to 2,2'-bipyridine, the loss of benzylic bromide and bromoacetyl functionalities was reduced and the bromine content of the resultant HBFP increased to the expected value.

Application of Interseal[®] 670 HS Epoxy Barrier Coating

The two component system of Interseal[®] 670 HS was mixed at a ratio of 8 mL:1 mL of Part A:Part B. The system was applied to glass microscope slides *via* a draw down method in a fabricated aluminum mold with a 0.5 mm clearance between the top of the

glass slides and the lip of mold (**Figure 3.1**). Coatings with Interseal[®] 670 HS were cured at room temperature for 24 h under N₂ atmosphere.

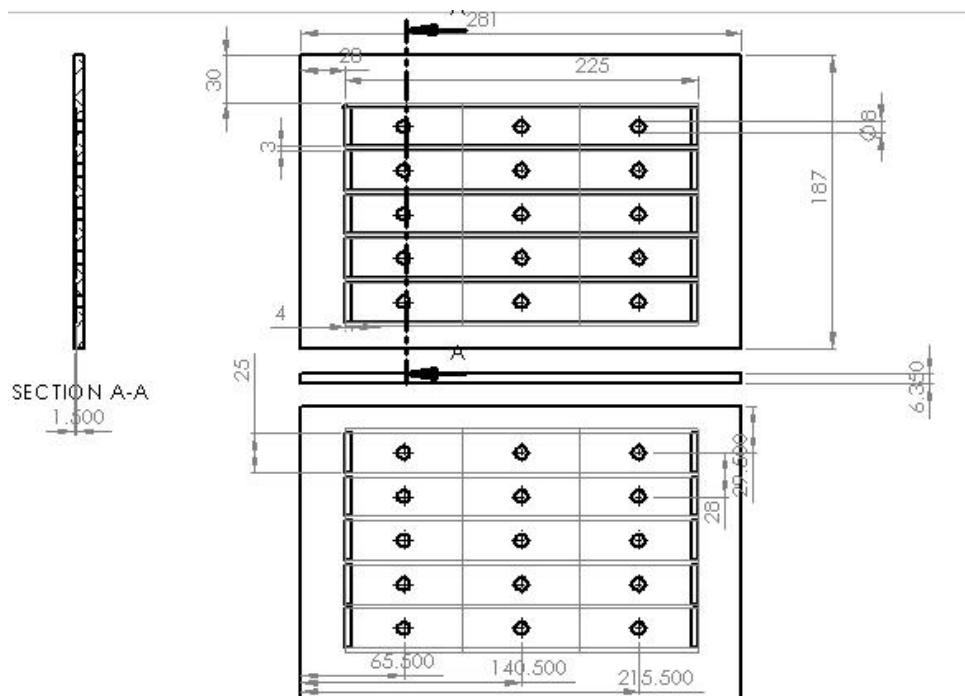


Figure 3.1. Schematic of the mold used to coat glass microscope slides with Interseal[®] 670 HS.

Application of Terpolymer Film onto Interseal[®] 670 HS Epoxy Barrier Coating.

The following general procedure was followed for each sample, as defined here for the terpolymer network having 75 wt % of each PEG and PDMS. To a scintillation vial was added HBFP (1.67 g, 0.199 mmol), bis(3-aminopropyl)-terminated PEG (1.25 g, 0.83 mmol, 75 wt % with respect to HBFP), bis(3-aminopropyl)-terminated PDMS (1.25 g, 0.50 mmol, 75 wt % with respect to HBFP), THF (150 mL) and N,N-

diisopropylethylamine (DIPEA) (0.93 mL, 5.3 mmol) and the mixture was stirred magnetically until homogeneous. The film was then applied to the Interseal[®] 670 HS coated glass microscope slides *via* an airbrush applicator (Central Pneumatic) using an application pressure of 50 psi from a distance of 15 cm. The film was then cured in an oven at 110 °C for 45 min under N₂ atmosphere to afford the dry coatings. IR = 3035, 1840, 1710, 1630, 1610, 1560, 1350, 1285, 1210, 1110, 1080, 1060, 980 and 930 cm⁻¹.

Atomic Force Microscopy and Surface Force Spectral Mapping

Atomic force microscopy was performed under ambient conditions in air. The AFM instrumentation consisted of a MFP-3D-BIO AFM (Asylum Research; Santa Barbara, CA) and standard silicon tips (type, OTESPA-70; L, 160 μm; normal spring constant, 50 N/m; resonance frequency, 246-282 kHz). Force spectroscopy mapping was performed *via* AFM measurements using a Bruker Multimode 8 system in PeakForce[™] tapping mode. This imaging method also provides direct surface maps of modulus, dispersion, deformation and adhesion.⁶⁰ In brief, the PeakForce[™] QNM[™] imaging mode uses a modified Hertzian model, the DMT model, to directly extract a reduced Young's modulus (E_r).³³ The DMT model takes into account surface-tip interactions neglected in the Hertz model and also allows for mapping of adhesion force, deformation and dissipation energy. This method is described elsewhere in detail.³²

In these measurements, a ScanAsyst-Air (Bruker) with manufacturer specification for a spring constant of $k = 0.4$ was used. For this study, no formal calibration was performed as the relative values for purposes of chemical identification were sought.

Arbitrary values for tip size and the Poisson ratio were used. Thermal tuning of the cantilever gave a resonant frequency of 93 kHz. However, as PeakForce™ imaging uses the cantilever in an off-resonance mode of 2 kHz, this finding is not critical to the qualitative value of the imaging.

Atomic Force Microscopy and Surface Force Spectral Mapping

Atomic force microscopy was performed under ambient conditions in air. The AFM instrumentation consisted of a MFP-3D-BIO AFM (Asylum Research; Santa Barbara, CA) and standard silicon tips (type, OTESPA-70; L, 160 μm; normal spring constant, 50 N/m; resonance frequency, 246-282 kHz).

Infrared Spectroscopy

IR spectra were obtained on a Shimadzu IR Prestige attenuated total reflectance Fourier-transform infrared spectrometer (ATR-IR). Spectra were analyzed using IRsolution software package (Shimadzu).

Static Water Contact Angle

Contact angles were measured as static contact angles using the sessile drop technique with an Attension Theta optical tensiometer (Biolin Scientific)⁷⁸. Drops were fitted with a Young-Laplace formula to calculate the static contact angle in the Theta software (Biolin Scientific). Coatings were dried in a desiccator *in vacuo* for 30 m prior to measurements.

Fluorescence Microscopy

Fluorescence microscopy was conducted on an Olympus IX70 inverted microscope equipped with a mercury arc lamp and an Olympus DP72 digital camera. Images were

collected through a 20× objective (Olympus UPlanFl). Excitation and emission collections were achieved with the use of an Olympus U-MNIBA3 filter cube (excitation: 470–495 nm, emission: 510–550 nm). All collections during fluorescence imaging were done with the same optics set and with the same collection time and CCD gain in order to maintain comparability from frame-to-frame.

Cytotoxicity Assays

Coatings containing the fully cured terpolymer network spray coated onto the Interseal[®] 670 HS undercoat were immersed in deionized water (18 mL) for 48 h. After 48 h, the coatings were removed and dried in a desiccator *in vacuo* before determining the mass loss of the films gravimetrically. The concentration of the leachate was then calculated using this value.

RAW 264.7 mouse macrophages (2×10^4 cells/well) were plated in a 96-well plate in DMEM medium supplemented with 10% fetal bovine serum and 1% penicillin-streptomycin. Cells were incubated at 37 °C in a humidified atmosphere containing 5% CO₂. The medium was replaced with fresh medium 24 h after seeding. Formulations were prepared by serial dilutions of leachate from the terpolymer coatings in phosphate buffered saline (PBS) to yield concentrations that ranged from 0.174–0.001 mg/mL. For each well, 20 μL of every formulation was added to 100 μL of the medium. Negative controls were created by addition of 20 μL of PBS to wells containing 100 μL of the medium. The cells were incubated for 24 h, and after this period the media was replaced with 100 μL of the complete medium. Then, 20 μL of the MTS combined reagent was added to each well (Cell Titer 96[®] Aqueous Non-Radioactive Cell Proliferation Assay,

Promega Co.). The cells were incubated with the reagent for 3 h at 37 °C in a humidified atmosphere containing 5% CO₂, and protected from light. Absorbance was measured at 490 nm using SpectraMax M5 (Molecular Devices Co.). The cell viability was calculated based on the relative absorbance to the control untreated cells.

Culture of Barnacles at the University of Newcastle

Larvae were obtained from laboratory cultures of two barnacle species *Balanus* (=Amphibalanus) *improvisus* and *Balanus* (=Amphibalanus) *amphitrite*. The former are maintained in semi-continuous culture at Newcastle University from founder stock sourced originally from the Sven Lovén Centre for Marine Sciences at Tjärnö, Sweden. *Balanus amphitrite* adults were shipped from the Duke University Marine Laboratory at Beaufort, North Carolina. *Balanus. improvisus* were maintained in a 19 °C recirculating aquarium in brackish conditions (25 ppt Tropic Marin), whereas *Balanus amphitrite* were kept in aerated aquaria in full salinity (35 ppt) natural seawater filtered to 10 µm and UV-sterilized. Both were fed daily with *Artemia* sp. and *ad libitum* with the chlorophyte *Tetraselmis suecica*.

To collect larvae, barnacles of either species were removed from water overnight. On re-immersion, they released stage 1 nauplius larvae into the water and these larvae were collected subsequently by attraction to a point light source. Larvae were removed in batches to temporary storage in a solution of *Tetraselmis suecica*. Once 10,000 larvae had been collected, they were transferred into 10 L buckets containing aerated seawater of the appropriate salinity. *Balanus amphitrite* were fed throughout with *Tetraselmis suecica*, whereas *Balanus improvisus* began with a 50:50 mixture of *T. suecica* and

Thalassiosira pseudonana with the proportion of *Tetraselmis pseudonana* reducing to zero by the third day of culture.

Both species took between 4-5 days to metamorphose into cyprids, at which point they were filtered through a 250 µm mesh. *Balanus improvisus* were used immediately following removal from the culture, whereas *Balanus. amphitrite* were stored for 3 days at 6 °C prior to use in assays.

Settlement Assay at the University of Newcastle

Settlement assays were conducted on terpolymer coated microscope slides. 1 mL of seawater adjusted to the appropriate salinity was added in a droplet to each slide, contained within Quadriperm plates (Sarstedt). The droplets were of sufficient height to allow free movement of the cyprid larvae at an amount of 20 cyprids per drop. Once all surfaces had cyprids applied, the plates were closed and covered in moist tissue paper to minimise evaporation. The *Balanus amphitrite* and *Balanus improvisus* assays were then incubated for 48 h in the dark at 28 °C and 23 °C, respectively. Numbers of larvae settled at 24 and 48 h time points were expressed as a proportion of the total, averaged per treatment and then compared between treatments.

Removal Assay at the University of Newcastle

After the settlement assay, the surfaces were wiped clean using a soft sponge, the drops were re-applied and several hundred larvae were added to each surface. After 24 h, unattached larvae were washed from the surfaces and the remaining attached larvae were immersed for 6 days in a dilute solution of *T. suecica*. At this time the locations of all juvenile barnacles were noted and the surfaces were subjected to a calibrated wall-shear

stress of 92 Pa for 2 minutes in the turbulent flow channel at Newcastle University. Later, those juvenile barnacles remaining attached were noted and expressed as a proportion of the original. Numbers removed were then compared between treatments.

3.3 Results and Discussion

Synthesis and Generation of Coatings

The ability to rapidly generate crosslinked terpolymer systems on various surfaces used in the marine environment is of the utmost importance with careful attention being placed on the cure conditions and the ability for the systems to be used on different substrates used. However, the different substrates used can present problems to the terpolymer network for a variety of reasons, most notably, the low surface adhesion of both the fluoropolymer and siloxane components of the coating and the possibility of delamination of the coatings due to water swelling from the hydrophilic PEG domains of the system. Because of these factors, the process of covalently attaching the terpolymer network to an undercoat was explored. The rationale for choosing the epoxy-based undercoat, Interseal[®] 670HS, was based on two main reasons. First, depending on the stability of the epoxy undercoat in ambient conditions, the resultant epoxy coating has multiple functional handles which can be exploited for further covalent crosslinking. Second, Interseal[®] 670HS is approved for use by the United States Navy as a qualified barrier coating for their vessels and allows for the possibility of coating much larger substrates without difficulties in scale-up of the undercoat ⁷⁹.

The epoxy barrier coating was cast using a modification of the recommended ratio of the two component system (Part A:Part B = 5.67:1 by volume) through the increased use

of Part A of the system (A:B = 8:1 by volume). This ratio was chosen to incorporate an excess amount of epoxide functionality on the surface due to Part A containing a bisphenol A epichlorohydrin polymer. Interseal[®] 670HS was deposited onto glass slides through the use of a roller and mold to create coatings with homogeneous thicknesses of 0.5 mm. The coatings were cured at 25 °C for 24 h in an inert atmosphere at ambient temperature to preserve epoxide functionality on the surface. After curing, the terpolymer network was deposited on the epoxide barrier coating and subsequently cured at 110 °C for 45 m (**Figure 3.2a**).

As outlined in **Figure 3.2**, there are a number of different hypotheses for the covalent attachment of the terpolymer network to the surface. **Figure 3.2a** details the ideal scenario with the preservation of the epoxide functionality on the surface, with the bulk of the covalent attachment occurring through the reaction of the amine termini of both the PDMS and the PEG polymers with epoxides present on the surface of the coating. Ring opening of the epoxide through these polymers may allow for reactions between the hydroxyl group of the surface with the bromide functionalities of the HBFP as well.

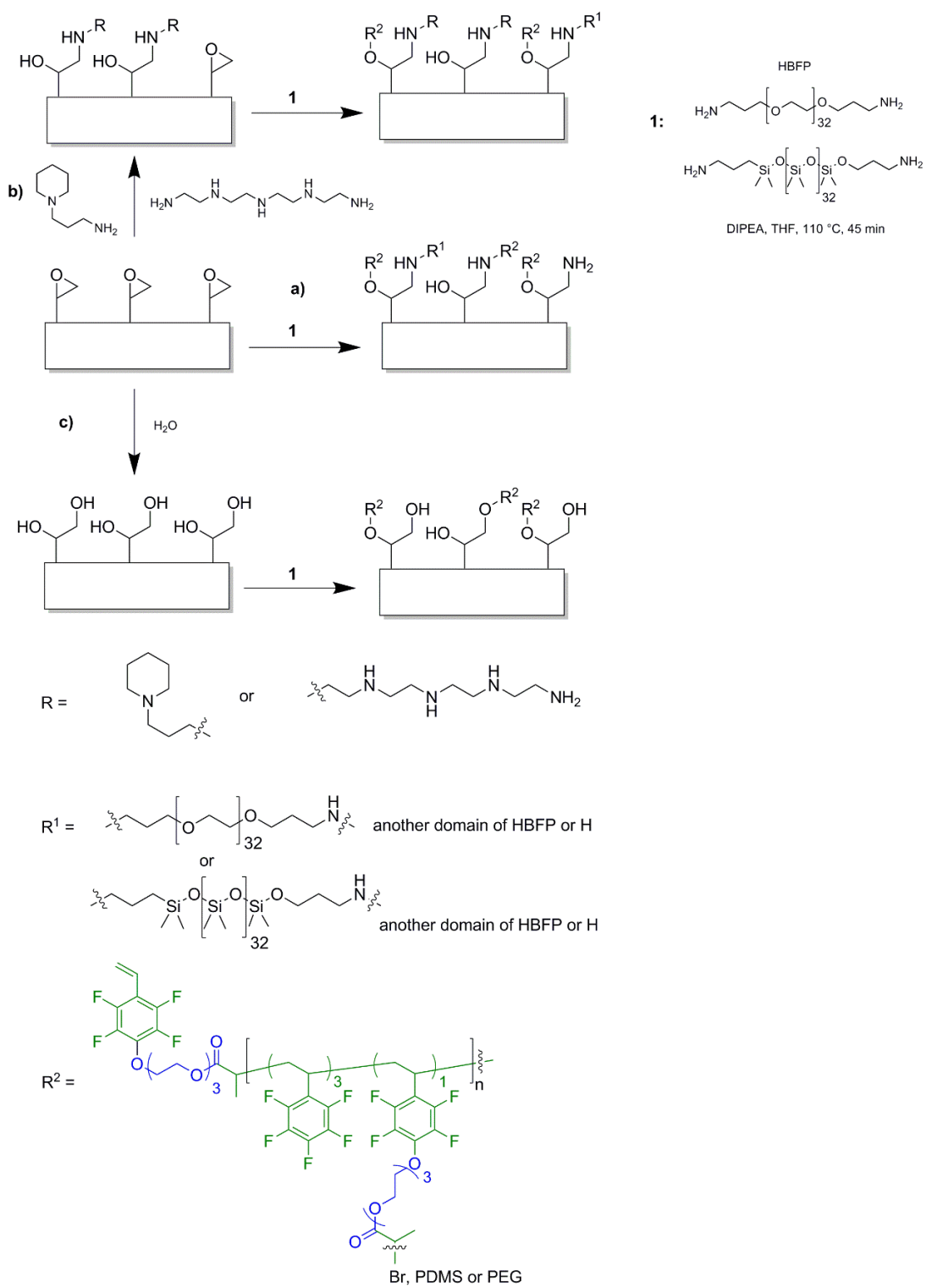


Figure 3.2. Generation of terpolymer coatings on an epoxy undercoat.

In an alternate scenario, **Figure 3.2b** represents when excess crosslinking at the surface occurs, exposing a mixture of epoxide functionalized groups and opened epoxides at the surface through reactions with aminopropyl morpholine and tetraethylenepentamine from Part B of the Interseal[®] 670HS during curing. This scenario would still allow for the same covalent attachments as stated in **Figure 3.2a**, but with the majority of the coating being attached to the surface *via* the functional bromide termini of the HBFP.

Lastly, **Figure 3.2c** represents a non-ideal scenario when hydrolysis of epoxide units at the surface occurs and leaves predominately hydroxyl groups present at the surface. This scenario still allows for the covalent attachment of the terpolymer coatings *via* a reaction between the hydroxyl groups of the surface and the terminal bromides of the HBFP. While the authors cannot deduce the specific method of covalent attachment to the surface at this time, the combination of two or more of the scenarios is the most likely occurrence and will be investigated more in-depth in future studies.

Atomic Force Microscopy, IR Spectroscopy and Static Water Contact Angle

To determine if surface features were lost upon adhering the terpolymer network to the epoxy barrier coating, atomic force microscopy was performed on both the epoxy barrier coating and a terpolymer coating containing 75 wt% PEG and 75 wt % PDMS. As seen in **Figure 3.3**, the epoxy barrier coating displayed very minimal changes in regards to surface roughness and topography.

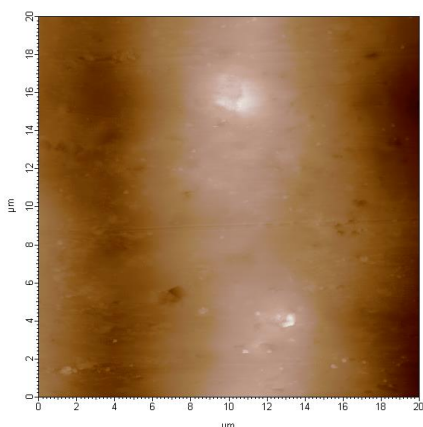


Figure 3.3. AFM micrographs of the epoxy barrier coating, 20 micron \times 20 micron field of view.

In comparison, the terpolymer network coated to the epoxy barrier layer displayed topological variations on both the nano- and micro-scales (**Figure 3.4**).

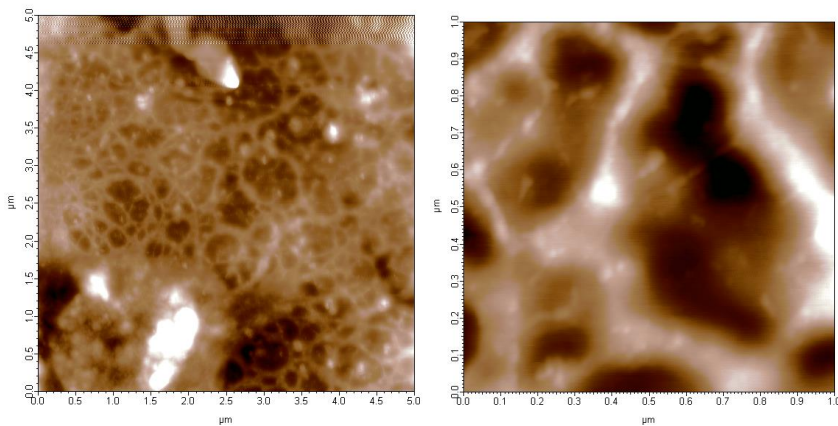


Figure 3.4. AFM micrographs of the terpolymer network with 75 wt % PEG and 75 wt % PDMS (left), and an expanded view of the surface topography (right).

To further understand the chemical stability of the surface crosslinking of the terpolymer coatings after long-term exposure in a marine environment, coatings containing 75 wt % PEG and 75 wt % PDMS were analyzed with ATR-IR spectroscopy and static water contact angle to determine if there was a change in the surface properties. Synthetic seawater was chosen as a media for immersion for the coatings to best replicate the intended environment of the coatings. The coatings were measured prior to immersion, 30 days post-water immersion and 90 days post-water immersion (**Figure 3.5**). While the characteristic signals of the epoxy undercoat dominate the majority of the IR spectra in the terpolymer network spectra, there are four characteristic peaks at 1060, 1080, 1630 and 1840 cm^{-1} , which reveal information regarding the surface composition expressed at the surface of these coatings. Based on previous results using IR spectroscopy, the 1630 and 1840 cm^{-1} signals are associated with HBFP, and the 1060 and 1080 cm^{-1} signals are attributed to PDMS expressed at the surface.⁴² It can be further stated that the results of this study correlate well with previous results from our laboratory stating the gross expression of PDMS at the surface of the terpolymer films after wetting.

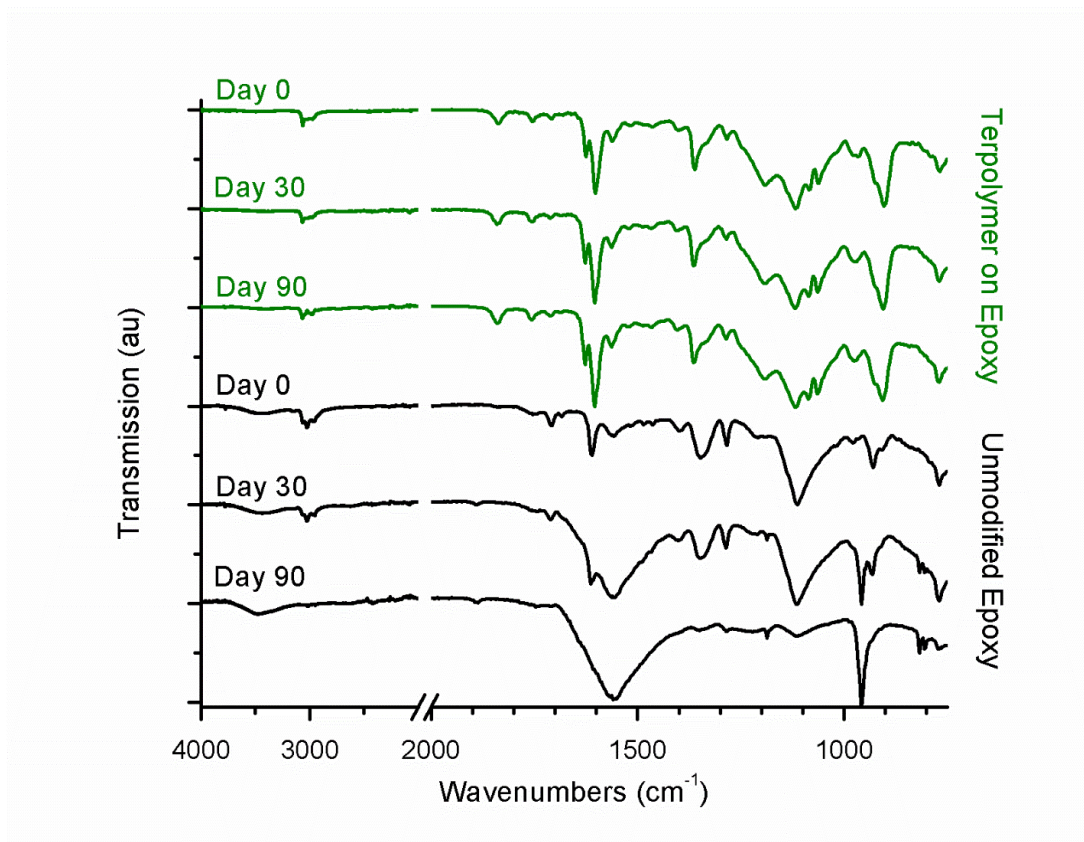


Figure 3.5. ATR-IR spectra of the terpolymer network spray coated on the epoxy coating (top three spectra) and an unmodified epoxy coatings (bottom three spectra) after 90 days of immersion in synthetic seawater.

Additionally, static water contact angle experiments were performed to determine if the surface lost any of the intended amphiphilic surface properties after long-term immersion in synthetic seawater. The results summarized in **Table 6** show no change in the static water contact angle values of the terpolymer network after 90 days of water immersion. Conversely, the bare epoxy coating showed an increase in hydrophilic character after water immersion. This result may be significant as well as it further suggests epoxide functionality on the surface prior to water immersion, which undergoes

hydrolysis after water immersion leading to an increase in hydrophilic character. This hypothesis is supported by the IR spectra through the signals most commonly associated with water and hydroxyl groups.

Table 6. Static water contact angle results of the terpolymer network spray coated on the epoxy coating and an unmodified epoxy coatings after 90 days of immersion in synthetic seawater.

Days Post-Water Immersion	Terpolymer Network on Epoxy	Unmodified Epoxy
0	102 ± 2°	65 ± 5°
30	103 ± 5°	44 ± 3°
90	103 ± 3°	47 ± 6°

Thickness of Terpolymer Coatings

When generating coatings for anti-biofouling coatings, the thickness of the final coating can affect its anti-biofouling and fouling release properties. In previous systems based on different iterations of HBFP-PEG, it was seen that nano- and microscopically complex surfaces in regards to morphological and topographical heterogeneities can be achieved by varying the coating thickness.⁴¹ Additionally, thickness can control the fracture mechanics at the interface of a surface of elastomeric coatings.⁸⁰ PDMS-based coatings typically display a decrease in the shear stress for the removal of fouling organisms as film thickness increases, with films having increasing fouling release properties as the thickness increases to 700 μm.^{28, 81} Because the composition of the

coating displays elastomeric properties due to the incorporation of PDMS, it is hypothesized that a coating with a thickness in the range of the hundreds of microns will display the greatest fouling release properties.

Film thicknesses were measured *via* confocal laser scanning microscopy with an excitation of 470–495 nm and an emission of 510–550 nm with contrast achieved from the emission of the HBFP.³² The thicknesses were found to vary from local minima of $330 \pm 20 \mu\text{m}$ and local maxima of $380 \pm 20 \mu\text{m}$ from FWHM of representative cross-sections ($n = 5$) (**Figure 3.6**).

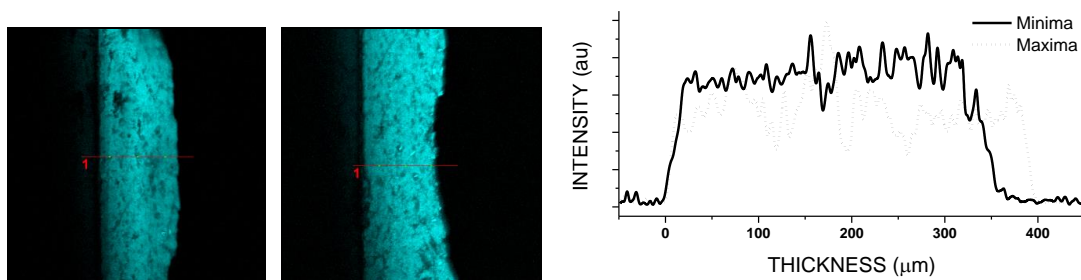


Figure 3.6. Cross-section of local maxima (left), minima (center) and intensity profiles for both (left). *Note: left of the emission is the basecoat material and to the right of the emission is open air.*

Cell Viability

As previous methods of controlling biofouling have proved to be environmentally toxic, the toxicity of the components of the coatings and possible leachates from the system are of the utmost concern⁷⁵. To test the toxicity of the possible leachates from the terpolymer system, cell viability studies were performed with RAW 264.7 macrophages.

While not present in a marine environment, this cell line was chosen to act as a general, non-inclusive model for testing cytotoxicity. After leaching the coatings in water for 48 h, the amount of water soluble compounds in the solution was measured gravimetrically and found to range from 0.127–0.174 mg/mL. Serial dilutions were then performed to give a range of concentrations from 0.002–0.174 mg/mL, in aggregate. Results from testing all concentrations of the leachates demonstrated 100% cell viability in all experiments performed indicating no apparent cytotoxicity issues.

Anti-biofouling Assays with *Balanus amphitrite* and *Balanus improvisus*

The anti-biofouling and fouling release performances of the terpolymer networks were investigated to determine if the resistance to non-specific proteins as previously seen extended to select marine organisms. Cyprids of two barnacle species, *Balanus amphitrite* and *Balanus improvisus*, were chosen as these organisms have enormous evolutionary pressures to adhere to surfaces to continue their life cycles to sessile barnacles as well as their generalist nature with regards to surface preference.⁸² Three terpolymer networks were analysed using these organisms, with PDMS content ranging from 25-75 wt %. The networks were then compared against two standards, polystyrene and the Interseal[®] HS epoxy coating. The settlement of *Balanus amphitrite* cyprids was assessed after 48 h of incubation on the coatings and settlement of the terpolymer surfaces was very low, ranging between 2 and 7%, with the polystyrene control having 37% settlement and the Interseal[®] control having 34% settlement. (**Figure 3.7**). The negligible settlement of this species on the test surfaces made it impossible to perform removal experiments.

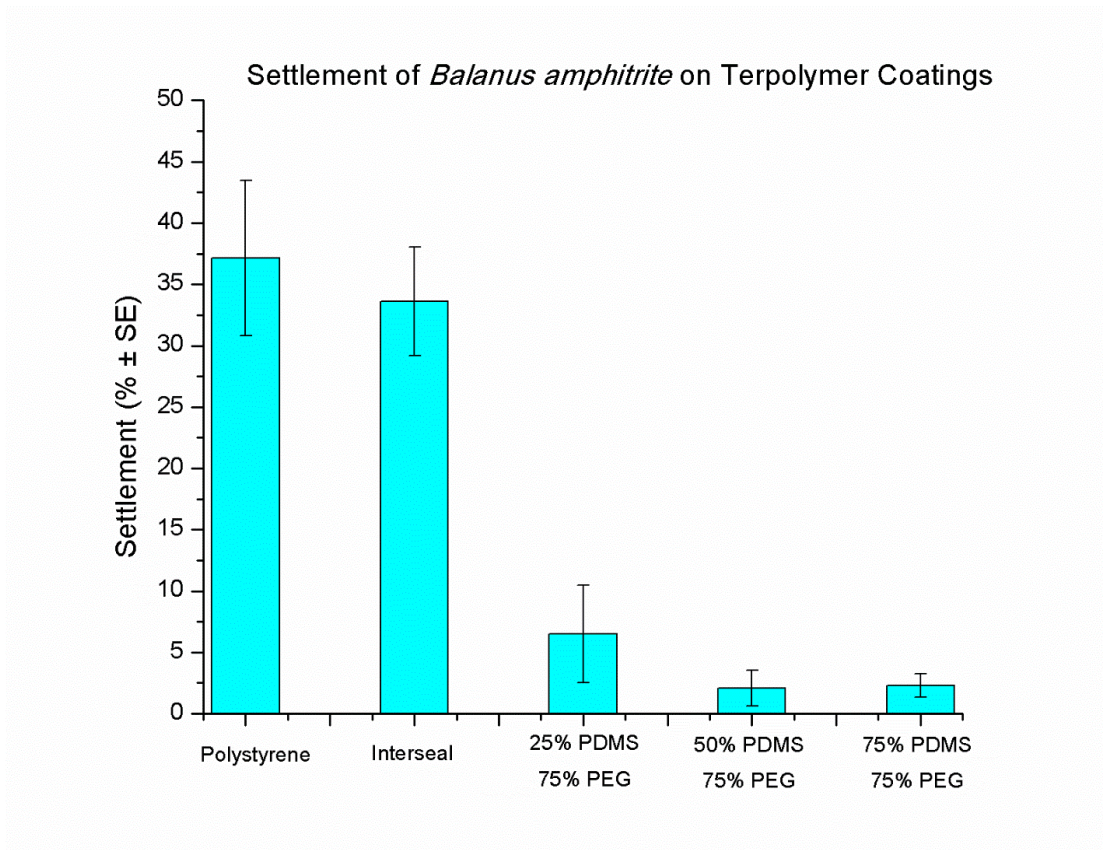


Figure 3.7. Percent settlement of *Balanus amphitrite* on the terpolymer coatings after 48 h of exposure.

In contrast to the *Balanus amphitrite* larvae, *Balanus improvisus* larvae settled on these surfaces in larger numbers. Settlement of this species was 57% on the Interseal[®] control after 48 h of incubation, with settlement on the terpolymer surfaces reducing from 36 to 10% in relation to increasing content of PDMS (**Figure 3.8**). For *Balanus improvisus*, removal was measurable and correlated inversely with settlement with higher removal from terpolymers with higher wt % of PDMS (**Figure 3.9**). Settlement was lowest on those polymers from which the barnacles were removed most easily (**Figure 3.10**).

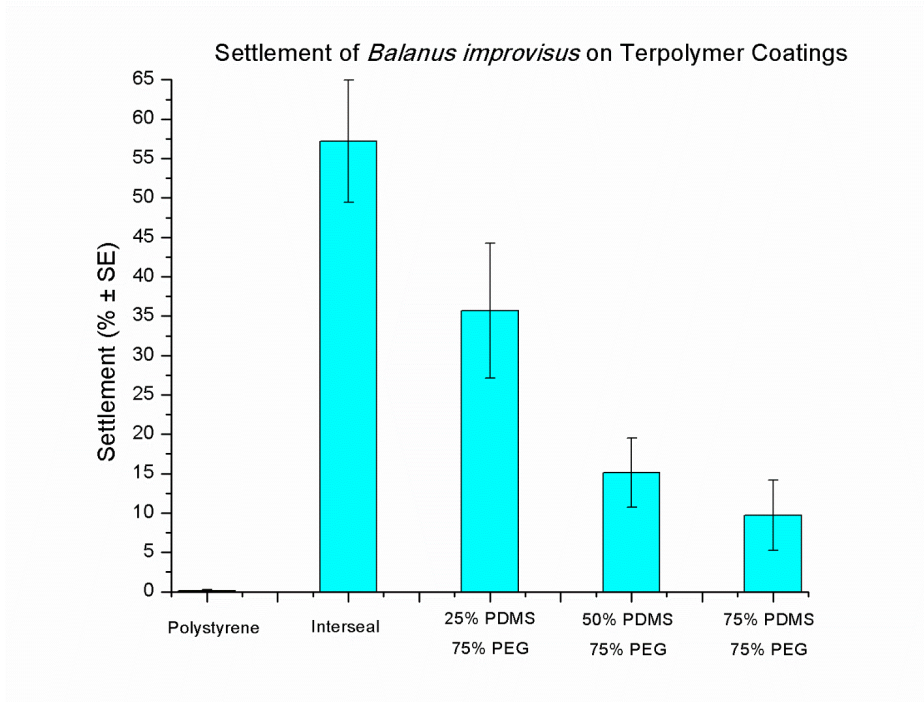


Figure 3.8. Percent settlement of *Balanus improvisus* on the terpolymer coatings after 48 h of exposure.

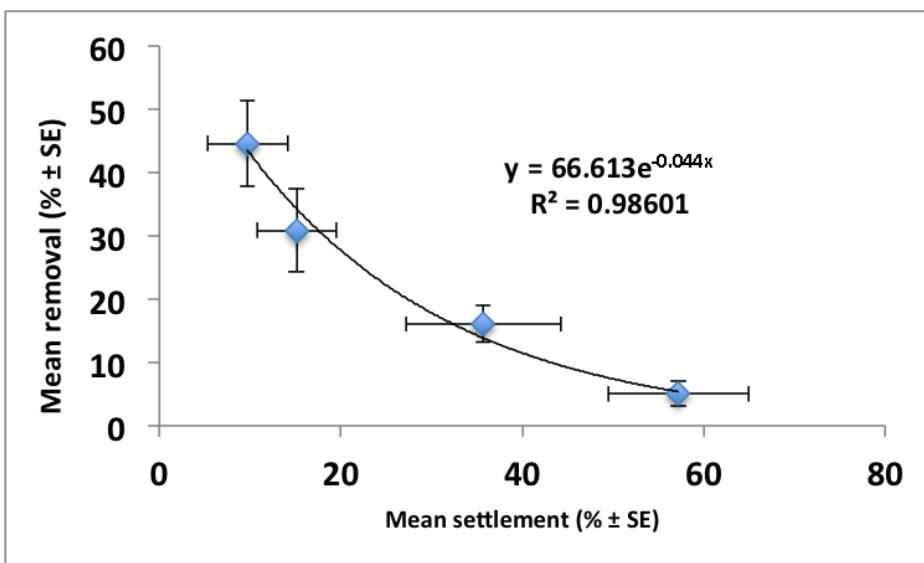


Figure 3.9. Mean removal strength (in Pa) vs. mean settlement of *Balanus improvisus* for all samples.

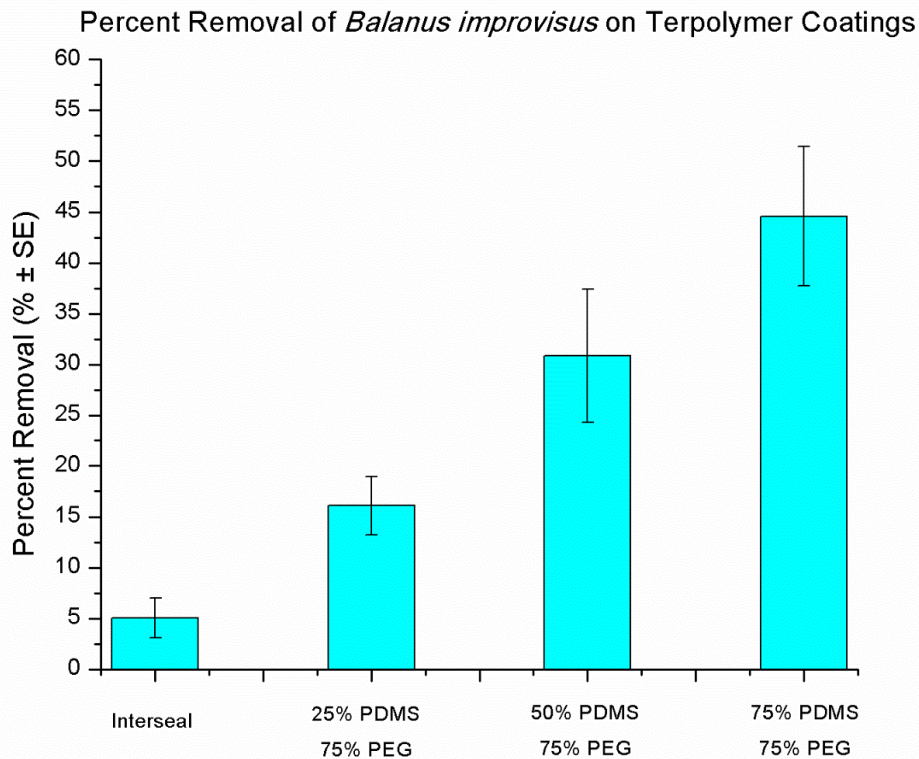


Figure 3.10. Percent removal of *Balanus improvisus* on the terpolymer coatings after 48 h of exposure.

For both species, settlement on the terpolymers was much lower than on the Interseal[®] control. Settlement of *Balanus amphitrite* was negligible on the terpolymers, as noted by Imbesi *et al.* on a previous incarnation of these materials based on HBFP-PEG³². Settlement of *Balanus improvisus* reduced in line with increasing wt % of PDMS. It is suggested, therefore, that in the context of these surfaces, *Balanus improvisus* can be considered a more aggressive fouler than *Balanus amphitrite*. This difference in surface selectivity points to the importance of testing developmental surfaces with more than one fouling organism and, if possible, more than one species within a single group of

organisms. It is also interesting to relate these findings to the previous work of Petrone *et al.* and Di Fino *et al.*, who used a range of self-assembled monolayers to compare the settlement of these two barnacles species in relation to surface free energy and charge.⁸³⁻

⁸⁴ These authors found only one difference; *Balanus improvisus* had a significant preference for hydrophobic surfaces, whereas *Balanus amphitrite* did not. These findings may explain the increasing settlement of the former with increasing wt % of PDMS in the surface composition.

It has been shown previously that settlement of *Balanus amphitrite* larvae relates directly to their likelihood of removal on textured surfaces.⁸⁵⁻⁸⁶ Cyprids settle in higher numbers on textured surfaces from which their likelihood of removal is lowest. Here, this relationship extends to surface chemistry. In the absence of variation in surface roughness, there was a direct correlation between settlement and removal of *Balanus improvisus*, with cyprids settling in larger numbers to surfaces from which fewer juveniles were removed. Excluding the potential hydrodynamic and refuge effects of a textured surface during removal assays, we can now relate settlement rate of barnacles to their adhesion strength with improved confidence. Whether potential adhesion strength is measured by larvae *via* mechanical testing during temporary adhesion, or if it is more predictive based on the chemical composition of the surface, however, remains unknown.

3.4 Conclusions

A method for the rapid generation of coatings based on terpolymer networks composed of HBFP, PEG and PDMS was developed. The method uses an epoxy barrier coating to

covalently attach the terpolymer network to the substrate. The terpolymer coatings expressed similar surface features in ATR-IR spectroscopy and static water contact angle prior to water immersion and after 90 days of water immersion, which supports that these coatings can be used in a marine setting for extended timeframes. The thickness of the coatings was measured to range from $330 \pm 20 \mu\text{m}$ to $380 \pm 20 \mu\text{m}$, which corresponds well to elastomeric coatings with beneficial fouling release properties. Leachates from the coatings displayed no cytotoxicity against RAW 264.7 macrophages. To determine the effect of PDMS on anti-biofouling and fouling release performance in the terpolymer network, anti-biofouling studies with *Balanus amphitrite* and *Balanus improvisus* were performed with three formulations of terpolymer coatings varying in the wt % of PDMS. Through these studies, the coatings with a formulation containing 75 wt % PEG and 75 wt % PDMS demonstrated the best performance against both species of barnacle cyprid. The results obtained from the anti-biofouling assays are promising, but studies testing against a wider variety of marine organisms in field testing are currently in progress. However, the results of this study demonstrate a useful platform for the covalent attachment of the terpolymer coatings to substrates with improved anti-biofouling properties.

CHAPTER IV

**LONG-TERM STATIC IMMERSION TESTING OF HYPERBRANCHED
FLUOROPOLYMER-POLYDIMETHYLSILOXANE-POLY(ETHYLENE
GLYCOL) CROSSLINKED TERPOLYMER NETWORKS**

4.1 Introduction

Marine fouling is a persistent problem which leads to an increase in operational costs of vessels, ranging into the billions of dollars per year for the shipping and transportation industries.⁷ The increased operational costs are mostly due to an increase in fuel consumption because of an increase in frictional drag on the hull of the ship, but costs related to hull cleaning and painting also add to the costs generated by fouling.⁶ In the past, many effective anti-fouling paints were developed that incorporated various biocides in their formulations, however, the negative environmental impact of these compounds has led to greater regulations governing their use in the shipping industry.⁸⁷ One such example of the biocide based paints are triorganotin-based paints, which prevent the recruitment and growth of organisms on the surface.¹³ To deter fouling in the marine environment using a method which is environmentally-benign, research has focused on two types of coatings for the prevention of fouling, anti-fouling (AF) and fouling release (FR) coatings.⁸⁸ While the two can be of similar composition, AF films exhibit properties which passively or actively deter the settlement of organisms on the coating, while FR coatings allow weak adhesion by organisms which facilitates their removal through hydrodynamic shear forces.⁸⁹

For both the AF and FR coatings, many different polymeric systems have been investigated.⁹⁰ Fluoropolymers, siloxanes and poly(ethylene glycols) (PEG) have all demonstrated the potential to be viable next-generation AF coatings. Coatings based on fluoropolymers have been investigated because of their low surface energies and their well-organized surfaces that deter fouling.²⁸⁻²⁹ Siloxanes also display low surface energy, however, the dominant factor that these coatings operate by is through the encouragement of bond fracturing at their surface.^{28, 91} In addition to these systems, amphiphilic systems containing combinations of fluorinated, PEGylated or siloxane components have displayed superior anti-fouling properties compared to single component systems.^{39, 92} Amphiphilicity is a strong deterrent for fouling because many proteins in a marine environment bind preferentially to either hydrophobic or hydrophilic surfaces, and the combination of the two components can deter the settlement of both proteins⁹³. However, marine organisms still present a challenge as they have a vast amount of methods to adhere to a surface, which require additional methods to prevent fouling such as nanoscopically and microscopically complex surfaces in regards to their composition, topography and topology.⁹⁴ The heterogeneities presented through the surface complexities has been shown to prevent the settlement of organisms and to have improved fouling release properties when compared to surfaces of the same composition without the complexities.⁹⁵ In a specific example from our laboratory, crosslinking of hyperbranched fluoropolymer (HBFP) and PEG created heterogeneities on the nanoscale which inhibited the settlement of proteins, lipopolysaccharides and *Ulva* zoospores.²⁹

More recent work in our laboratory has still focused on the generation of complex coatings through the crosslinking of thermodynamically incompatible components, but with different generations of HBFP.³⁶ The HBFP used in more recent studies is generated through an atom transfer radical self-condensing vinyl copolymerization between an inimer and pentafluorostyrene. Upon crosslinking this polymer with bis-amino-functionalized PEG, a thermodynamic phase segregation of the components coincident with kinetic trapping leads to unique topographical and compositional heterogeneities on the surface.³² In further work, it has been demonstrated that this concept can be expanded to a terpolymer network through the use of a third component, that of a bis-amino-functionalized polydimethylsiloxane (PDMS). These coatings also were able to be applied to an epoxy undercoat through covalent crosslinking of the functional handles of the three components with the epoxide functionalities of the surface for the rapid generation of terpolymer coatings. These coatings displayed optimal resistance to the settlement of two species of barnacle cyprids, *Balanus amphitrite* and *Balanus improvisus*.

The focus of the work presented here is to address the long-term AF and FR capabilities of three formulations of terpolymer coatings based upon the crosslinking of HBFP, PEG and PDMS. The three formulations explored in the study differed in the PDMS content of the system, with 25 wt %, 50 wt % and 75 wt % of PDMS relative to HBFP with PEG content of the system was kept constant at 75 wt % relative to HBFP. This study extends on the previous work of these systems through the testing of these coatings at static water immersion sites across the United States. The importance of

testing at multiple sites is because there are statistically significant differences in the type and intensity of fouling and barnacle adhesion among different static water immersion sites⁹⁶. Additionally, factors which influence fouling and coating performance, such as water temperature, salinity and variation in species, differ greatly from site to site⁹⁶. Herein, we discuss the long-term exposure of our coatings in a static water immersion site over a one to three month period to determine the influence of surface compositions on fouling resistance and release performance.

4.2 Materials and Methods

Coatings were produced using a similar method as discussed in Chapter 3, differing only in the substrate on which the epoxy barrier coating and the subsequent terpolymer network were deposited. The substrates used in this study were 4 × 8 inch aluminum panels which were coated with the epoxy barrier coating and cured prior to the deposition and curing of the terpolymer network. One bare epoxy barrier coating and three formulations of the terpolymer network were sent to the different static water immersion test sites with the following ratios for the terpolymer coatings: HBFP:PEG:PDMS = 4:3:1 (75 wt % PEG & 25 wt % PDMS); 4:3:2 (75 wt % PEG, 50 wt % PDMS); 4:3:3 (75 wt % PEG & 75 wt % PDMS). A minimum of three replicates were sent to each test site in accordance with the protocol set forth by the laboratory.

Static Immersion Testing in Port Canaveral, Florida

The test facility is a 7-m long twin hulled floating structure located at Port Canaveral, Florida, (28°24'28.76"N, 80°37'39.11"W) by Kelli A. Zargiel of the Florida Institute of Technology. The port was created in 1953 and is a hub for cruise and cargo ships, US

Navy and Coastguard, fishing vessels and recreational boats. It is an area of high fouling activity. The average salinity is 35 ± 1.2 ppt, the average temperature is 25 ± 4.2 °C and the water depth exceeds 2.0 m. The facility includes a bay for static immersion.

Three replicates of each coating were attached to two PVC frames with cable ties and submerged at a depth of 1.0 m below the surface. Both frames were caged with 13 mm galvanized steel mesh to prevent grazing and predation.

Biofilms were sampled every 4-5 weeks on four separate occasions starting on on 25 March 2014 and were observed monthly over 3 months. Biofilms were collected after two weeks due to the onset of macrofouling. This ensured sufficient growth of biofilm for sampling on the FR coatings, but the panels were not covered with macrofouling. After sampling and adhesion testing, the panels were hand cleaned with a cloth so as not to damage the coatings, and redeployed. Cleaning panels were chosen rather than deploying a new set each time because a cleaning panel better represents the lifecycle of a coating on a ship hull and it also insures the surfaces are acclimated to the environment.

Upon removing the test panels from the water, panels were visually inspected to note surface condition and photographed. A representative area of biofilm was randomly selected from each panel for collection. This area was lightly rinsed with filtered seawater to remove any loosely attached silt and debris.⁹⁷ A 1×3 in (2.5×7.6 cm) area of biofilm was removed from this area using a sterile polyethylene cell lifter and placed into a vial of filtered seawater. On panels that may have begun to experience settlement of macrofouling, smaller areas were sampled. This fact was taken into account when

quantifying the diatom community. The samples were kept on ice until returning to the laboratory where they were fixed with 37% formaldehyde.

Diatoms were counted and identified down to the lowest possible taxonomic level using a Nikon compound microscope equipped with a digital camera at 40× and 100×. When possible at least 300 valves of diatoms were counted and identified per sample. Taxonomic identification was assisted by references listed in Zargiel *et al.*⁹⁸

After the collection of biofilm, the adhesion was measured using the water jet method.⁹⁹ The water jet apparatus is comprised of a SCUBA tank filled with compressed air, a regulator to adjust the pressure from 0 to 1.38 MPa (0–200 psi), a SCUBA tank filled with seawater and a 1.6 mm diameter nozzle to apply the water pressure. A representative area of biofilm was chosen. The regulator on the water jet was set to 0.28 MPa (40 psi) and applied to the selected area. The nozzle was held approximately 1 in from the surface of the panel and rotated in a 1 in concentric circle for about 30 s. This was repeated at 0.55, 0.83, 1.10, and 1.38 MPa (80, 120, 160, and 200 psi) or until the surface was visibly clean. If after 1.28 MPa there was still biofilm present, then the surface was declared unclean. For statistical purposes, an unclean surface was given a value of 2.41 MPa (350 psi). No water jet testing was performed on the BRA (copper coating) because it erodes the coating and does not provide useful data.

Diatom community composition was used to calculate the richness, evenness, and the Shannon–Wiener diversity index of the species. Biofilm adhesion, diatom abundance, species evenness, species richness and diversity were analyzed using a three-way analysis of variance (ANOVA) and a Holm–Sidak post hoc treatment to determine variations in

diatom communities on AF coatings, between treatments, and among sampling dates. All data were tested for homogeneity. If the data failed, then appropriate transformations were made (eg log x, sqrt x). When no transformations were able to correct for non-homogenous data, ANOVAs were run on ranked data. Ordination of sites, coatings, and sampling dates were conducted with the non-metric multidimensional scaling (MDS) of Bray- Curtis similarities. Multivariate analysis was performed on the diatom community data using PRIMER version 6.0. Similarity percentage (SIMPER) was used to determine which diatom species may be contributing the most to the similarity or dissimilarity among coatings.

Static Immersion Testing in Morro, Bay, California

The terpolymer coatings were applied to aluminum panels as described above and deployed at a static immersion test site in Morro Bay, CA for a series of field tests by Lenora H. Brewer of California Polytechnic State University. Panels were submerged 1 m below the surface from a floating dock. Panels were deployed on 22 April 2014 at the beginning of the heaviest fouling season and were observed monthly over 3 months. Panels were subjected to tests quantifying AF and FR performance. AF performance was quantified in accordance with ASTM standard D6990-05. FR performance was estimated using two separate tests, viz. removal of adult barnacles in accordance with ASTM standard D5618-94 and an adaptation of water jet testing.⁹⁹⁻¹⁰⁰

Adult barnacles (*Balanus crenatus*) were recruited directly onto panels in the field and then removed from test panels in accordance with ASTM standard D5618-94. Barnacle removal testing was conducted on 27 May 2014 once all individuals met the minimum

size requirements for testing according to the ASTM standard. Values of CRS were calculated for all barnacles that could be removed from test panels with less than an estimated 10% basal plate remaining on the coating surface as per the ASTM standard. All barnacles that were isolated and met the minimum size requirements were removed from each panel replicate so sample sizes were not equal. Few barnacles settled and grew on the IS900 control panel so this sample size was much smaller than for the other two test coatings. However, the CRS was consistent with what has been observed in other field trials.

One replicate panel of each formulation was reserved for water-jet testing to provide another measure of FR performance. A pressurized stream of water was applied perpendicular to and 25 mm away from the surface as evenly as possible across the entire surface of the panel at a series of pressures (40, 80, 120, 180 and 240 psi). Panels were observed after each water pressure was applied and assessed for complete removal of organisms or estimated percentage cover remaining. These estimates were then used to rank coatings based on how easily fouling could be removed. All water jet testing was done after *ca.* 1 months' accumulated fouling

AF and physical performance of coatings were evaluated as outlined in ASTM standard D6990-05. Each panel was given a fouling rating with 100 being completely free of fouling.

Static Immersion Testing in Pearl Harbor, Hawaii

The experiment was conducted at the University of Hawaii's test site on the southeast end of Ford Island in Pearl Harbor, Oahu, Hawaii by Audrey Asahina. This area is

characterized by relatively constant water temperature and salinity. The site consists of a number of aluminum frames attached to pilings on the south side of Pier F-1 1/2, which extend between 1 to 2 m beneath the surface of the water, depending upon the state of the tide. The experimental panels were mounted to PVC racks which could be raised from and lowered into the water on the aluminum frames. This arrangement allowed individual panels to rotate in tidal currents or prop wash, and facilitated inspection of both faces of each panel.

The supply of competent larvae, the intensity of settlement and the subsequent survival and growth of macrofouling organisms vary strongly over many spatial scales. The investigation was designed to determine not only whether fouling varied due to the experimental coatings, but also whether there was spatial variation in fouling across the test site. Under these conditions a blocked design is appropriate.¹⁰¹ One replicate panel of each coating was assigned to each of three blocks. The first block was immersed at the end of the pier closest to Ford Island, and the second and third blocks were immersed progressively farther down the pier and away from the island. Each block of four panels was approximately 1.77 m in width. The first and second blocks were separated by 14.91m, and the second and third blocks by 7.45 m. The panels were exposed on 6 March 2014 and retrieved on 30 May 2014.

The structure of the fouling communities occurring on the test coatings was described in terms of functional groups. The groups were defined by combining higher taxa with growth form.¹⁰² This approach was taken because the fouling community in Pearl Harbor is extremely diverse, and many of the species present are either unidentified or

impossible to identify rapidly in the field with the unaided eye. Eleven functional groups of macrofouling organisms were scored, *viz.* hydrozoans (effectively including all Cnidaria), tubeworms with calcareous tubes, solitary tunicates, colonial tunicates, arborescent bryozoans, encrusting bryozoans, sponges, molluscs (mainly bivalves although scores did include a small number of vermetid gastropods), barnacles, sediment tubes (constructed by both amphipods and polychaete worms) and macroalgae. A twelfth 'functional group' consisted of free space. The abundance of the functional groups was estimated as percentage cover. Coverage was assessed three times over the length of the experiment. For scoring, a transparent acetate marked with 4, 30 mm x 50 mm quadrats containing 20 randomly spaced points was laid over the face of the panel, and the occurrence of any organism attached to the primary substratum (i.e. the surface of the coating) under each point was noted. Thus, the percentage cover of each functional group on each panel face was estimated from a total of 80 points. The same 4 locations on each panel face were scored at each sampling date, but a different set of random points was used each time.

The raw coverage data from each sampling date were combined into a single data set. This set was then subjected to a principal component analysis in an effort to reduce the number of variables describing the fouling communities present on the coatings. Principal component analysis (PCA) reduces the size of multivariate data sets by taking the original, correlated, variables (*e.g.*, coverages of individual functional groups) and generating combinations of these variables to produce a reduced set of variables (principal component scores) that are uncorrelated. These uncorrelated variables

measure distinct characteristics (or dimensions) of the original data.¹⁰³ PCA may be a useful technique for identifying patterns in community structure that might otherwise be obscured in a multivariate analysis of variance or separate univariate analyses. The principal component scores for each replicate coating at each sampling date were used in a repeated measures analysis. This analysis tested for the effects of coating type, block, time, and time x coating and time x block interactions. For purposes of the analysis, it was assumed that coating x block interactions were not significant. One IN5 panel was damaged before the last sampling date and could not be scored for coverage, in order to maintain a balanced design, all the data from this last inspection were eliminated from the repeated measures analysis (but not from the PCA). All statistical analyses were conducted using SAS (SAS Institute Incorporated, 1989).

4.3 Results

After a month of static water immersion at the test site at Pearl Harbor, Hawaii, the terpolymer coatings and an epoxy standard were assessed for anti-fouling properties and fouling release properties. The coating with 75 wt % PEG & 25 wt % PDMS (coating 3) and with 75 wt % PEG & 75 wt % PDMS (coating 1) greatly outperformed the epoxy standard (control), with a total coverage of 16% and 13% coverage, respectively, compared to 31% coverage for the epoxy (**Figure 4.1**). The FR properties of the terpolymer coatings also outperformed the epoxy coating as seen through the water jet assays performed on both tubeworms, *Hydroides elegans*, and bivalve, *Ostrea hanleyana* (**Figure 4.2** and **Figure 4.3**). The removal assay determined the average strength of removal for tubeworms and bivalves to be 150 ± 14 and 152 ± 25 kPa for the 75 wt %

PEG & 25 wt % PDMS coating (coating 3) 109 ± 13 and 109 ± 23 kPa for the 75 wt % PEG & 50 wt % PDMS coating (coating 2) and 123 ± 12 and 147 ± 41 kPa for the 75 wt % PEG & 75 wt % PDMS coating (coating 1), respectively.

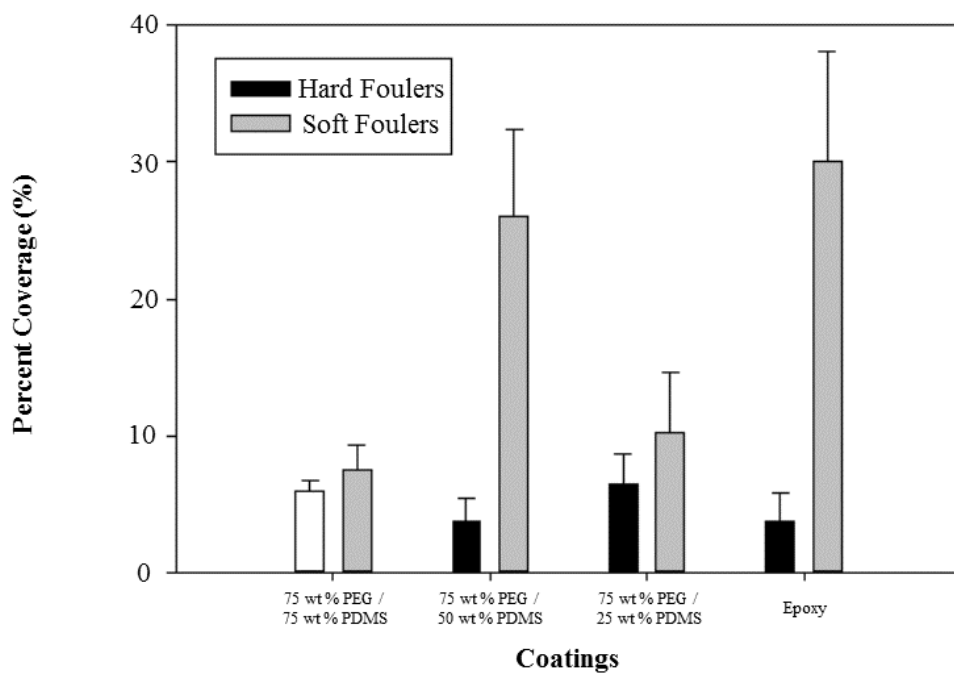


Figure 4.1. Percent coverage of hard and soft foulers on experimental coatings after one month of static water immersion testing at Pearl Harbor, Hawaii. Coating 3 had the greatest amount of cover of hard foulers (6.5 ± 2) as compared to coating 1 (6 ± 7) and 2 (3.7 ± 1.6). Coating 2 had the greatest amount of soft foulers (26 ± 6).

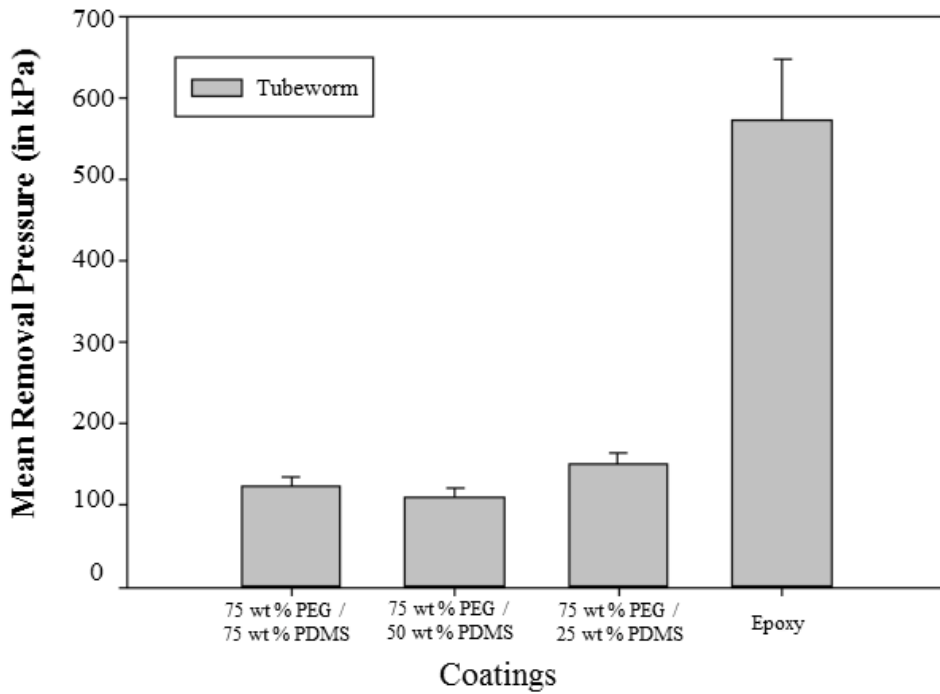


Figure 4.2. Mean pressure in kPa required to remove tubeworm, *Hydroides elegans*, from experimental coatings after one month of static water immersion testing at Pearl Harbor, Hawaii. Coating 1 (123 ± 12), 2 (109 ± 13), and 3 (150 ± 14 kPa) had mean pressures that were significantly less than the control coating (ANOVA, $p < 0.05$). Data were log transformed prior to performing nonparametric tests. Error bars=1 standard error.

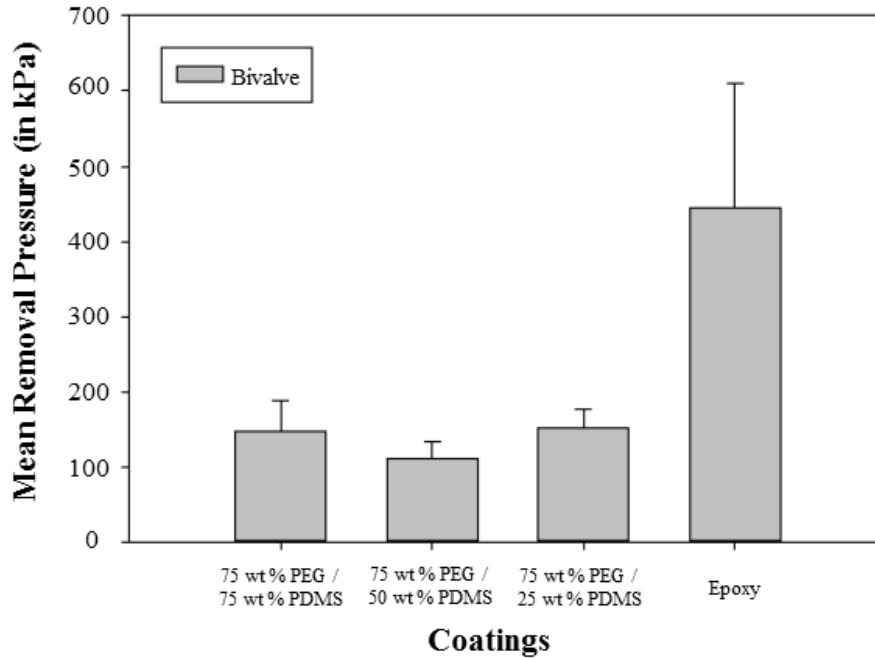


Figure 4.3. Mean pressure in kPa required to remove the bivalve, *Ostrea hanleyana*, from experimental coatings after one month of static water immersion testing at Pearl Harbor, Hawaii. Coating 1 (147 ± 41), 2 (109 ± 23), and 3 (152 ± 25) had mean pressures that were significantly less than the control coating (ANOVA, $p < 0.05$). Data were log transformed prior to performing nonparametric tests. Error bars=1 standard error.

After two months of static water immersion, the total coverage of the terpolymer surfaces decreased with increasing PDMS content with the coverage on the surfaces was dominated by soft foulers (**Figure 4.4**). Removal assays performed with both *Hydroïdes elegans* and *Ostrea hanleyana* determined the removal strength to be 166 ± 15 and 168 ± 21 kPa for the 75 wt % PEG & 25 wt % PDMS coating (coating 3) 121 ± 10 and 103 ± 15 kPa for the 75 wt % PEG & 50 wt % PDMS coating (coating 2) and 119 ± 9 and 153 ± 21 kPa for the 75 wt % PEG & 75 wt % PDMS coating (coating 1), respectively (**Figure 4.5** and **Figure 4.6**).

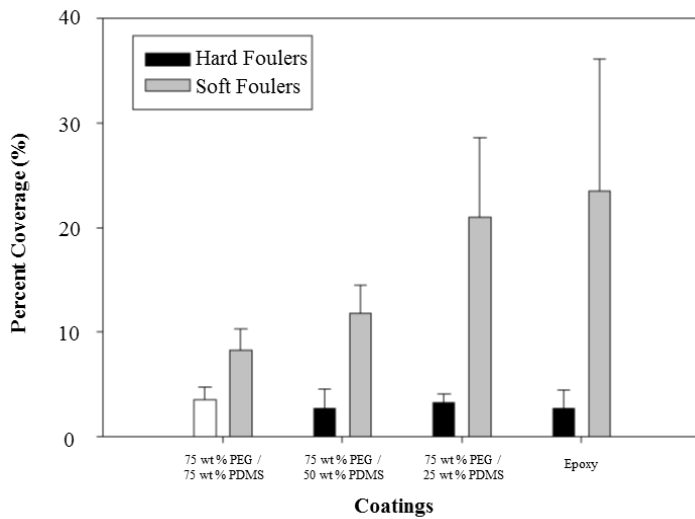


Figure 4.4. Percent coverage of hard and soft foulers on experimental coatings after two months of static water immersion testing at Pearl Harbor, Hawaii. Coating 1 had the greatest amount of cover of hard foulers (4 ± 1) as compared to coating 2 (3 ± 2) and 3 (3 ± 1). Coating 3 had the greatest amount of soft foulers (21 ± 8).

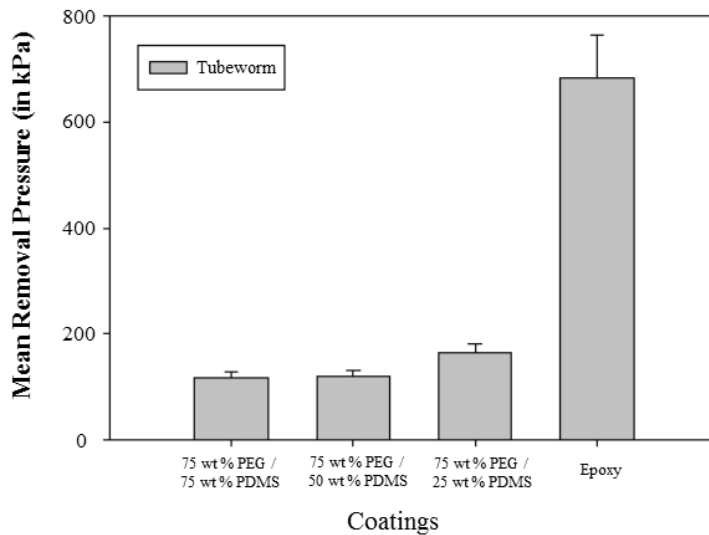


Figure 4.5. Mean pressure in kPa required to remove tubeworm, *Hydroides elegans*, from experimental coatings after two months of static water immersion testing at Pearl Harbor, Hawaii. Coating 1 (119 ± 9), 2 (121 ± 10), and 3 (166 ± 15 kPa) had mean pressures that were significantly less than the control coating (684 ± 79) (ANOVA, $p < 0.05$). Data were log transformed prior to performing nonparametric tests. Error bars=1 standard error.

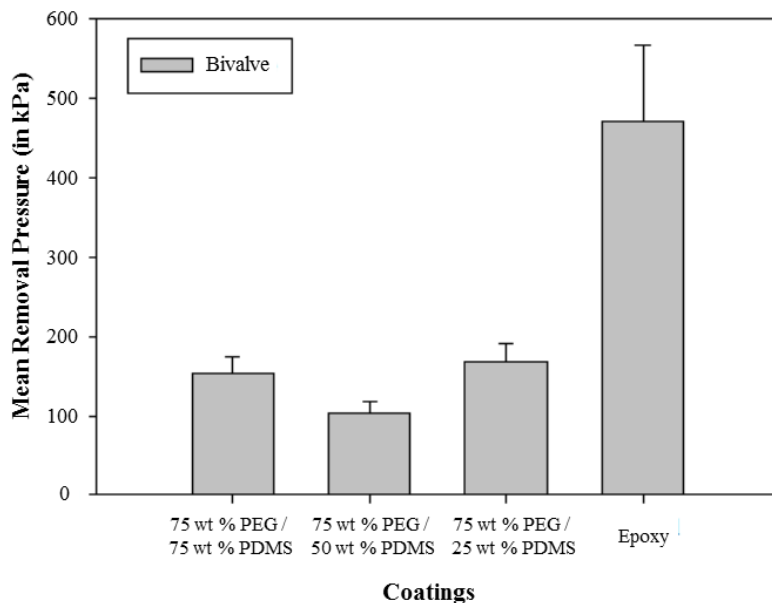


Figure 4.6. Mean pressure in kPa required to remove the bivalve, *Ostrea hanleyanai*, from experimental coatings after two months of static water immersion testing at Pearl Harbor, Hawaii. Coating 1 (153 ± 21), 2 (103 ± 15), and 3 (168 ± 21) had mean pressures that were significantly less than the control coating (471 ± 96) (ANOVA, $p < 0.05$). Data were log transformed prior to performing nonparametric tests. Error bars=1 standard error.

AF/FR Properties in Field Testing at Port Canaveral, Florida

The three terpolymer coatings all had a higher percentage of fouling after both one month of static water immersion testing and did not perform as well as either the BRA 640 or the Intersleek 900 controls. After one month of immersion, the predominant species accounting for 90% of the fouling on the terpolymer networks were classified as biofilms, which include diatoms, initial algae germination and low form algae and bacterial growth. The average removal strength required to remove the biofilm after one month decreased with increasing amounts of PDMS. After three months of testing, all terpolymer films had greater than 95% surface fouling, much higher than the 63%

fouling for both the BRA 640 and Intersleek 900 controls. The predominant species on all three samples, regardless of composition, were tunicates, soft animals that may be solitary or colonial. For the coating with 75 wt % PDMS, the second predominant fouling type was encrusting bryozoans, while the coatings with 25 and 50 wt % PDMS had polychaete calcareous tubeworms as their second predominant species.

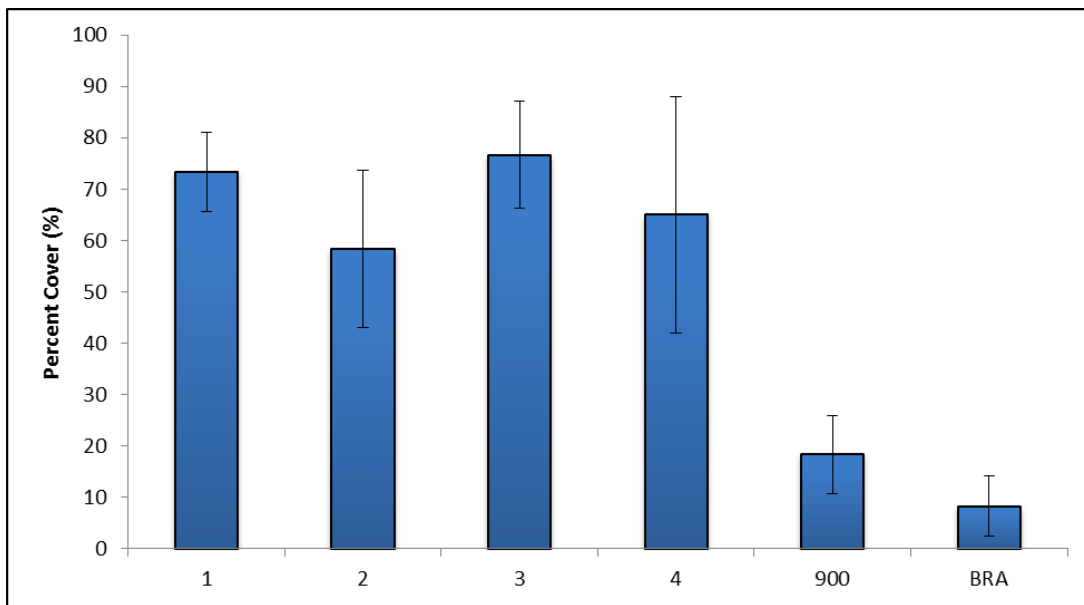


Figure 4.7. Average percent cover of fouling organisms observed on April 11, 2014.

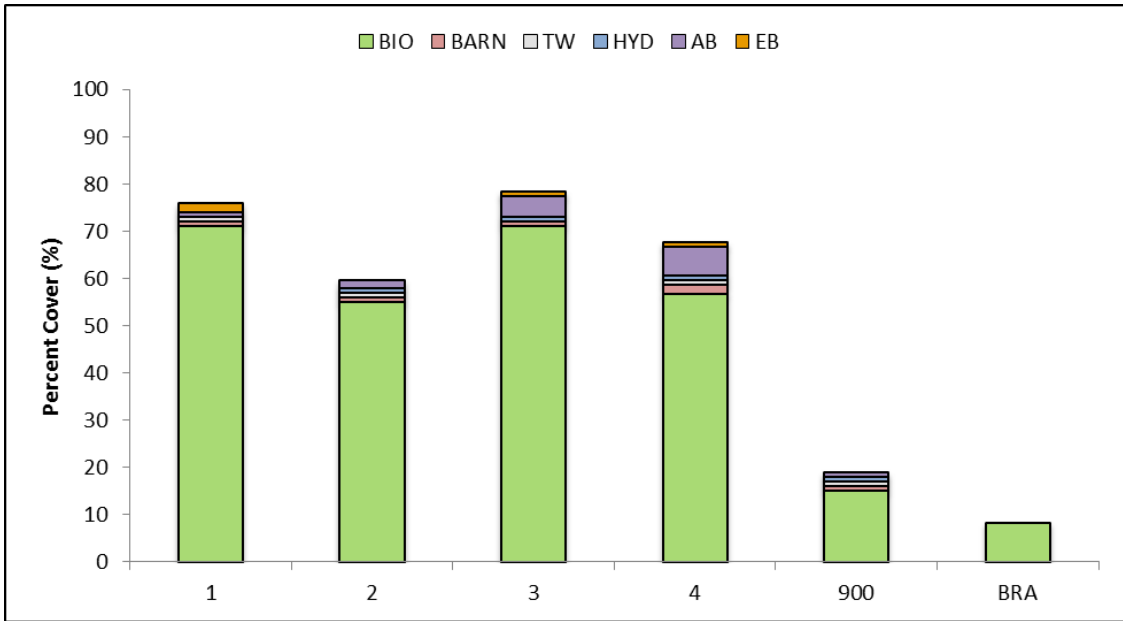


Figure 4.8. Average relative abundance of fouling organisms observed on April 11, 2014.

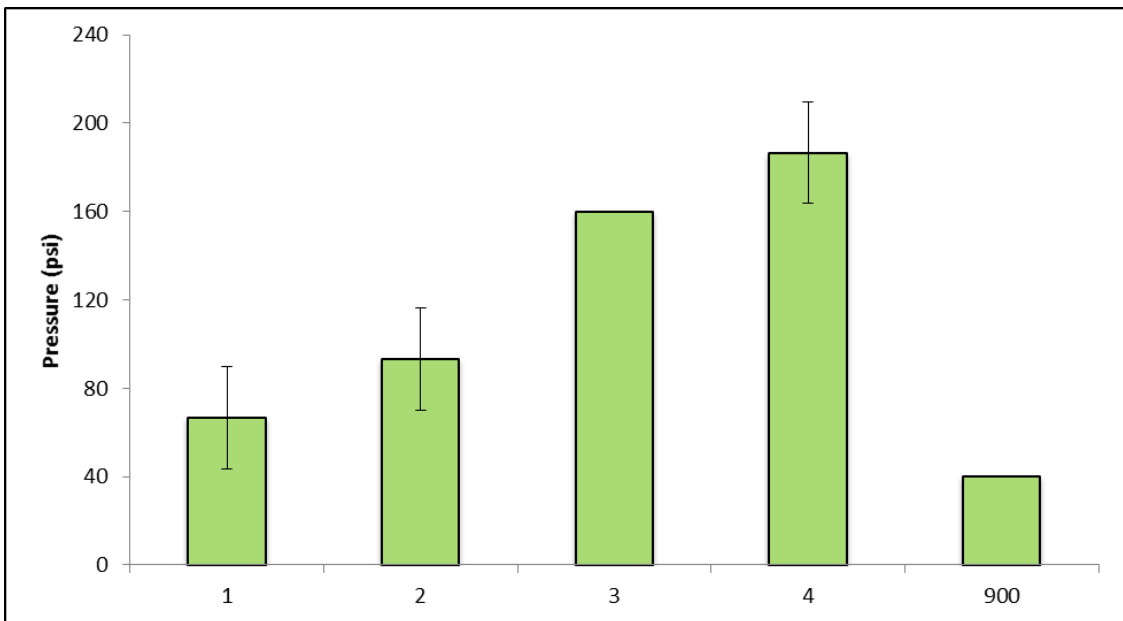


Figure 4.9. Average water jet pressure required to remove biofilm from panels on April 11, 2014. Note: this test was not performed on the Antifouling Standard (BRA 640).

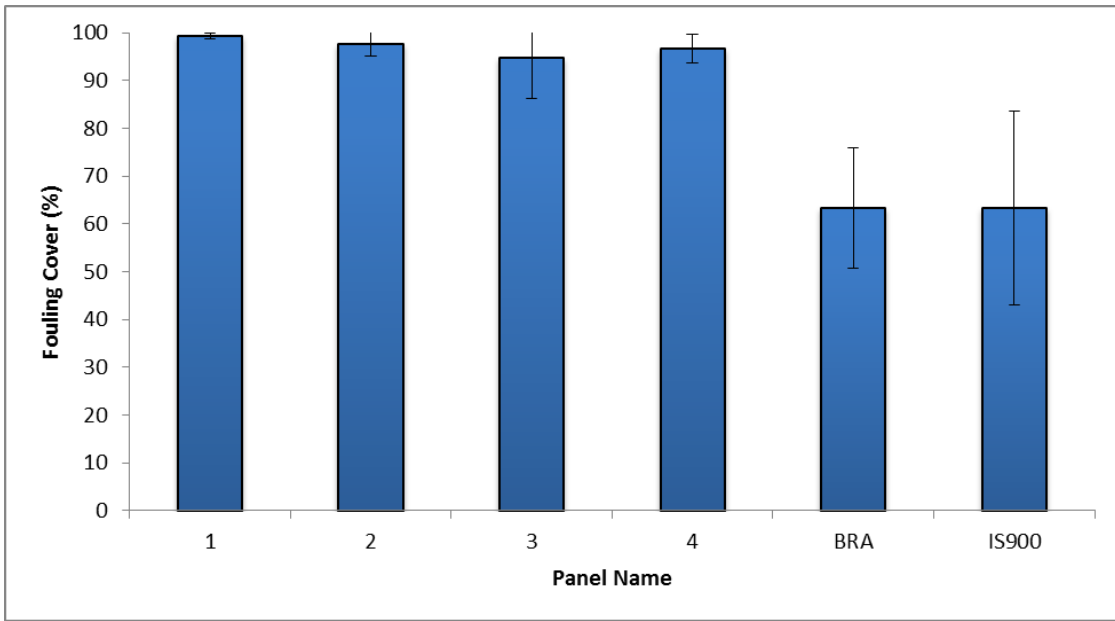


Figure 4.10. Average percent cover of fouling with standard deviation observed on June 18, 2014.

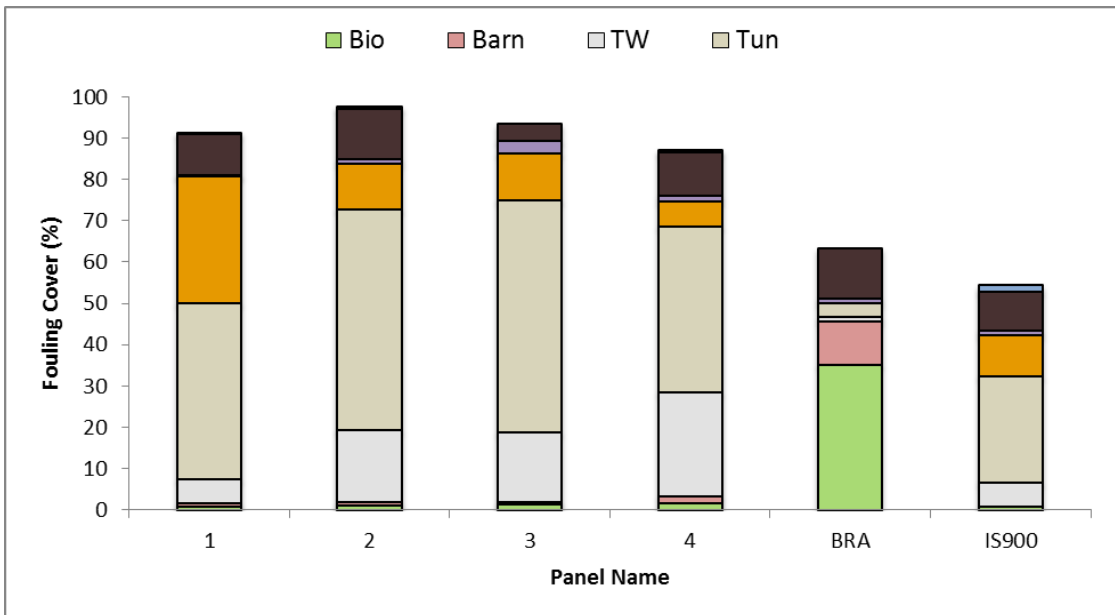


Figure 4.11. Average relative abundance of fouling organisms observed on June 18, 2014.

AF/FR properties in Field Testing at Morro Bay, California

The terpolymer coatings with 75 wt % PEG & 25 wt % PDMS (HBFP:PEG:PDMS = 4:3:1), 75 wt % PEG & 50 wt % PDMS (4:3:2) and 75 wt % PEG & 75 wt % PDMS (4:1:1) were assessed for AF and FR properties under static immersion conditions at Morro Bay, California. In general, the performance of all terpolymer networks decreased after three months of water immersion (**Figure 4.12**). While the terpolymer networks did not perform as well as BRA 640, the coatings, on averaged outperformed the epoxy undercoat and Interseal[®] 670. The best performing terpolymer network in this study had 75 wt % PEG & 50 wt % PDMS, with fouling ratings of 77 ± 7 , 67 ± 8 and 62 ± 8 after April, May and June, respectively. In contrast to Intersleek 900, this formulation of the terpolymer network had comparable results (in the three months of testing, fouling ratings of 69 ± 7 , 79 ± 3 and 67 ± 4 compared to 77 ± 7 , 67 ± 8 and 62 ± 8 for the HBFP:PEG:PDMS = 4:3:2 coating). The results of the water jet assay reveal that BRA 640 outperforms all other standards and terpolymer coatings, with 0% fouling remaining after water jet assays at 40 psi (**Table 7**). The assays performed on the terpolymer networks display the coatings with 75 wt % PEG & 50 wt % PDMS and 75 wt % PEG & 75 wt % PDMS had the greatest removal of slime and macrofouling after three months of static water immersion conditions.

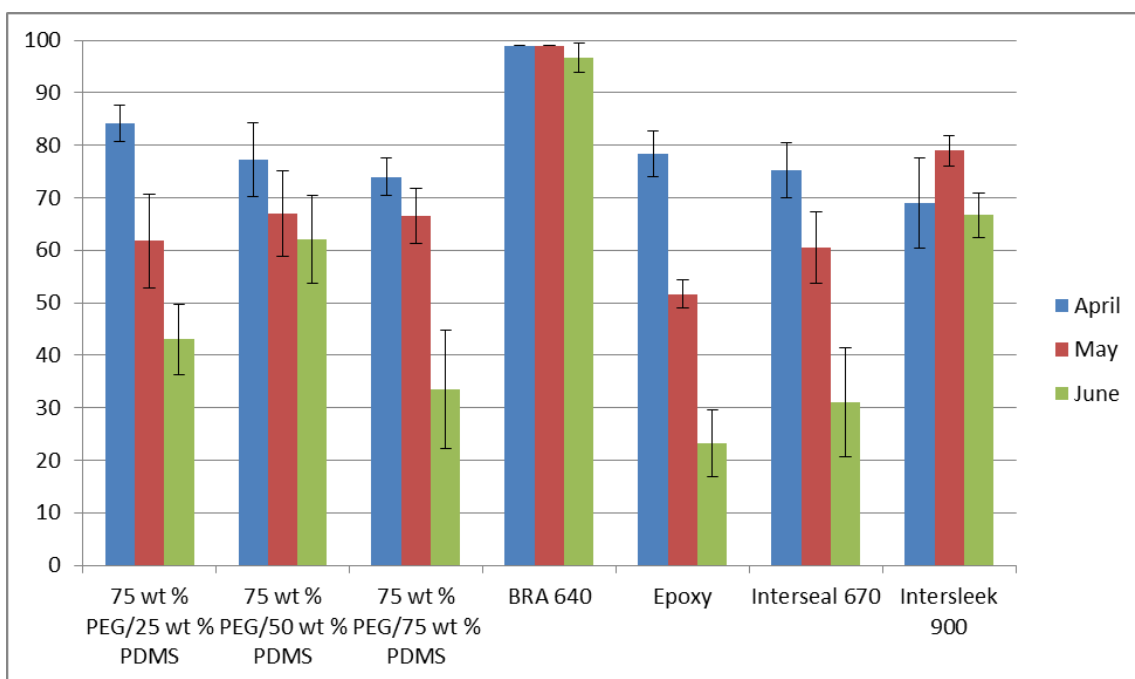


Figure 4.12. Fouling rating of the terpolymer networks and controls after 1, 2 and 3 months of static water immersion conditions, respectively. A fouling rating of 100 represents a completely unfouled surface, while a fouling rating of 0 represents a completely fouled surface.

Table 7. Results of water jet testing for all coatings. Data are shown as the estimated percent coverage of organisms remaining at the pressure indicated. Categories were split into biological slime and total macrofouling.

Coating	22 April 2014		27 May 2014		19 June 2014	
	Slime	Macrofouling	Slime	Macrofouling	Slime	Macrofouling
4:3:1	10% ^a	0% ^c	70% ^a	2% ^a	75% ^a	1% ^a
4:3:2	13% ^a	0% ^c	70% ^a	18% ^a	30% ^a	4% ^a
4:3:3	45% ^a	0% ^d	60% ^a	14% ^a	50% ^a	3% ^a
Interseal 670 HS	70% ^a	15% ^a	15% ^a	84% ^a	40% ^a	1% ^a
BRA 640	0% ^b	N/A	0% ^d	N/A	0% ^c	0% ^b
Intersleek 900	8% ^a	0% ^b	10% ^a	0% ^b	0% ^a	0% ^b
Epoxy	80% ^a	8% ^a	60% ^a	27% ^a	20% ^a	30% ^a

^a: 240 psi; ^b: 40 psi; ^c: 80 psi; ^d: 120 psi.

4.4 Discussion

Previously, it was determined the terpolymer networks presented good anti-fouling performance against two types of barnacle cyprids, *Balanus amphitrite* and *Balanus improvisus*, with increasing AF and FR properties with increasing amounts of PDMS. This finding is hypothesized to occur because the increased hydrophobic character expressed by PDMS creates a more chemically-complex surface as there is a greater degree of heterogeneity of the three components on the surface. The study warranted longer term fouling studies in a static water immersion testing facility due to the beneficial properties they exhibited. From the present studies, more variations in the data sets were seen. The general trends of the data display the coatings containing 50 wt

% PEG & 50 wt % PDMS and 75 wt % PEG & 75 wt % PDMS to be the best performing coatings over the length of the assays. After the first month of testing at the Port Canaveral, Florida, the same trends of FR release properties were observed which matched well with previous data against barnacle cyprids (**Figure 4.9**). Furthermore, the average removal pressure for biofilm on the panels containing the coating with 75 wt % PDMS was 60% greater than that of Intersleek 900 (67 ± 20 psi vs. 40 psi). Interestingly, the coating with 50 wt % PDMS displayed greatest resistance to settlement in these waters, with the least amount of fouling, and the least amount of the predominant fouler in that timeframe, biofilm. However, after three months, panels for all formulations were completely fouled, differing only in the predominant fouling species on the surface. This result possibly signifies a change in overall surface chemistry which favors the preferential settlement of different fouling types. The results from the static water immersion testing in Pearl Harbor, Hawaii present data suggesting the viability of the terpolymer networks as suitable anti-fouling coatings. While the fouling may not be as aggressive as other test sites, the coatings displayed optimal performances over the course of the static water immersion testing. The static water immersion testing in Morro Bay, California exhibited interesting results after three months. The terpolymer coatings did not perform as well as the BRA 640 control, with much decreased fouling ratings compared to this coating, however, the coating with 75 wt % PEG & 50 wt % PDMS performed very similarly to Intersleek 900 in regards to its fouling ratings in the testing period. Also, the best performing coating in other studies, the 75 wt % PEG & 75 wt % PDMS was the least optimal terpolymer network tested in

this study, suggesting that variations in the marine conditions at each site may play a unique role in the surface reorganization of the film with regards to its chemical composition and surface topography. Variations in the water jet assays as compared to Intersleek 900 were seen as well, with the Intersleek 900 coatings exhibiting higher FR properties than any of the coatings after three months of immersion. The variations are unusual as one would expect the AF properties and, thus, the fouling ratings of the terpolymer coatings, specifically the coating with 75 wt % PEG & 75 wt % PDMS, to be affected because of the overall decrease in FR properties over time, but this finding is opposite from what was found. The data seems to indicate that, while the FR properties of the surface may decrease over time, the ability to deter fouling has less of a drop-off. In aggregate, the terpolymer networks were less optimal than Intersleek 900 and BRA 640 in regards to their AF and FR properties. Additionally, the variations in weight percentages of PDMS did not seem to have a great effect on the long-term properties of the coatings with the exception of the testing in Pearl Harbor. However, there are a couple of positives which can be extrapolated from the data as a whole. Coatings with a higher percentage of PDMS (50-75 wt %) display improved properties in regards to AF and FR performances. Also, the enhanced performance of BRA 640 may be due to the fact that the formulation contains a biocide and maintains a performance level due its ablative nature. In other studies, it was seen that the terpolymer coatings were not greatly outperformed by Intersleek 900, with one formulation of the terpolymer network yielding similar fouling ratings after three months of static water immersion testing (**Figure 4.12**), as well as the results from Pearl Harbor, Hawaii indicating a promising

coating technology. These data suggest that the AF properties of the systems studied may be optimized further as more specific changes in the system are made, such as optimizing the content of PDMS and PEG and determining what leads to the variability of the coatings in different environments. To expand on this concept of variability of the coatings, more studies on the long-term property changes of the terpolymer networks may explain the decrease in performance in the studies. As the films undergo surface rearrangement upon water immersion, the timeframe of these changes may play a role in the decreased performance over time. Another hypothesis related to the surface rearrangement of the films suggests a change in the surface properties of the system after a fouling event. If protein secreted from a marine organism is not fully removed from the surface on the nano- or micrometer scale, it is plausible to see a decrease in performance that would not match up with visual assessments of the coatings. Because of this possible outcome, more advanced analytical techniques will be performed in the future that determine the surface composition after fouling, such as time-of-flight secondary ion mass spectrometry (TOF-SIMS) to determine if there is any change in the fluorine or silicon components of the system after a fouling event occurs. In summary, the studies presented in this paper represent the first step in the long-term studies of the terpolymer networks in regards to their AF and FR performance, and, if optimized for longevity, may present a coating which matches or outperforms current industrial standards.

CHAPTER V
THIOL-ENE CROSSLINKED, MULTIPLY-COMPLEX FLUORINATED-
ZWITTERIONIC-SILSESQUIOXANE COATINGS FOR ANTI-BIOFOULING
APPLICATIONS

5.1 Introduction

Since the beginning of the 21st century, there has been an increase in the research of zwitterionic and charged materials for their applications in the field of biomaterials.^{24, 104-107} Specifically, the area of marine fouling has focused much research into coatings based on zwitterionic polymers or charged materials containing zwitterions because of the beneficial anti-fouling properties they impart on the resultant system.^{20, 108-110} These exceptional properties are hypothesized to occur because of the tightly bound surface hydration layer which forms a physical and energetic barrier to prevent protein adsorption onto the surface.^{30, 111} Additionally, the electrostatically induced surface hydration of the zwitterions, such as carboxybetaine, sulfobetaine and phosphobetaine, has been shown to be much stronger than the hydrogen bonding of water to hydrophilic materials.³¹ While this surface hydration effect is effective in the deterrence of protein adsorption, proteins in a marine environment can display a preference for both hydrophobic and hydrophilic surfaces, citing a need for more complex surfaces.¹¹² The development of amphiphilic surfaces containing zwitterionic functionalities to create anti-fouling surfaces has been studied and has shown to be effective in the reduction of nonspecific protein adsorption and the settlement of *Ulva* zoospores.¹¹⁰

Recently, our group has demonstrated terpolymer networks composed of hydrophobic, hydrophilic and fluorinated domains display potential as anti-fouling applications, and amphiphilic zwitterionic surfaces are able to deter settlement of *Ulva* zoospores. Silsesquioxanes also have been explored as the added hydrophobic component to increase the mechanical robustness of the resultant crosslinked network. These studies display that complex heterogeneities in the surface characteristics of the film, specifically chemical composition and topology, can be achieved through the crosslinking of the incompatible components and can be used to incorporate desired, better performing materials. In this work, we explored the use of a novel crosslinked terpolymer network composed of a hydrophobic silsesquioxane, an amphiphilic, fluorinated small molecule, **1**, and a hydrophilic sulfobetaine zwitterion, **2**, to inhibit marine fouling. The generation of the films focused on the development of two unique small molecules with fluorinated and zwitterionic character, which could be reacted with a thiol-terminated silsesquioxane using thiol-ene click chemistry. Four coatings were made varying in the molar ratio of the fluorinated and zwitterionic components. Through ATR-IR spectroscopy, an increase in the signatures attributed to water suggest an increase in zwitterionic character at the surface of the coatings with increasing amounts of the sulfobetaine in the system. Static water contact angle experiments also agree with this observation as a decrease in these values in both a dry and wet state were seen with increasing amount of zwitterion. The coatings displayed unique properties as seen through AFM and surface force spectroscopy, with the compressive moduli of the films ranging from 50 MPa to *ca.* 90 MPa as zwitterionic character of the films

decreased. The films with zwitterionic content also exhibited greater resistance to *Ulva* zoospores as zwitterionic content increased.

5.2 Experimental Section

Materials

Reagents were purchased from Sigma Aldrich and used as received unless otherwise noted. 2,3,4,5,6-Pentafluorostyrene (PFS) was purchased from Oakwood Chemical and filtered through a plug of neutral alumina prior to use. Thiopropyl T8/T10 silsesquioxane (POSS) was purchased as a 1:1 mixture of isomers from Mayaterials Inc. Sylgard 184[®] elastomer was purchased from Dow Corning and prepared according to their protocol. Bovine serum albumin (BSA) conjugated to Alexa Fluor 680 was purchased from Invitrogen. *Ulva* was purchased from Gray St. Aquatics. Alga-Gro seawater medium was received and used as from Carolina Biological Supply Company. 20 µm nylon net filters were purchased from EMD Millipore Corporation. Synthetic seawater was purchased from Ricca Chemical Company and filtered with 20 µm nylon net filter.

Nuclear Magnetic Resonance Spectroscopy and Mass Spectrometry

Briefly, compounds were characterized by ¹H, ¹³C and ¹⁹F nuclear magnetic resonance (NMR) spectroscopies using a Varian Inova 300 spectrometer. ¹H and ¹³C NMR spectra were analyzed using the solvent signal as an internal reference and ¹⁹F NMR spectra were analyzed with CF₃COOH as an external standard. High-resolution mass spectrometry (HRMS) for the monomers was conducted on an Applied Biosystems PE SCIEX QSTAR.

Atomic Force Microscopy and Surface Force Spectral Mapping

Atomic force microscopy (AFM) was performed under ambient conditions in air. AFM and force spectroscopy mapping was performed *via* AFM measurements using a Bruker Multimode 8 system in PeakForce™ tapping mode. This imaging method also provides direct surface maps of modulus, dispersion, deformation and adhesion.⁷⁸ In brief, the PeakForce™ QNM™ imaging mode uses a modified Hertzian model, the DMT model, to directly extract a reduced Young's modulus (E_r).¹¹³ The DMT model takes into account surface-tip interactions neglected in the Hertz model and also allows for mapping of adhesion force, deformation and dissipation energy. This method is described elsewhere in detail.

In these measurements, a ScanAsyst-Air (Bruker) with manufacturer specification for a spring constant of $k = 0.4$ was used. For this study, calibration was performed with a PDMS standard to determine the effective tip size. Thermal tuning of the cantilever gave a resonant frequency of 93 kHz. However, as PeakForce™ imaging uses the cantilever in an off-resonance mode of 2 kHz, this finding is not critical to the qualitative value of the imaging.

Infrared Spectroscopy

IR spectra were obtained on a Shimadzu IR Prestige attenuated total reflectance Fourier-transform infrared spectrometer (ATR-IR). Spectra were analyzed using IRsolution software package (Shimadzu). The coatings were analyzed pre- and post-water immersion in synthetic seawater.

Static Surface Contact Angle

Contact angles were measured as static contact angles using the sessile drop technique with an Attension Theta optical tensiometer (Biolin Scientific).⁷⁸ Drops were fitted with a Young-Laplace formula to calculate the static contact angle in the Theta software (Biolin Scientific). The coatings were analyzed pre- and post-water immersion in synthetic seawater.

Confocal Microscopy

Confocal imaging was performed on an Olympus FV 1000 system laser scanning confocal microscope operating with a 10× objective, a 635 nm diode laser and fluorescence collection selected by a wide band monochromator from 655 to 755 nm.

Synthesis of Fluorinated Small Molecule, 1

To a 100 mL two-necked round bottom flask was added 60 % sodium hydride (1.33 g, 33.3 mmol). The flask was placed under inert atmosphere and into an ice bath. THF (75 mL) was added dropwise to the flask. To solution was added triethylene glycol (2.00 g, 13.3 mmol) in THF (25 mL) followed by PFS (7.75 g, 39.9 mmol). The solution was then warmed to ambient temperature and allowed to stir for 18 h. Upon completion, the solution was concentrated *in vacuo* and dissolved in 250 mL of dichloromethane. The crude product was washed with brine (3 x 275 mL) and the organic layer was dried over anhydrous MgSO₄. The product was then concentrated and isolated using column chromatography. The product was then dried *in vacuo* to yield 4.42 g of product (66.6 %). IR: 2941, 2875, 1869, 1739, 1697, 1647, 1485, 1454, 1427, 1406, 1365, 1354, 1330, 1290, 1246, 1151, 1118, 1078, 1030, 1018, 966, 931, 856, 783, 753, 711 cm⁻¹. ¹H

NMR (CDCl₃) δ = 3.70 (s, 4H, -OCH₂CH₂O), 3.83 (t, J = 4.56 Hz, 4H, Ar-OCH₂CH₂O-), 4.37 (t, J = 4.57 Hz, 4H, Ar-OCH₂CH₂O), 5.63 (d, J = 11.92 Hz, 2H, *cis* CHH=CHAr), 6.03 (d, J = 18.02, 2H, *trans* CHHdCHAr), 6.62 (dd, J = 4.56 and 11.92 Hz, 2H, CH₂=CHAr) ppm. ¹³C-NMR (CDCl₃, ppm): δ 70.3, 71.0, 74.2, 110.7, 122.1, 136.5, 140.2, 142.1, 144.0 and 146.1 ppm. ¹⁹F NMR (CDCl₃) δ = -159 (s, 2F, *meta*-F), -147 (s, 2F, *ortho*-F) ppm. *T_c* = 47 °C, *T_m* = 51 °C. HRMS (m/z): calcd for C₂₂H₁₈F₈O₄, 499.1156; found, 499.1135 [M]⁺.

Synthesis of Alkene Functionalized Sulfobetaine, 2

To a dry 250 mL round bottom flask was added *N,N*-dimethylallylamine (10.0 g, 115 mmol), 1,3-propane sultone (17.2 g, 138 mmol) and acetone (100 mL). The solution was stirred for 14 hours overnight under inert atmosphere. The solution was centrifuged to remove acetone and the solid was washed with acetone (50 mL). The product was dried *in vacuo* to afford a white powder in 93% yield (26.6 g). IR: 3030, 3010, 2970, 2230, 1649, 1485, 1465, 1448, 1431, 1419, 1398, 1348, 1321, 1292, 1238, 1203, 1180, 1134, 1111, 1064, 1033, 1006, 958, 933, 908, 844, 794, 7663, 750, 655 cm⁻¹. ¹H NMR (CDCl₃, ppm): δ 2.1 (m, 2H, R-N-CH₂-CH₂-CH₂-S-R'), 2.8 (t, J = 7.42 Hz, 2H, -CH₂-CH₂-S-R'), 2.9 (s, 6H, (CH₃)₂-N-R) 3.3 (m, 2H, R-N-CH₂-CH₂-CH₂-S-R'), 3.9 (d, J = 7.22 Hz, 2H, CH₂=CH-CH₂-N-R), 5.6 (m, 2H, H₂C=CH-R) and 5.9 (m, 1H, *cis* CH₂=CH-R) ppm. ¹³C-NMR (CDCl₃, ppm): δ 18.2, 47.3, 50.0, 62.0, 66.4, 124.2 and 129.3 ppm. HRMS (m/z): calcd for C₈H₁₇NO₃S, 208.1007; found, 208.0994 [M]⁺.

Silanization of Glass Substrates

Microscope glass slides were cut into 10 × 10 mm substrates. The glass substrates were cleaned in a UV ozone cleaner for 20 m. The slides were then soaked in a solution of allyltrimethylsilane (0.5 wt %) in 300 mL of a mixture of ethanol and water (ethanol:water = 95:5). The slides were then taken out of the solution and cured in an oven at 120 °C for 18 h. The slides were stored *in vacuo* until the deposition of the coatings.

General Procedure for Preparation of Ternary Coatings on Silanized Glass Substrates

The following general procedure was followed for each sample, as defined here for the ternary coating having a **POSS:1:2** ratio of 1:4:1. To a scintillation vial was added POSS (100 mg, 0.079 mmol), **1** (157 mg, 0.32 mmol), **2** (16 mg, 0.077 mmol), 2,2-dimethoxy-2-phenylacetophenone (DMPA) (54 mg, 0.21 mmol) and a dioxane:water mixture (dioxane:water = 9:1, 9 mL) and the mixture was stirred magnetically until homogeneous. The solution was drop cast (0.08 mL per slide) onto 10 × 10 mm silanized glass slides. A period of *ca.* 10 min allowed for the solvent to evaporate, and then the coating was cured under in a UV oven at 365 nm for 2 h. After curing, the coatings were stored *in vacuo* until measurements were performed.

***Ulva* Zoospores Settlement and Growth**

Ulva zoospores were collected and suspended into synthetic seawater. The zoospore suspension was filtered with 20 µm nylon net filters and further diluted to an OD₆₀₀ of 0.24. For each type of substrate, six replicates were placed in a polystyrene petri dish

and 7 mL of zoospores suspension were added. The substrates were incubated in the zoospores suspension for 3 hours in the dark before being rinsed lightly with synthetic seawater (3×). Three replicates were fixed with 2.5% glutaraldehyde and rinsed lightly with nanopure water. Z-stacked confocal fluorescence images were taken of the zoospores exposed surfaces and the resultant intensity histograms were used for quantification of the autofluorescence of chlorophyll present in the zoospores. The remaining three replicates of each substrate were incubated in Alga-Gro seawater medium with a light to dark cycle of 16:8 hours and medium was changed every 2 days for one week.

5.3 Results and Discussion

The synthetic strategy for the synthesis of the generated films was based on a byproduct from the synthesis of hyperbranched fluropolymer. The byproduct of the reaction, **1**, holds great potential in the development of novel materials because of the inherent amphiphilic character of the molecule coupled with the bis-functionality presented via the styrenyl heads. To synthesize compound **1**, a nucleophilic aromatic substitution reaction was performed between two pentafluorostyrene units with triethylene glycol in the presence of sodium hydride to generate the desired product (**Figure 5.1**). A second synthesis was used to incorporate an alkene-functionalized zwitterionic molecule, **2**. Compound **2** was formed through a ring opening reaction of 1,3-propanesultone with N,N-dimethylamine to synthesize the desired zwitterionic product in a 93% yield (**Figure 5.2**).

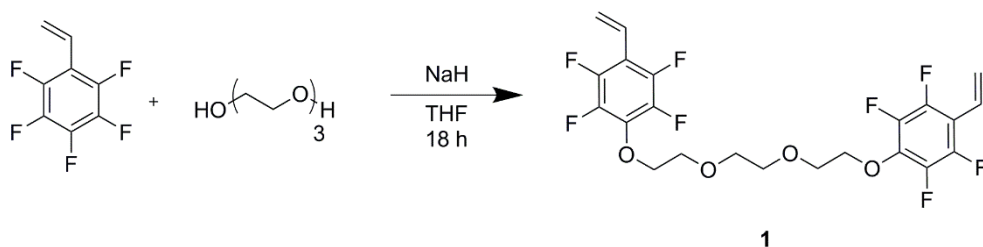


Figure 5.1. Synthesis of the fluorinated small molecule, **1**.

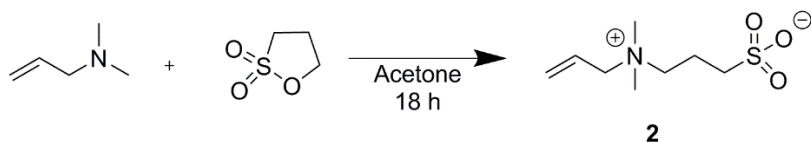


Figure 5.2. Synthesis of alkene functionalized sulfobetaine, **2**.

The synthesized molecules, **1** and **2**, were then prepared for crosslinking with a thiol terminated silsesquioxane in the presence of a photoinitiator, DMPA. The styrenyl heads of compound **1** in combination with the thiol terminated silsesquioxane allow for a high modulus system to be created with very little synthetic effort. The alkene functionalized zwitterion, **2**, allows for the ability to distribute charges throughout the bulk of the film in an effort to minimize losing zwitterionic character due to surface reorganization upon submersion in water and allow for a high probability of surface bound water to deter further settlement by marine organisms.

To determine the influence of the fluorinated and zwitterionic characteristics of the systems, four coatings were generated varying in the stoichiometric ratios of compounds **1** and **2**, while maintaining a constant amount of POSS (**Figure 5.3, Table 8**). It should

be noted that because compound **1** has the bis-functional styrenyl heads, its loading concentrations in the films cannot be lowered further as to maintain the ability for the film to be crosslinked. The solutions were deposited onto an alkene functionalized glass surface using solvent deposition prior to reacting in a UV oven at 365 nm for 2 hours to generate the crosslinked ternary coatings.

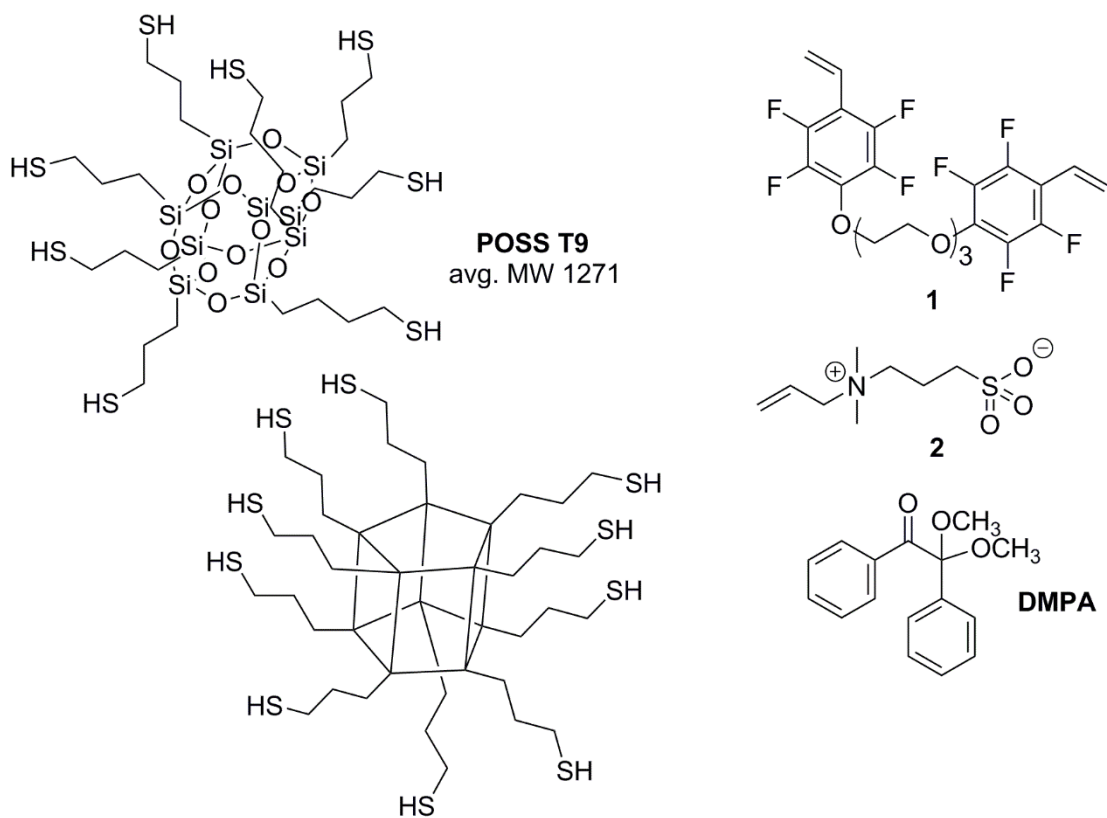


Figure 5.3. Compounds of the ternary coatings.

Table 8. Ratios of the compounds in the composition of the ternary coatings.

Coating	POSS	1	2	DMPA
A	1	4.5	0	2.7
B	1	4	1	2.7
C	1	3.5	2	2.7
D	1	3	3	2.7

To initially investigate the surface composition of the various coatings, attenuated total reflectance-infrared spectroscopy (ATR-IR) was performed (**Figure 5.4**). The measurements were performed pre- (dry) and post-water (wet) immersion to assess the changes in the surface after exposure to synthetic seawater. In the dry state, there are very subtle spectroscopic changes from coating **A** to **C**. The differences in the coatings are manifested in the characteristic water signal around 3350 cm^{-1} as well as at 1035 cm^{-1} and 1650 cm^{-1} , which becomes more prevalent with increasing amounts of molecule **2**. These signals are more pronounced in the films post-water immersion because of the zwitterionic content of the films as films with higher concentrations of compound **2** have increasingly higher intensities in their water signals.

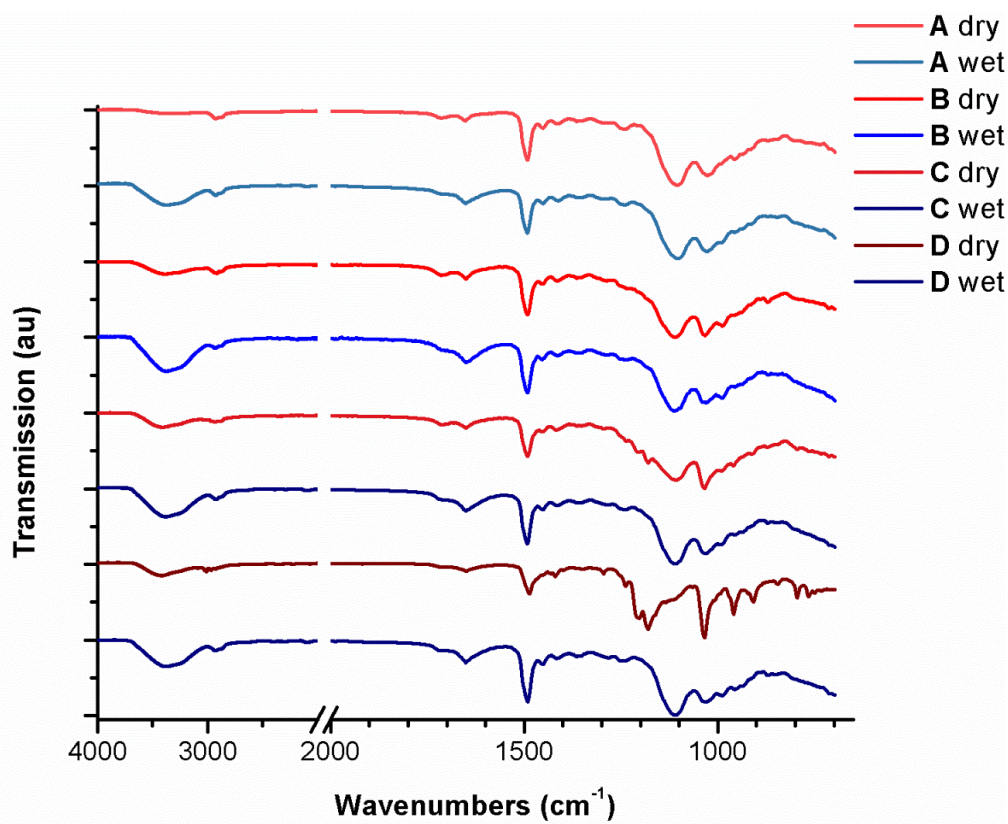


Figure 5.4. ATR-IR spectra for coatings A, B, C and D pre- (dry) and post-water (wet) immersion.

A static water contact angle experiment was performed pre- and post-water immersion of the coatings to determine if the influence of compound **2** on the system as a whole (**Table 9**). In the dry state, there is an overall decrease upon increasing amounts of zwitterionic character to the system. Upon testing the surfaces post-water immersion, there is an overall decrease in the static water contact of all the systems, indicating normal wetting behavior upon exposure to water. There is also a general trend towards a decreasing static water contact angle upon addition of the zwitterions, which is in agreement with the data from ATR-IR studies. While coating **A** displayed a lower static

water contact angle in the wet state than coating **B**, this finding is most likely because molecule **1** is present in the system. This molecule contains a triethylene glycol moiety, which could be exposed at the surface and lead to a decrease in the static water contact angle.

Table 9. Summary of static water contact angle data for all coatings pre- and post-water immersion.

Coating	Pre-Water Immersion	Post-Water Immersion
A	91 ± 1°	82 ± 3°
B	90 ± 4°	82 ± 5°
C	87 ± 2°	77 ± 4°
D	82 ± 7°	76 ± 3°

To test the topographical variations on the nanoscale and microscale, atomic force microscopy (AFM) was used. As displayed in previous work, surface force spectroscopy measurements can be performed simultaneously as AFM using quantitative nanomechanical mapping (QNM) to determine the compressive moduli at the nanoscale. Through these experiments, the most unique coating, in regards to topography, was seen to be coating **A**, the coating which contained no zwitterionic character (**Figure 5.5**). Coating **A** also shows an aggregates at the surface about 25 nm in height, and the aggregates have a higher compressive modulus than the surrounding areas, suggesting portions of the coating which are predominantly stiffer and composed of higher amounts of POSS (**Figure 5.6**). Upon the addition of the zwitterionic component, **2**, to the

system, there is an overall decrease in the surface roughness of the coatings. These three coatings, **B**, **C** and **D**, display no differences in surface topography in comparison with each other through the average roughness values (R_a) and root mean squared roughness values (R_q) (**Figure 5.5** and **Table 10**).

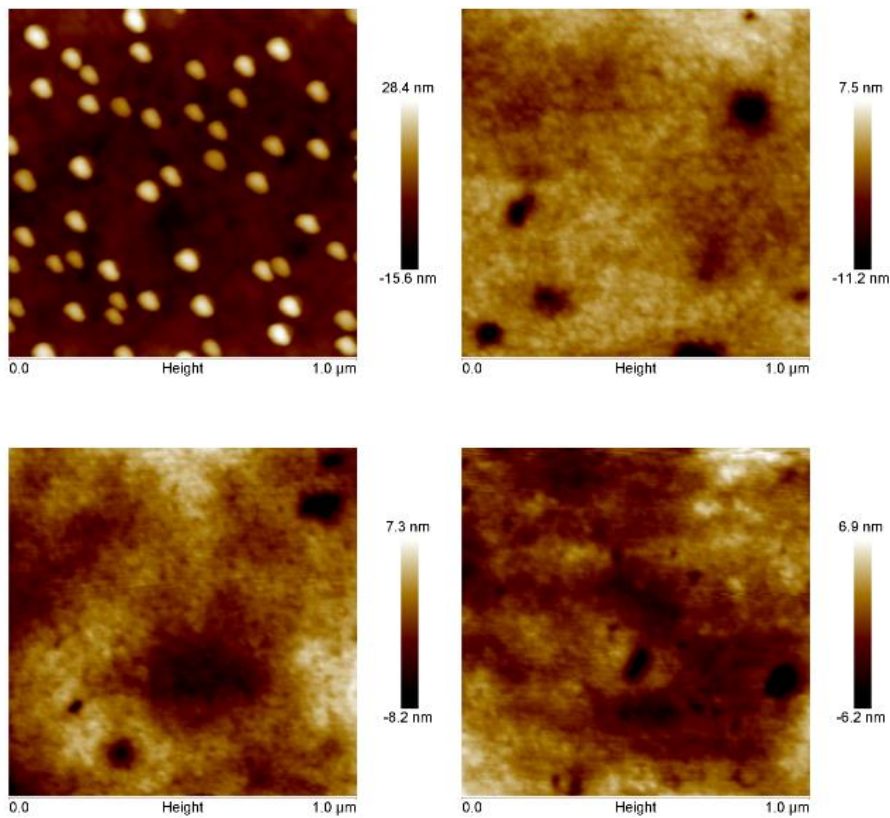


Figure 5.5. AFM micrographs of coating A (top left), B (top right), C (bottom left) and D (bottom right), 1 mm × 1 mm field of view.

However, there is a difference seen in the compressive moduli at this scale for the three coatings, with an overall decrease of the compressive moduli upon increasing

amounts of **2** (Table 10). This result is not surprising and is hypothesized to occur due to two reasons. The first reason is that there is a decrease in the crosslink density of the system with increasing amounts of compound **2**, which could possibly lead to an overall decrease in the compressive moduli of the coatings. The second reason is the inclusion of the zwitterionic component into the system, as there could be more water bound to the coating dermally and subdermally with increasing amounts of the sulfobetaine, leading to softer surface features and compressive moduli values.

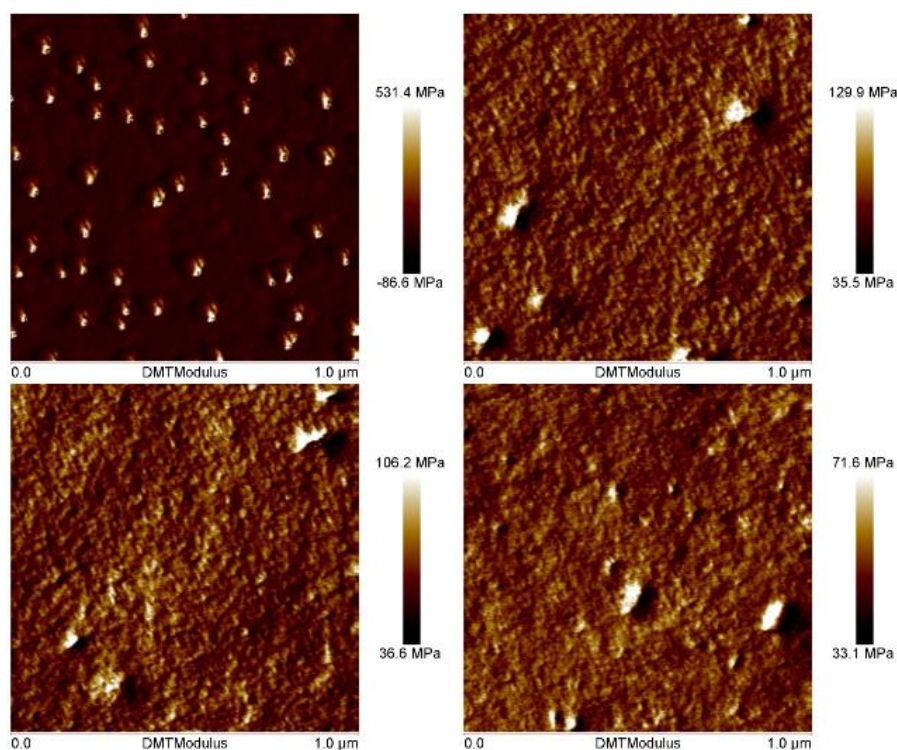


Figure 5.6. Force spectra of the compressive modulus channel transposed on AFM micrographs of coating A (top left), B (top right), C (bottom left) and D (bottom right), 1 mm × 1 mm field of view.

Table 10. Summary of AFM and surface force spectroscopy data for all coatings.

Coating	R_a (nm)	R_q (nm)	Mean Compressive Modulus (MPa)
A	4.6	6.6	77.8
B	1.6	2.2	76.9
C	1.7	2.2	67.1
D	1.5	2.0	50.9

To assess the coatings' anti-fouling performance, an settlement assay was performed with *Ulva* zoospores. *Ulva*, a genus of common, green macroalgae found throughout the world, are a widely studied fouling organism and act as a model for soft foulers.¹¹⁴ The coatings were soaked in a solution of *Ulva* zoospores prior to incubating the samples for one week. The coatings were also tested against three standards, glass, silanized glass and a known PDMS anti-fouling standard, Sylgard 184[®]. After one week of incubation, all of the coatings outperformed the PDMS standard, with *ca.* 50% or less fouling present (**Figure 5.7**). As the zwitterionic character of the system increased due to compound **2**, there was an increase in the deterrence of fouling on the surface. The zwitterionic character allows for a decrease in the surface energy of the system due to a greater amount of water hydration, which also extends to an improved anti-fouling ability. The results of this study indicate a suitable platform for anti-fouling technologies which will be tested further with larger scale assays with various marine organisms.

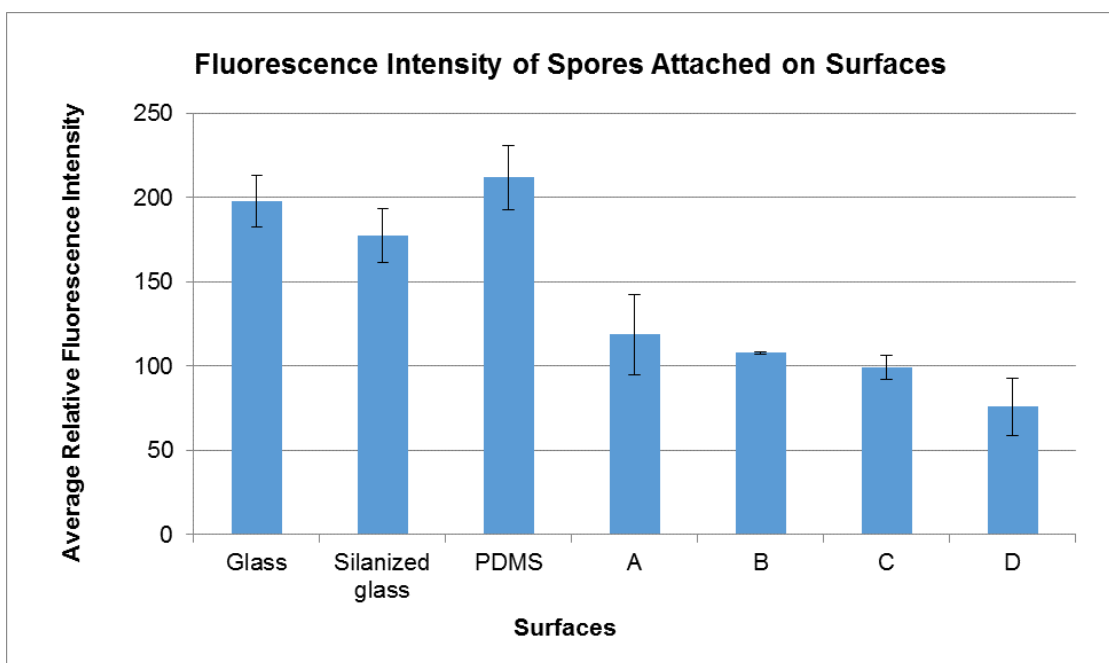


Figure 5.7. Average fluorescence intensity of *Ulva* zoospores on standard coatings and the different variations of zwitterionic coatings after one week of incubation.

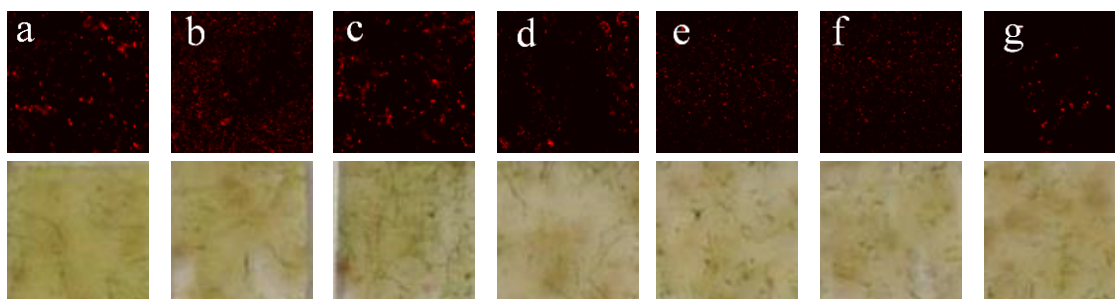


Figure 5.8. Confocal micrographs of the surfaces *Ulva* incubation for one week. a) glass; b) silanized glass; c) Sylgard® 184; d) coating A; e) coating B; f) coating C; g) coating D. Each micrograph is a combined z-stack image of a 10 μm depth field of view taken at 1 μm increments. The x-y field of view is 2 mm. Excitation occurred via a 635 nm diode laser, with emission collection selected from 655 nm to 755 nm using a monochromator and a PMT.

5.4 Conclusions

In summary, a series of amphiphilic, zwitterionic coatings have been generated using thiol-ene click chemistry with variations in the stoichiometric ratios of both the fluorinated and zwitterionic components. As the zwitterionic content of the system increased, there was a decrease in the static water contact angle pre- and post-water immersion as well. The films displayed robust mechanical properties on the micron and sub-micron scales with compressive moduli in ranging from 50 to 90 MPa, with the compressive moduli decreasing for films with increasing concentrations of sulfobetaine. Lastly, anti-fouling assays were performed with *Ulva* zoospores and films with zwitterionic character were shown to display superior anti-fouling properties compared to a PDMS standard. Among the films studied with zwitterionic character, the inhibition of settlement of the *Ulva* zoospores increased with an increase in zwitterionic character of the system, indicating a potential system for future anti-fouling coatings.

CHAPTER VI

CONCLUSIONS

6.1 Conclusions

In closing, this dissertation presents work that has led to significant advancements in the development of anti-biofouling coatings, specifically in regards to systems based on HBFP crosslinked systems. Through the incorporation of PDMS in combination with HBFP and PEG, the system shows improved fouling release performance compared to both the HBFP-PEG binary system and a commercially-available siloxane standard. The work was then extended further through the development of a spray coating technique, allowing for the polymeric network to be deposited onto an epoxy barrier coating without the issue of coating delamination and reducing the amount of materials needed to generate the terpolymer network, driving down the cost of production of the HBFP-PEG-PDMS systems. Using this application method, panels were coated with the terpolymer network and tested in drydock harbors around the United States. In this testing, the networks show inferior settlement compared to a commercially-available anti-biofouling coating, but show comparable results in fouling release studies. Lastly, the ability to modify the system through the use of three new chemical components was investigated. This system allowed for the introduction of a silsesquioxane as a hydrophobic component and a zwitterion as the hydrophilic component to allow for added mechanical robustness and surface water hydration to allow for an increase in anti-biofouling performance.

Chapter 2 introduces the concept of the ternary system, specifically expressed as a system blending three unique classes of polymers, fluoropolymer, siloxanes and PEGylated materials. In this chapter, the method of producing HBFP-PEG-PDMS coatings and the properties which they displayed were discussed. A series of HBFP-PEG-PDMS coatings were generated with varying concentrations of PEG and PDMS. Surface analysis of the networks in both the pre-water swollen and post-water swollen states presented information regarding the surface composition of each of the systems, with the most notable findings being the dynamic surface reorganization which occurs in the films upon exposure to water and the ability for the surface energy of the surfaces to be modified *via* a change in the weight percentages of PEG and PDMS. An in-depth study of one terpolymer network using surface force spectroscopy demonstrated a surface dominated by HBPF and PDMS in the raised nanoscopic features of the system and PEG dominant in the valleys between the raised features. A non-specific protein adsorption study was performed with BSA and displayed the ability for the terpolymer systems to resist fouling events. Finally, the mechanical properties of the system were tested and were seen to be robust enough for both marine and biomedical environments. This study provided a method of generating of multiply-complex systems composed of HBFP, PEG and PDMS which could be used as next generation anti-biofouling coatings.

Chapter 3 expands upon the concept of the terpolymer network, but addressed the problems associated with attaching these systems on a larger scale. Through the use of an epoxy barrier coating, the terpolymer network was adhered to substrates for anti-biofouling assays. The systems displayed optimal attachment to the undercoat and were

seen to show no loss of surface properties for 90 days of testing. A series of coatings was then prepared with a constant amount of PEG, 75 wt %, and concentrations of PDMS, 25, 50 and 75 wt %, respectively, and tested against two species of barnacle cyprids, *Balanus amphitrite* and *Balanus improvisus*. Results from these studies demonstrated the terpolymer networks had an increase in the ability to deter and release fouling with increasing amounts of PDMS. Future studies with these organisms can allow for more optimizations to be made in the terpolymer coatings, specifically in regards to the amount of PEG and PDMS in the system to determine an optimal concentration of each which leads to the most optimal anti-fouling and fouling release properties.

In Chapter 4, long-term static immersion testing was performed on the terpolymer coatings created in Chapter 3. This study aimed to address the anti-fouling and fouling release properties of the systems against the wide spectrum of organisms present in various marine environments across the United States. The ability for the coatings to deter fouling was seen to be variable dependant on the testing site, but a general trend was seen with coatings having 75 wt % PEG & 50 wt % PDMS and 75 wt % PEG and 75 wt % PDMS outperforming the coatings with 75 wt % PEG and 25 wt % PDMS in anti-fouling and fouling release studies. Results from the Morro Bay, California site yielded an interesting result with the coatings containing 75 wt % PEG & 50 wt % PDMS having similar fouling ratings to a commercially used anti-fouling paint, Intersleek 900, after 3 months. The results from Pearl Harbor, Hawaii also exhibited the ability to deter fouling on a longer timescale, with all coatings having less than 20%

fouling after two months of immersion in this location. Overall, this study demonstrated the complexity of fouling organisms and how variations in the species and their specific methods of attachment to surfaces as well as the differences present in water salinity and temperature can affect the long-term performance of anti-fouling coatings. The shortcomings and variability of the terpolymer coatings in this study will need to be addressed prior to future static water immersion testing. These shortcomings lie in the performance of the HBFP-PEG-PDMS systems and the reasoning for the reduction in fouling performance will need to be addressed. Future studies will be directed at using more advanced analytical techniques, such as environmental scanning electron microscopy or SIMS, on the coatings pre- and post-fouling to allow for more direct correlations to be made between the decreased performance and the chemical composition at the surface.

The concept of the ternary networks was expanded in Chapter 5 through the generation of UV-crosslinked systems composed of an amphiphilic, fluorinated small molecule, a hydrophobic silsesquioxane and a sulfobetaine zwitterion. These coatings aimed to elaborate on the concept of the ternary systems through the use of the silsesquioxane, which would add mechanical robustness to the system, and the zwitterion, which possibly allows for a higher degree of surface bound water to the system. A series of coatings were generated varying in the stoichiometric ratios of both the fluorinated and zwitterionic components, and investigated using static water contact angle and ATR-IR spectroscopy pre- and post-water immersion. These studies displayed that coatings with increasing amounts of zwitterions had decreasing static water contact angle and

increasing amounts of water as seen through the ATR-IR spectra. The films with sulfobetaine had very similar surface features as measured through AFM, but had decreasing compressive moduli values with increasing amounts of sulfobetaine. The coatings were then tested against *Ulva*, and displayed an increasing resistance to fouling with increasing amounts of zwitterionic content. This study exhibited the ability for further development of the ternary system through the incorporation of different functionalities which enable the resultant system to have a blend of the best properties of each individual component. Future work in this project will aim to test the anti-fouling capabilities of these coatings against a variety of marine organisms including *Ulva linza*, *Balanus amphitrite* and *Navicula incerta*.

The work presented in this dissertation has contributed in the advancement of anti-fouling coatings based on HBFP as well as coatings consisting of three unique chemical components. The ability to create systems with varying functionalities which display heterogeneities on the nano- and micro-scales can allow for the generation of increasingly complex systems that may deter greater amounts of fouling in a marine environment. The ability to adhere these systems to an undercoat is also of great importance as it provides a relevant platform for the widespread use of these coatings and reduces the cost of the system through the use of decreased amounts of the terpolymer networks. However, while the current iteration of the epoxy undercoat is an accomplishment, the long-term fouling capabilities of the terpolymer coatings is a concern. Currently, it is unknown if any changes in the surface chemistry of the systems are due to further surface rearrangement, or if the fouling release properties are

compromised due to initial fouling events on the surface. The surface reorganization on the films can be analyzed through static water contact angle measurements to more accurately determine the timescale on which surface reorganization occurs. Additionally, future coatings studied with anti-fouling assays will need to be analyzed in-depth pre- and post-water immersion, as well as post-fouling events. Because of the possibility of minor changes in the surfaces of the systems, more sensitive techniques will be necessary to monitor nanoscopic variations in the surface chemistry to determine possible causes of the decrease in fouling properties.

The curing conditions of the terpolymer coating, 110 °C for 45 min, is not necessarily feasible on an industrial scale and can be addressed through two differing routes. The first route involves curing the coatings at ambient temperatures for prolonged times (*ca.* 24 h), and the second involves using different crosslinking chemistries such as thiol-ene click chemistry to generate coatings more rapidly. Both routes offer possible solutions to the problem, but each has drawbacks as well. A drawback of curing at ambient temperatures leaves a possibility for incomplete crosslinking to occur as the chain ends become locked into set conformations after partial curing, while using changing the chemistries used requires variations of functional handles of the polymers being used to facilitate the reactions. Both routes, as well as current crosslinking conditions with all variations of the ternary networks, will need to be analyzed in-depth using sol-gel studies to determine the extent of crosslinking. There is also the possibility of incorporating additional functionality in the terpolymer systems through molecules that present alternate methods of fouling rejections, such as zwitterionic molecules or active

deterrents. Using a similar approach to the BRA 640 may also yield improvements in the terpolymer systems through the addition of ablative properties. Ablation would allow for the heterogeneity of the terpolymer networks to be expressed over extended periods and could allow for the release of the problematic microbial fouling, which was seen throughout the static water immersion testing facilities. However, the challenges in making an ablative coating, such as creating a film that ablates slowly, displays suitable thickness to prevent reapplication of the coatings and expresses the heterogeneities over years would need to be addressed when considering these systems.

In summary, biofouling creates a very complex problem to control, especially when considering the vast enormity in structural and fouling variations as seen in biological systems, and this research contributes to the advancement of the current technologies and gives insight into the direction of anti-fouling coatings in the future.

REFERENCES

1. Videla, H. A., Prevention and Control of Biocorrosion. *International Biodeterioration & Biodegradation* **2002**, *49*, 259-270.
2. Kirschner, C. M.; Brennan, A. B., Bio-Inspired Antifouling Strategies. *Annual Review of Materials Research* **2012**, *42*, 211-229.
3. Mansouri, J.; Harrison, S.; Chen, V., Strategies for Controlling Biofouling in Membrane Filtration Systems: Challenges and Opportunities. *Journal of Materials Chemistry* **2010**, *20*, 4567-4586.
4. Baier, R. E., Conditioning Surfaces to Suit the Biomedical Environment: Recent Progress. *Journal of Biomechanical Engineering* **1982**, *104*, 257-271.
5. Baier, R. E.; Meyer, A. E., Aspects of Bioadhesion. In *Fundamentals of Adhesion*, Lee, L.-H., Ed. Springer US: 1991; pp 407-425.
6. Maréchal, J.-P.; Hellio, C., Challenges for the Development of New Non-Toxic Antifouling Solutions. *International Journal of Molecular Sciences* **2009**, *10*, 4623-4637.
7. Schultz, M. P.; Bendick, J. A.; Holm, E. R.; Hertel, W. M., Economic Impact of Biofouling on a Naval Surface Ship. *Biofouling* **2010**, *27*, 87-98.
8. Townsin, R. L., The Ship Hull Fouling Penalty. *Biofouling* **2003**, *19*, 9-15.
9. Tribou, M.; Swain, G., The Use of Proactive In-water Grooming to Improve the Performance of Ship Hull Antifouling Coatings. *Biofouling* **2009**, *26*, 47-56.
10. Turner, A., Marine Pollution from Antifouling Paint Particles. *Marine Pollution Bulletin* **2010**, *60*, 159-171.
11. Champ, M. A., A Review of Organotin Regulatory Strategies, Pending Actions, Related Costs and Benefits. *Science of The Total Environment* **2000**, *258*, 21-71.
12. Dafforn, K. A.; Lewis, J. A.; Johnston, E. L., Antifouling Strategies: History and Regulation, Ecological Impacts and Mitigation. *Marine Pollution Bulletin* **2011**, *62*, 453-465.
13. Champ, M. A., Economic and Environmental Impacts on Ports and Harbors from the Convention to Ban Harmful Marine Anti-fouling Systems. *Marine Pollution Bulletin* **2003**, *46*, 935-940.

14. Banerjee, I.; Pangule, R. C.; Kane, R. S., Antifouling Coatings: Recent Developments in the Design of Surfaces That Prevent Fouling by Proteins, Bacteria, and Marine Organisms. *Advanced Materials* **2011**, *23*, 690-718.
15. Buskens, P.; Wouters, M.; Rentrop, C.; Vroon, Z., A Brief Review of Environmentally Benign Antifouling and Foul-release Coatings for Marine Applications. *J Coat Technol Res* **2013**, *10*, 29-36.
16. Yebra, D. M.; Kiil, S.; Dam-Johansen, K., Antifouling Technology — Past, Present and Future Steps Towards Efficient and Environmentally Friendly antifouling Coatings. *Progress in Organic Coatings* **2004**, *50*, 75-104.
17. Gudipati, C. S.; Greenlief, C. M.; Johnson, J. A.; Prayongpan, P.; Wooley, K. L., Hyperbranched Fluoropolymer and Linear Poly(ethylene glycol) Based Amphiphilic Crosslinked Networks as Efficient Antifouling Coatings: An Insight into the Surface Compositions, Topographies, and Morphologies. *Journal of Polymer Science Part A: Polymer Chemistry* **2004**, *42*, 6193-6208.
18. Efimenko, K.; Finlay, J.; Callow, M. E.; Callow, J. A.; Genzer, J., Development and Testing of Hierarchically Wrinkled Coatings for Marine Antifouling. *ACS Applied Materials & Interfaces* **2009**, *1*, 1031-1040.
19. Callow, M. E.; Fletcher, R. L., The Influence of Low Surface Energy Materials on Bioadhesion — A Review. *International Biodeterioration & Biodegradation* **1994**, *34*, 333-348.
20. Krishnan, S.; Weinman, C. J.; Ober, C. K., Advances in Polymers for Antibiofouling Surfaces. *Journal of Materials Chemistry* **2008**, *18*, 3405-3413.
21. Xu, Q.; Barrios, C. A.; Cutright, T.; Zhang Newby, B.-m., Evaluation of Toxicity of Capsaicin and Zosteric Acid and their Potential Application as Antifoulants. *Environmental Toxicology* **2005**, *20*, 467-474.
22. Majumdar, P.; Crowley, E.; Htet, M.; Stafslie, S. J.; Daniels, J.; VanderWal, L.; Chisholm, B. J., Combinatorial Materials Research Applied to the Development of New Surface Coatings XV: An Investigation of Polysiloxane Anti-Fouling/Fouling-Release Coatings Containing Tethered Quaternary Ammonium Salt Groups. *ACS Combinatorial Science* **2011**, *13*, 298-309.
23. Ekblad, T.; Bergström, G.; Ederth, T.; Conlan, S. L.; Mutton, R.; Clare, A. S.; Wang, S.; Liu, Y.; Zhao, Q.; D'Souza, F.; Donnelly, G. T.; Willemsen, P. R.; Pettitt, M. E.; Callow, M. E.; Callow, J. A.; Liedberg, B., Poly(ethylene glycol)-Containing Hydrogel Surfaces for Antifouling Applications in Marine and Freshwater Environments. *Biomacromolecules* **2008**, *9*, 2775-2783.

24. Jiang, S.; Cao, Z., Ultralow-Fouling, Functionalizable, and Hydrolyzable Zwitterionic Materials and Their Derivatives for Biological Applications. *Advanced Materials* **2010**, *22*, 920-932.
25. Brady, R. F.; Bonafede, S. J.; Schmidt, D. L., Self-assembled Water-borne Fluoropolymer Coatings for Marine Fouling Resistance. *Surface Coatings International* **1999**, *82*, 582-585.
26. Pieper, R.; Ekin, A.; Webster, D.; Cassé, F.; Callow, J.; Callow, M., Combinatorial Approach to Study the Effect of Acrylic Polyol Composition on the Properties of Crosslinked Siloxane-polyurethane Fouling-release Coatings. *J Coat Technol Res* **2007**, *4*, 453-461.
27. Brady, R. F.; Singer, I. L., Mechanical Factors Favoring Release from Fouling Release Coatings. *Biofouling* **2000**, *15*, 73-81.
28. Brady Jr, R. F., A Fracture Mechanical Analysis of Fouling Release from Nontoxic Antifouling Coatings. *Progress in Organic Coatings* **2001**, *43*, 188-192.
29. Gudipati, C. S.; Finlay, J. A.; Callow, J. A.; Callow, M. E.; Wooley, K. L., The Antifouling and Fouling-Release Performance of Hyperbranched Fluoropolymer (HBFP)-Poly(ethylene glycol) (PEG) Composite Coatings Evaluated by Adsorption of Biomacromolecules and the Green Fouling Alga *Ulva*. *Langmuir* **2005**, *21*, 3044-3053.
30. Chen, S.; Li, L.; Zhao, C.; Zheng, J., Surface Hydration: Principles and Applications Toward Low-fouling/nonfouling Biomaterials. *Polymer* **2010**, *51*, 5283-5293.
31. He, Y.; Hower, J.; Chen, S.; Bernards, M. T.; Chang, Y.; Jiang, S., Molecular Simulation Studies of Protein Interactions with Zwitterionic Phosphorylcholine Self-Assembled Monolayers in the Presence of Water. *Langmuir* **2008**, *24*, 10358-10364.
32. Imbesi, P. M.; Finlay, J. A.; Aldred, N.; Eller, M. J.; Felder, S. E.; Pollack, K. A.; Lonnecker, A. T.; Raymond, J. E.; Mackay, M. E.; Schweikert, E. A.; Clare, A. S.; Callow, J. A.; Callow, M. E.; Wooley, K. L., Targeted Surface Nanocomplexity: Two-dimensional Control over the Composition, Physical Properties and Anti-biofouling Performance of Hyperbranched Fluoropolymer-Poly(ethylene glycol) Amphiphilic Crosslinked Networks. *Polym. Chem.* **2012**, *3*, 3121-3131.
33. Krishnan, S.; Wang, N.; Ober, C. K.; Finlay, J. A.; Callow, M. E.; Callow, J. A.; Hexemer, A.; Sohn, K. E.; Kramer, E. J.; Fischer, D. A., Comparison of the

Fouling Release Properties of Hydrophobic Fluorinated and Hydrophilic PEGylated Block Copolymer Surfaces: Attachment Strength of the Diatom *Navicula* and the Green Alga *Ulva*. *Biomacromolecules* **2006**, *7*, 1449-1462.

34. Weinman, C. J.; Finlay, J. A.; Park, D.; Paik, M. Y.; Krishnan, S.; Sundaram, H. S.; Dimitriou, M.; Sohn, K. E.; Callow, M. E.; Callow, J. A.; Handlin, D. L.; Willis, C. L.; Kramer, E. J.; Ober, C. K., ABC Triblock Surface Active Block Copolymer with Grafted Ethoxylated Fluoroalkyl Amphiphilic Side Chains for Marine Antifouling/Fouling-Release Applications. *Langmuir* **2009**, *25*, 12266-12274.
35. Martinelli, E.; Suffredini, M.; Galli, G.; Glisenti, A.; Pettitt, M. E.; Callow, M. E.; Callow, J. A.; Williams, D.; Lyall, G., Amphiphilic Block Copolymer/Poly(dimethylsiloxane) (PDMS) Blends and Nanocomposites for Improved Fouling-release. *Biofouling* **2011**, *27*, 529-541.
36. Bartels, J. W.; Cheng, C.; Powell, K. T.; Xu, J.; Wooley, K. L., Hyperbranched Fluoropolymers and their Hybridization into Complex Amphiphilic Crosslinked Copolymer Networks. *Macromolecular Chemistry and Physics* **2007**, *208*, 1676-1687.
37. Chisholm, B., J.; Christianson, D., A. Amphiphilic Fouling Release Coatings. U.S. Patent 20120255480, Oct. 11, 2012.
38. Feng, S.; Wang, Q.; Gao, Y.; Huang, Y.; Qing, F.-L., Synthesis and Characterization of a Novel Amphiphilic Copolymer Capable as Anti-biofouling Coating material. *Journal of Applied Polymer Science* **2009**, *114*, 2071-2078.
39. Martinelli, E.; Sarvothaman, M. K.; Alderighi, M.; Galli, G.; Mielczarski, E.; Mielczarski, J. A., PDMS Network Blends of Amphiphilic Acrylic Copolymers with Poly(ethylene glycol)-fluoroalkyl Side Chains for Fouling-release Coatings. I. Chemistry and Stability of the Film Surface. *Journal of Polymer Science Part A: Polymer Chemistry* **2012**, *50*, 2677-2686.
40. Bartels, J. W.; Cheng, C.; Powell, K. T.; Xu, J.; Wooley, K. L., Hyperbranched Fluoropolymers and their Hybridization into Complex Amphiphilic Crosslinked Copolymer Networks. *Macromol. Chem. Phys.* **2007**, *208*, 1676-1687.
41. Gan, D.; Mueller, A.; Wooley, K. L., Amphiphilic and Hydrophobic Surface Patterns Generated from Hyperbranched Fluoropolymer/Linear Polymer Networks: Minimally Adhesive Coatings via the Crosslinking of Hyperbranched Fluoropolymers. *Journal of Polymer Science Part A: Polymer Chemistry* **2003**, *41*, 3531-3540.

42. Powell, K. T.; Cheng, C.; Wooley, K. L., Complex Amphiphilic Hyperbranched Fluoropolymers by Atom Transfer Radical Self-Condensing Vinyl (Co)polymerization. *Macromolecules* **2007**, *40*, 4509-4515.
43. Dobretsov, S.; Romani, A. M.; Spratt, D. A.; Ready, D.; Pratten, J., Introduction to Microbial Fouling. In *Biofouling*, Dürr, S.; Thomason, J., Eds. Wiley-Blackwell: West Sussex, 2010; pp 121-122.
44. Edyvean, R., Consequences of Fouling on Shipping. In *Biofouling*, Dürr, S.; Thomason, J., Eds. Wiley-Blackwell: West Sussex, 2010; pp 217-225.
45. Finnie, A. A.; Williams, D. N., Paint and Coatings Technology for the Control of Marine Fouling. In *Biofouling*, Dürr, S.; Thomason, J., Eds. Wiley-Blackwell: West Sussex, 2010; pp 185-206.
46. Grozea, C. M.; Walker, G. C., Approaches in Designing Non-toxic Polymer Surfaces to Deter Marine Biofouling. *Soft Matter* **2009**, *5*, 4088-4100.
47. Ladd, J.; Zhang, Z.; Chen, S.; Hower, J. C.; Jiang, S., Zwitterionic Polymers Exhibiting High Resistance to Nonspecific Protein Adsorption from Human Serum and Plasma. *Biomacromolecules* **2008**, *9*, 1357-1361.
48. Yu, M.; Urban, M. W., Polymeric Surfaces with Anticoagulant, Antifouling, and Antimicrobial Attributes. *Macromolecular Symposia* **2009**, *283-284*, 311-318.
49. Webster, D. C.; Chisholm, B. J., New Directions in Antifouling Technology. In *Biofouling*, Dürr, S.; Thomason, J., Eds. Wiley-Blackwell: West Sussex, 2010; pp 366-387.
50. Wang, Y.; Betts, D. E.; Finlay, J. A.; Brewer, L.; Callow, M. E.; Callow, J. A.; Wendt, D. E.; DeSimone, J. M., Photocurable Amphiphilic Perfluoropolyether/Poly(ethylene glycol) Networks for Fouling-Release Coatings. *Macromolecules* **2011**, *44*, 878-885.
51. Yasani, B. R.; Martinelli, E.; Galli, G.; Glisenti, A.; Mieszkin, S.; Callow, M. E.; Callow, J. A., A Comparison Between Different Fouling-release Elastomer Coatings Containing Surface-active Polymers. *Biofouling* **2014**, *30*, 387-399.
52. Schumacher, J.; Carman, M.; Estes, T.; Feinberg, A.; Wilson, L.; Callow, M.; Callow, J.; Finlay, J.; Brennan, A., Engineered Antifouling Microtopographies - Effect of Feature Size, Geometry, and Roughness on Settlement of Zoospores of the Green Alga *Ulva*. *Biofouling* **2007**, *23*, 55-62.

53. Vaidya, A.; Chaudhury, M. K., Synthesis and Surface Properties of Environmentally Responsive Segmented Polyurethanes. *Journal of Colloid and Interface Science* **2002**, *249*, 235-245.
54. Hirao, A.; Sugiyama, K.; Yokoyama, H., Precise Synthesis and Surface Structures of Architectural Per- and Semifluorinated Polymers with Well-defined Structures. *Prog. Polym. Sci.* **2007**, *32*, 1393-1438.
55. Andruzzi, L.; Chiellini, E.; Galli, G.; Li, X.; Kang, S. H.; Ober, C. K., Engineering Low Surface Energy Polymers through Molecular Design: Synthetic Routes to Fluorinated Polystyrene-based Block Copolymers. *J. Mater. Chem.* **2002**, *12*, 1684-1692.
56. Li, X.; Andruzzi, L.; Chiellini, E.; Galli, G.; Ober, C. K.; Hexemer, A.; Kramer, E. J.; Fischer, D. A., Semifluorinated Aromatic Side-Group Polystyrene-Based Block Copolymers: Bulk Structure and Surface Orientation Studies. *Macromolecules* **2002**, *35*, 8078-8087.
57. Mueller, A.; Kowalewski, T.; Wooley, K. L., Synthesis, Characterization, and Derivatization of Hyperbranched Polyfluorinated Polymers. *Macromolecules* **1998**, *31*, 776-786.
58. Mark James, E., Overview of Siloxane Polymers. In *Silicones and Silicone-Modified Materials*, American Chemical Society: 2000; Vol. 729, pp 1-10.
59. Gasteier, P.; Reska, A.; Schulte, P.; Salber, J.; Offenhäusser, A.; Moeller, M.; Groll, J., Surface Grafting of PEO-Based Star-Shaped Molecules for Bioanalytical and Biomedical Applications. *Macromolecular Bioscience* **2007**, *7*, 1010-1023.
60. Neumann, A. W. G., R.J., *Techniques of Measuring Contact Angles*. Plenum Press, : New York (1979), 1979; Vol. Vol. 11.
61. Lutz, J.-F.; Matyjaszewski, K., Nuclear Magnetic Resonance Monitoring of Chain-End Functionality in the Atom Transfer Radical Polymerization of Styrene. *Journal of Polymer Science Part A: Polymer Chemistry* **2005**, *43*, 897-910.
62. Cheng, C.; Wooley, K. L.; Khoshdel, E., Hyperbranched Fluorocopolymers by Atom Transfer Radical Self-condensing Vinyl Copolymerization. *J. Polym. Sci., Part A: Polym. Chem.* **2005**, *43*, 4754-4770.
63. Makal, U.; Uslu, N.; Wynne, K. J., Water Makes It Hydrophobic: Contraphilic Wetting for Polyurethanes with Soft Blocks Having Semifluorinated and 5,5-Dimethylhydantoin Side Chains. *Langmuir* **2006**, *23*, 209-216.

64. Mirabella Jr., F. M., Practical Spectroscopy Series: Internal Reflection Spectroscopy: Theory and Applications. Marcel Dekker, Inc.: New York, 1993; pp 17-52.
65. Fitridge, I.; Dempster, T.; Guenther, J.; de Nys, R., The Impact and Control of Biofouling in Marine Aquaculture: A Review. *Biofouling* **2012**, *28*, 649-669.
66. Baker, J. S.; Dudley, L. Y., Biofouling in Membrane Systems — A Review. *Desalination* **1998**, *118*, 81-89.
67. Richmond, M. D.; Seed, R., A Review of Marine Macrofouling Communities with Special Reference to Animal Fouling. *Biofouling* **1991**, *3*, 151-168.
68. Lappin-Scott, H. M.; Costerton, J. W., Bacterial Biofilms and Surface Fouling. *Biofouling* **1989**, *1*, 323-342.
69. Sorte, C. J. B.; Williams, S. L.; Zerebecki, R. A., Ocean Warming Increases Threat of Invasive Species in a Marine Fouling Community. *Ecology* **2010**, *91*, 2198-2204.
70. Kotrikla, A., Environmental Management Aspects for TBT Antifouling Wastes from the Shipyards. *Journal of Environmental Management* **2009**, *90*, Supplement 1, S77-S85.
71. Muñoz, J.; Gallego, M.; Valcárcel, M., Speciation of Organometallic Compounds in Environmental Samples by Gas Chromatography after Flow Preconcentration on Fullerenes and Nanotubes. *Analytical Chemistry* **2005**, *77*, 5389-5395.
72. López-Serrano Oliver, A.; Sanz-Landaluze, J.; Muñoz-Olivas, R.; Guinea, J.; Cámara, C., Zebrafish Larvae as a Model for the Evaluation of Inorganic Arsenic and Tributyltin Bioconcentration. *Water Research* **2011**, *45*, 6515-6524.
73. Wong, T.-S.; Kang, S. H.; Tang, S. K. Y.; Smythe, E. J.; Hatton, B. D.; Grinthal, A.; Aizenberg, J., Bioinspired Self-repairing Slippery Surfaces with Pressure-stable Omniphobicity. *Nature* **2011**, *477*, 443-447.
74. Eshet, I.; Freger, V.; Kasher, R.; Herzberg, M.; Lei, J.; Ulbricht, M., Chemical and Physical Factors in Design of Antibiofouling Polymer Coatings. *Biomacromolecules* **2011**, *12*, 2681-2685.
75. Callow, J. A.; Callow, M. E., Trends in the Development of Environmentally Friendly Fouling-resistant Marine Coatings. *Nat Commun* **2011**, *2*, 244.
76. Sommer, S.; Ekin, A.; Webster, D. C.; Staflien, S. J.; Daniels, J.; VanderWal, L. J.; Thompson, S. E. M.; Callow, M. E.; Callow, J. A., A Preliminary Study on the

- Properties and Fouling-release Performance of Siloxane–polyurethane Coatings Prepared from Poly(dimethylsiloxane) (PDMS) Macromers. *Biofouling* **2010**, *26*, 961-972.
77. Xu, J.; Bohnsack, D. A.; Mackay, M. E.; Wooley, K. L., Unusual Mechanical Performance of Amphiphilic Crosslinked Polymer Networks. *Journal of the American Chemical Society* **2006**, *129*, 506-507.
78. Neumann, A. W.; Good, R. J., Techniques of Measuring Contact Angles. In *Surface and Colloid Science*, Good, R.; Stromberg, R., Eds. Springer US: 1979; pp 31-91.
79. Finlay, J. A.; Bennett, S. M.; Brewer, L. H.; Sokolova, A.; Clay, G.; Gunari, N.; Meyer, A. E.; Walker, G. C.; Wendt, D. E.; Callow, M. E.; Callow, J. A.; Detty, M. R., Barnacle Settlement and the Adhesion of Protein and Diatom Microfouling to Xerogel Films with Varying Surface Energy and Water Wettability. *Biofouling* **2010**, *26*, 657-666.
80. Brady Jr, R. F., Properties which Influence Marine Fouling Resistance in Polymers Containing Silicon and Fluorine. *Progress in Organic Coatings* **1999**, *35*, 31-35.
81. Kim, J.; Chisholm, B. J.; Bahr, J., Adhesion Study of Silicone Coatings: The Interaction of Thickness, Modulus and Shear rate on Adhesion Force. *Biofouling* **2007**, *23*, 113-120.
82. Maruzzo, D.; Aldred, N.; Clare, A. S.; Høeg, J. T., Metamorphosis in the Cirripede Crustacean *Balanus amphitrite*. *PLoS ONE* **2012**, *7*, e37408.
83. Petrone, L.; Di Fino, A.; Aldred, N.; Sukkaew, P.; Ederth, T.; Clare, A. S.; Liedberg, B., Effects of Surface Charge and Gibbs Surface Energy on the Settlement Behaviour of Barnacle Cyprids (*Balanus amphitrite*). *Biofouling* **2011**, *27*, 1043-1055.
84. Di Fino, A.; Petrone, L.; Aldred, N.; Ederth, T.; Liedberg, B.; Clare, A. S., Correlation Between Surface Chemistry and Settlement Behaviour in Barnacle Cyprids (*Balanus improvisus*). *Biofouling* **2013**, *30*, 143-152.
85. Aldred, N.; Scardino, A.; Cavaco, A.; de Nys, R.; Clare, A. S., Attachment Strength is a Key Factor in the Selection of Surfaces by Barnacle Cyprids (*Balanus amphitrite*) During Settlement. *Biofouling* **2010**, *26*, 287-299.
86. Carl, C.; Poole, A. J.; Sexton, B. A.; Glenn, F. L.; Vucko, M. J.; Williams, M. R.; Whalan, S.; de Nys, R., Enhancing the Settlement and Attachment Strength of

- Pediveligers of *Mytilus Galloprovincialis* by Changing Surface Wettability and Microtopography. *Biofouling* **2012**, *28*, 175-186.
87. Jacobson, A. H.; Willingham, G. L., Sea-nine Antifoulant: An Environmentally Acceptable Alternative to Organotin Antifoulants. *Science of The Total Environment* **2000**, *258*, 103-110.
 88. Chambers, L. D.; Stokes, K. R.; Walsh, F. C.; Wood, R. J. K., Modern Approaches to Marine Antifouling Coatings. *Surface and Coatings Technology* **2006**, *201*, 3642-3652.
 89. Lejars, M.; Margaillan, A.; Bressy, C., Fouling Release Coatings: A Nontoxic Alternative to Biocidal Antifouling Coatings. *Chemical Reviews* **2012**, *112*, 4347-4390.
 90. Magin, C. M.; Cooper, S. P.; Brennan, A. B., Non-toxic Antifouling Strategies. *Materials Today* **2010**, *13*, 36-44.
 91. Hoipkemeier-Wilson, L.; Schumacher, J. F.; Carman, M. L.; Gibson, A. L.; Feinberg, A. W.; Callow, M. E.; Finlay, J. A.; Callow, J. A.; Brennan, A. B., Antifouling Potential of Lubricious, Micro-engineered, PDMS Elastomers against Zoospores of the Green Fouling Alga *Ulva* (Enteromorpha). *Biofouling* **2004**, *20*, 53-63.
 92. Wang, Y.; Pitet, L. M.; Finlay, J. A.; Brewer, L. H.; Cone, G.; Betts, D. E.; Callow, M. E.; Callow, J. A.; Wendt, D. E.; Hillmyer, M. A.; DeSimone, J. M., Investigation of the Role of Hydrophilic Chain Length in Amphiphilic Perfluoropolyether/Poly(ethylene glycol) Networks: Towards High-performance Antifouling Coatings. *Biofouling* **2011**, *27*, 1139-1150.
 93. Martinelli, E.; Agostini, S.; Galli, G.; Chiellini, E.; Glisenti, A.; Pettitt, M. E.; Callow, M. E.; Callow, J. A.; Graf, K.; Bartels, F. W., Nanostructured Films of Amphiphilic Fluorinated Block Copolymers for Fouling Release Application. *Langmuir* **2008**, *24*, 13138-13147.
 94. Bazaka, K.; Crawford, R. J.; Ivanova, E. P., Do Bacteria Differentiate Between Degrees of Nanoscale Surface Roughness? *Biotechnology Journal* **2011**, *6*, 1103-1114.
 95. Schumacher, J. F.; Carman, M. L.; Estes, T. G.; Feinberg, A. W.; Wilson, L. H.; Callow, M. E.; Callow, J. A.; Finlay, J. A.; Brennan, A. B., Engineered Antifouling Microtopographies – Effect of Feature Size, Geometry, and Roughness on Settlement of Zoospores of the Green Alga *Ulva*. *Biofouling* **2007**, *23*, 55-62.

96. Swain, G.; Anil, A. C.; Baier, R. E.; Chia, F. S.; Conte, E.; Cook, A.; Hadfield, M.; Haslbeck, E.; Holm, E.; Kavanagh, C.; Kohrs, D.; Kovach, B.; Lee, C.; Mazzella, L.; Meyer, A. E.; Qian, P. Y.; Sawant, S. S.; Schultz, M.; Sigurdsson, J.; Smith, C.; Soo, L.; Terlizzi, A.; Wagh, A.; Zimmerman, R.; Zupo; Valerio, Biofouling and Barnacle Adhesion Data for Fouling-release Coatings Subjected to Static Immersion at Seven Marine Sites. *Biofouling* **2000**, *16*, 331-344.
97. Zargiel, K. A.; Swain, G. W., Static vs Dynamic Settlement and Adhesion of Diatoms to Ship Hull Coatings. *Biofouling* **2013**, *30*, 115-129.
98. Zargiel, K. A.; Coogan, J. S.; Swain, G. W., Diatom Community Structure on Commercially Available Ship Hull Coatings. *Biofouling* **2011**, *27*, 955-965.
99. Swain, G. W.; Schultz, M. P., The Testing and Evaluation of Non-toxic Antifouling Coatings. *Biofouling* **1996**, *10*, 187-197.
100. Sokolova, A.; Cilz, N.; Daniels, J.; Staflien, S. J.; Brewer, L. H.; Wendt, D. E.; Bright, F. V.; Detty, M. R., A Comparison of the Antifouling/Foul-release Characteristics of Non-biocidal Xerogel and Commercial Coatings Toward Micro- and Macrofouling Organisms. *Biofouling* **2012**, *28*, 511-523.
101. Sokal, R.; Rohlf, F., Biometry. *The Principles and Practice of Statistics in Biological Research* **1981**.
102. Butler, A. J., Recruitment of Sessile Invertebrates at Five Sites in Gulf St. Vincent, South Australia. *Journal of Experimental Marine Biology and Ecology* **1986**, *97*, 13-36.
103. Manly, B. F., *Multivariate Statistical Methods: A Primer*. CRC Press: 2004.
104. Blaszykowski, C.; Sheikh, S.; Thompson, M., Surface Chemistry to Minimize Fouling from Blood-based Fluids. *Chemical Society Reviews* **2012**, *41*, 5599-5612.
105. Cao, B.; Tang, Q.; Cheng, G., Recent Advances of Zwitterionic Carboxybetaine Materials and their Derivatives. *Journal of Biomaterials Science, Polymer Edition* **2014**, 1-12.
106. Chang, Y.; Chang, W.-J.; Shih, Y.-J.; Wei, T.-C.; Hsiue, G.-H., Zwitterionic Sulfobetaine-Grafted Poly(vinylidene fluoride) Membrane with Highly Effective Blood Compatibility via Atmospheric Plasma-Induced Surface Copolymerization. *ACS Applied Materials & Interfaces* **2011**, *3*, 1228-1237.
107. Yu, Q.; Zhang, Y.; Wang, H.; Brash, J.; Chen, H., Anti-fouling Bioactive Surfaces. *Acta Biomaterialia* **2011**, *7*, 1550-1557.

108. Yang, W. J.; Neoh, K.-G.; Kang, E.-T.; Teo, S. L.-M.; Rittschof, D., Polymer Brush Coatings for Combating Marine Biofouling. *Progress in Polymer Science* **2014**, *39*, 1017-1042.
109. Bauer, S.; Alles, M.; Finlay, J. A.; Callow, J. A.; Callow, M. E.; Rosenhahn, A., Influence of Zwitterionic SAMs on Protein Adsorption and the Attachment of Algal Cells. *Journal of Biomaterials Science, Polymer Edition* **2014**, 1-10.
110. Colak, S.; Tew, G. N., Amphiphilic Polybetaines: The Effect of Side-Chain Hydrophobicity on Protein Adsorption. *Biomacromolecules* **2012**, *13*, 1233-1239.
111. Chen, S.; Yu, F.; Yu, Q.; He, Y.; Jiang, S., Strong Resistance of a Thin Crystalline Layer of Balanced Charged Groups to Protein Adsorption. *Langmuir* **2006**, *22*, 8186-8191.
112. Cheng, G.; Li, G.; Xue, H.; Chen, S.; Bryers, J. D.; Jiang, S., Zwitterionic Carboxybetaine Polymer Surfaces and their Resistance to Long-term Biofilm Formation. *Biomaterials* **2009**, *30*, 5234-5240.
113. Young, T. J.; Monclus, M. A.; T L Burnett, T. L.; Broughton, W. R.; Ogin, S. L.; Smith, P. A., The Use of the PeakForce™ Quantitative Nanomechanical Mapping AFM-based Method for High-resolution Young's Modulus Measurement of Polymers. *Measurement Science and Technology* **2011**, *22*, 125703.
114. Chaudhury, M. K.; Finlay, J. A.; Chung, J. Y.; Callow, M. E.; Callow, J. A., The Influence of Elastic Modulus and Thickness on the Release of the Soft-fouling Green Alga *Ulva linza* (syn. *Enteromorpha linza*) from Poly(dimethylsiloxane) (PDMS) model networks. *Biofouling* **2005**, *21*, 41-48.